CHARACTERISATION OF STEADY STATE OF CRYSTALLISATION FROM MELT IN A CONTINUOUS OSCILLATORY BAFFLED CRYSTALLISER

Juliet Adelakun

Submitted for the degree of Doctor of Philosophy

Heriot-Watt University

Institute of Mechanical, Process and Energy Engineering

School of Engineering and Physical Science

May 2017

ABSTRACT

This is the first time that temporal and spatial data of crystal sizes and solute concentration are obtained and analysed for different operating conditions, such that useful parameters (such as agglomeration/attrition rates) could be predicted. Carrying out steady state analyses is an unchartered territory with respect to palm oil (a typical fat material) crystallisation and some interesting but useful correlations and discoveries were made.

Studies were undertaken in a batch OBC, investigating the effect of cooling profile and mixing on the kinetics parameter, e.g. MSZW and it was established that while cooling rate showed similar effects as it would be for a typical solution crystallisation in that higher cooling rate increased the crystallisation rate, mixing had a negligible effect; this is part of what distinguishes this process from a generic solution crystallisation. Generally, the MSZW for this palm oil system was between 17 – 22 °C. The effects of these parameters on filtration properties, such as filtration rate, yield, were also examined.

Continuous crystallisation of palm oil was performed in a continuous oscillatory baffled crystalliser where steady states of solute concentration and crystal size along the column length were examined with respect to process conditions. Temporal steady state of size was achieved for all the conditions considered with a $\leq 10\%$ change over a 30-min period while solute was continuously being consumed with time (based on the % transmittance data). However, the consumption reduced considerably when the flowrate was increased (effect short residence time), and when oscillation frequency was reduced (effect of high shear rates). Spatial size increase was observed between the measurements windows (Jn7 → Jn10) and this was attributed to agglomeration (as opposed to crystal growth) due to the minimal spatial change (1 – 4%) in the % transmittance (an indication of solute consumption) along this tube length. The rate of this agglomeration was averaged at 0.025 μm/s. Only the fast flowrate condition showed an opposite trend in that size decrease was observed from Jn7 to Jn10; another effect of short residence time. High mixing conditions had relatively more influence on the nucleation rate than the crystal size.

ACKNOWLEDGMENT

This is for all those that contributed in one way, shape, or form to the progress and completion of this research work.

First of all, I'll like thank the sponsors of this research work, EPSRC-CMAC for providing the funding required to make this research possible. I will then like to show my sincere gratitude to my supervisor, Prof. Xiong-Wei Ni for his endless support and guidance at every step of the way. My deep appreciation goes to a senior ex-colleague, Dr Cameron Brown for his earnest assistance during the first 1yr+ of this research programme. My appreciation also goes to the other members of the COBRA team – Craig, Hannah, Guillermo, Meifen, and Arabella – for their assistance through the progress of this research work.

Furthermore, I will like to recognise the commendable services of the technicians - Mr Andrew Haston, Mr Richard Kinsella, Mr Curtis Abbott, Mr Douglas Wagener, and Mr Cameron Smith, to mention but a few. The admirable support of the building superintendent, Mr Stuart McLean is also very well appreciated.

And finally, I'll like to appreciate my family and friends, who were always there to provide me with their moral support through this programme.

DECLARATION STATEMENT

TABLE OF CONTENTS

TABLE OF TABLES

TABLE OF FIGURES

LIST OF PUBLICATIONS

Journal Papers

Brown, C. J., **Adelakun, J. A**., & Ni, X. W. (2015). Characterization and modelling of antisolvent crystallization of salicylic acid in a continuous oscillatory baffled crystallizer. Chemical Engineering and Processing: Process Intensification, Vol. 97, 180-186.

Adelakun, Juliet A., and Xiong-Wei Ni. (2016). On the Kinetics of Palm Oil Crystallisation. International Journal of Engineering Research & Science, Vol 2, issue 10, 1-12

Conference Presentations

J. Adelakun and X.-W. Ni. Critical Analysis of Kinetics Models in the Study of Crystallisation of Refined, Bleached, Deodorised (RBD) Palm Oil. 10th European Congress of Chemical Engineering, Nice, France, September 2015

J. Adelakun and X.-W. Ni. Kinetics Study of Melt Crystallisation, Case Study: Palm Oil. British Association for Crystal Growth, Leeds, UK, June 2016

CHAPTER 1 – INTRODUCTION

1.1 Problem Statement

The concept of crystallisation has received a lot of attention with respect to research and developments both in academia and industries such as pharmaceuticals, fine chemicals, agro-chemical and food industries; this is due to the complex science and control associated with the operation. Since it is often adopted in recovering/separating *purer* materials from a multicomponent multiphase product, it is constantly desired to carry out this process as effective as possible, without compromising the efficiency of the downstream processes, such as filtration and drying. This forms a considerable part of the challenge faced by the industries that are constantly under the pressure of delivering high quality products consistently with effective use of both natural and financial resources, without negatively influencing the environment. Given that there are no *one-size-fits-all* theoretical models for the process, fundamental understanding of a particular process mechanism is often obtained through experiments carried out in the laboratory before it is being scaled up for commercial production. Major considerations during the design of a crystallisation process include purity, product control (size distribution, morphology) and process control (supersaturation, temperature profile).

1.1.1 Proffered Solution

Mixing and heat transfer are key parameters that greatly affect the eventual product qualities (consistency and desired properties). As can be expected, this challenge will be more prominent in fat/oil systems where the composition is more complex, and viscosity is higher. To address these issues, a *plug flow* system, where all the elements within the system have the same residence time, is often desired. This motivated the design and development of a novel technology, the Oscillatory Baffled Crystalliser (OBC); it is a tubular system with inserted (or in-built) orifice baffles positioned at regular intervals along the length of the tube; oscillatory motion is used to stimulate a radial flow motion through generation and cessation of eddies as the fluid flows through the baffle orifices. Studies have confirmed the capability of this technology in providing solutions to the pressing challenges with conventional stirred reactors[1].

The tubular geometry of the COBC (*C* = Continuous) allows for a better heat and mass transfer due to a larger specific area per unit volume, provides a consistent mixing environment for crystallisation and for uniform particle suspension due to the achievement of *pseudo*-plug flow; also, scale up parameter is linear, i.e. process mechanism remains the same in all scales. Besides improvement to the process operation mechanisms, other attractive enhancement brought about by this technology are reduced material consumption, reduced capital/operating costs and improved product control/quality. More information regarding this technology and its conventional counterparts are detailed later in this thesis.

1.1.2 Research Objectives

This research therefore aims to address the highlighted challenges by adopting this innovative mixing technology to gain better understanding of melt crystallisation with respect to kinetics and steady states. Therefore, the key drivers for this study are listed below:

- Understanding the science of crystallisation from melt as it compares with solution crystallisation.
- Develop operation and control for continuous crystallisation from melt
- Develop continuous filtration for crystallisation from melt

In view of this, the research work has been categorised into the following sections:

- Develop solubility curve for the model compound using different analysis techniques
- Examine the effect of operating parameters on metastable zone width
- Extract kinetics parameters and compare with solution crystallisation
- Examine the effects of operational parameters on filtration properties
- Examine the steady states of solute concentration and crystal sizes on a continuous platform.

1.2 Theory

There are two steps that make up the crystallisation process [2] – *nucleation* and *growth*, and they are driven by a deviation from thermodynamic equilibrium based on the concentration–temperature (C-T) relationship of a specific system; this deviation is referred to as *supersaturation*. Crystallisation is therefore the process with which the solution regains its equilibrium position; supersaturation can be achieved[3] primarily through cooling (change in temperature) or evaporation (change in concentration) processes; other methods include addition of anti-solvent materials and chemical reactions.

1.2.1 Crystallisation from Melt

The two steps above often involve solution systems– a homogeneous mixture of two or more substances[4]. However for this research work, the system involved is better referred to as *melt* – a homogeneous liquid mixture close to its freezing point, with constituents individually solidifying when cooled to ambient temperatures; though, no clear distinction has been made between the two systems (more so in relation to phase equilibria diagrams), it was stated that *crystallisation from solution* precipitates a pure state of only one component (for a binary mixture) while in *crystallisation from melt* (CfM), a mix of products is precipitated[5]. Therefore, CfM is targeted towards the separation/purification of each component within the mixture; this is often achieved by a controlled cooling process[6]. It is regarded more attractive than related processes (such as distillation and evaporation) due to the low energy involved; other advantageous feature of this process is low operating temperatures. However there are also some associated challenges which include poor product recovery (purity and yield), high viscosity at low temperatures, difficult process control, system incompatibility, difficult to measure process parameters as the solution being opaque, difficulties in filtration due to the viscosity, just to name but a few.

1.2.2 Model Compound

The model compound considered for this research work is *Refined, Bleached, and Deodorised* (RBD) ***palm oil***. Palm oil is a type of vegetable oil, naturally-rich in a wide range of triglycerides, thereby considered one of the most flexible edible oils. It consists of two major fractions – *olein* and *stearin*, the latter mainly made up of saturated fats thereby having a higher melting point. Due to the growing pressure against hydrogenated fat and the demand for

saturated fat products, palm oil is gaining increased attention as it is comprise of a wide range of fractions of which saturated fats are included[7]. In view of this, separation of the fractions is an essential process for the edible oil industries; and this is carried out based on the melting points of the constituent fractions – a process known as ***fractionation***[8] which is basically an industrial term for crystallisation from melt. More information on the process is provided later in this thesis.

1.3 Structure of Thesis

As seen already, the thesis commenced with an ***introduction*** as the first chapter which gave a brief overview of the CfM process, an insight into the major technology adopted, and an outline of the major problems to be addressed, together with aims and objectives of the research.

This is followed by a ***literature review*** in the second chapter which contains a detailed theoretical background of the crystallisation concept, including reports on findings/theories from previous studies relevant to the crystallisation from melt. The third chapter describes the ***experimental work*** of this research work, i.e. details of the major equipment used, experiments carried out, and analyses techniques adopted in the study.

The ***discussion & conclusions*** on the results obtained from the experiments carried out is articulated in the fourth chapter; logical reasoning behind results and comparison with some previous studies are shown in this section. The fifth chapter suggests ***future work*** in order to broaden the understanding of the research focus and also tackle some other related issues that were not addressed within the scope of the study.

At the end of this thesis there are the ***reference*** section and ***appendices*** section where additional information supporting some of the presented results are shown.

CHAPTER 2 – LITERATURE REVIEW

In this chapter, the background of crystallisation is established, which includes the theory behind the process, previous research work and the associated challenges in melt crystallisation.

2.1 Basics of Crystallisation

Crystallisation is a common unit operation for separating and purifying materials. *Supersaturation,* the driving force of any crystallisation process, is when the concentration of the solid materials present in a solution is higher than the equilibrium concentration at a specific temperature (and pressure)[9]. Since supersaturation is a deviation from the equilibrium position, crystallisation is the process with which the solution regains its equilibrium position. In thermodynamics, it is a function of the chemical potential (a measure of the potential energy released or absorbed during a chemical reaction or phase transition) of the solution with respect to the *excess* solid phase and the solute activities (or concentration) as shown in eq. (2.1), which is based on the Gibbs – Thomson equation. However due to the difficulty in determining the value of $\Delta\mu$ experimentally, supersaturation is expressed as a ratio of excess to equilibrium concentration and it is referred to as *relative supersaturation* (σ)[9].

$$\frac{\Delta\mu}{RT} = \ln\left(c/c^*\right) = \ln S$$

$$\sigma = \frac{c - c^*}{c^*} = \frac{c}{c^*} - 1 = S - 1 \qquad (2.1)$$

Where $\Delta\mu$ = Difference between actual and equilibrium chemical potential, J/mol

c and c^* = Actual and equilibrium concentrations respectively, g/g

R = Gas constant, J/mol-K

T = Temperature, K

S = Fundamental supersaturation

A *Solubility-Supersolubility* diagram, which shows the concentration-temperature (C–T) relationship, is used to classify and represent the degree of supersaturation of a solution **(Fig 2.1**). Below the *solubility* curve, where the solution contains less amount of solute than the equilibrium concentration, crystallisation cannot occur. Above the solubility curve is the

metastable zone, the solution becomes supersaturated but crystallisation is still unlikely. Beyond the metastable zone, the solution becomes unstable and crystallisation occurs spontaneously[10]. There are two major steps that are resulted from supersaturation on the crystallisation process; *nucleation* and *crystal growth*.

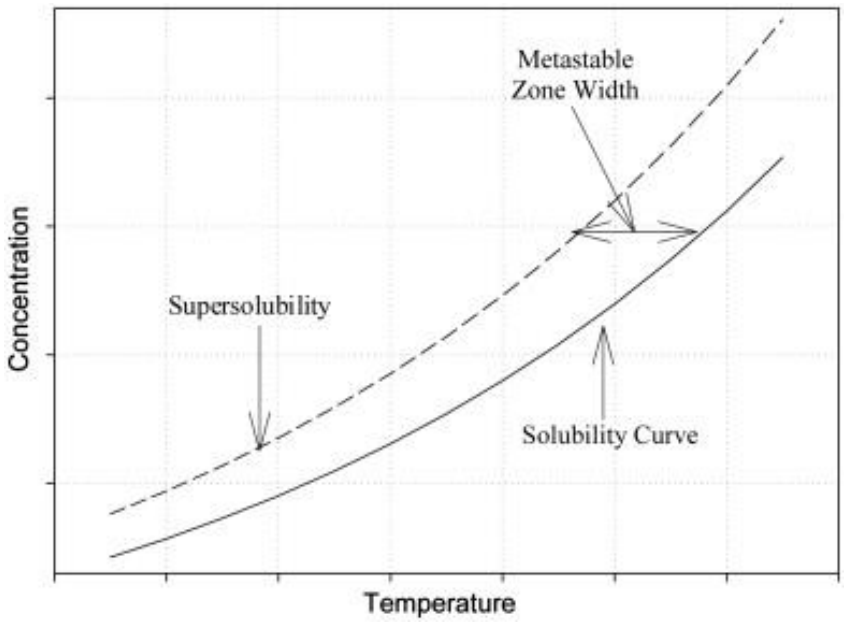

Fig 2.1: A typical solubility-supersolubility curve[11]

2.1.1 Nucleation

Nucleation is the creation of a new solid phase (nuclei) from a supersaturated solution. It can occur spontaneously (at high level of supersaturation, as stated above) and it can be induced artificially through seeds, mechanical agitation, shear force, lighting[12], cavitation of sub-cooled or over-pressurised liquid[13, 14] within the solution. In view of this, nucleation can be divided into two major categories[15]:

- ***Primary Nucleation***: When nuclei are formed spontaneously in the absence of crystalline materials or foreign bodies, it is referred to as *homogeneous*. However, when it is induced by the presence of foreign particles (impurities, rough surfaces), it is referred to as *heterogeneous*. The former is possible only when the supersaturation has reached the labile region while latter can occur within the metastable zone (Error! Reference source not found.).

- ***Secondary Nucleation***: Here, nucleation occurs due to the presence of crystalline material generated from within the supersaturated solution. This could be due to mechanical forces (attrition) or a deliberate addition of crystals referred to as 'seeds'. The type of nucleation could also be due to the interaction of the solution with the surrounding surfaces, e.g. impeller, walls, etc.[16]

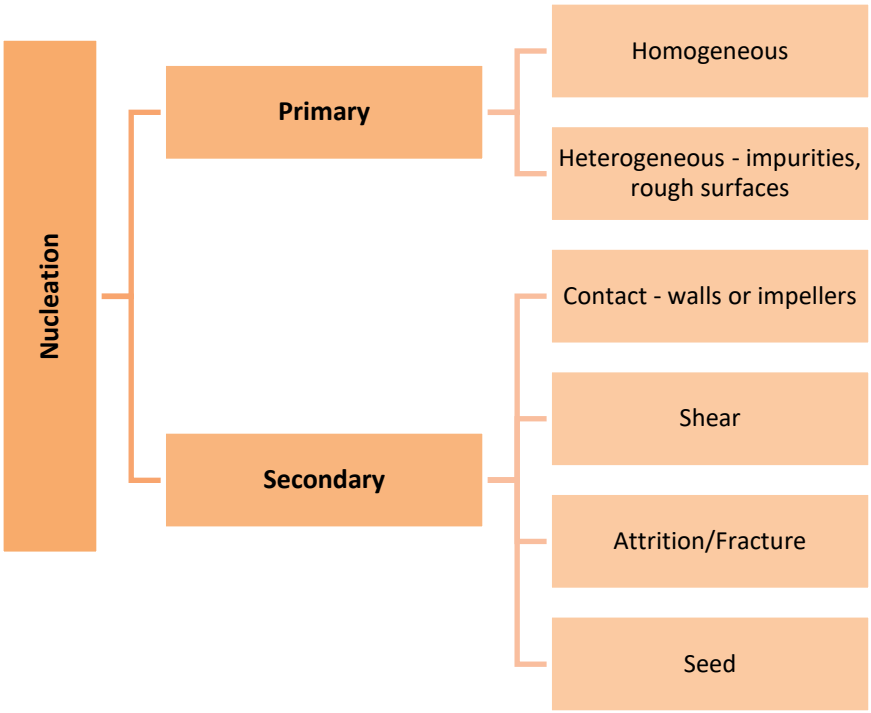

Fig 2.2: Different categories of nucleation events[15]

Kinetics

Nucleation is similar to a chemical reaction in that activation energy barrier needs to be overcome before a stable nucleus can be formed; this energy is referred to as free energy. It is characterised by the size of this stable nucleus (referred to as the *critical size*) and the degree of supersaturation of the solution; the magnitude of this barrier varies with the particular process of interest. According to Volmer *et al*[17], it was assumed that nucleation occurs by successive addition of molecules to one another thereby increasing in size until the critical size is reached, and that it is birthed by the formation of an interface layer between the solution and the new, solid phase. Therefore the expression that defines the overall free energy barrier is a function of the energy gained due to the phase transition (ΔG_V, negative) and that required to form the nucleus surface (ΔG_S, positive); it is given as below[16]:

$$\Delta G = \Delta G_s + \Delta G_v$$
$$= 4\pi r^2\gamma - \frac{4}{3v}\pi r^3\Delta\mu \quad (2.2)$$

Where r = radius of *nucleus* (assumed nucleus is spherical), m

γ = interfacial tension between the new solid surface and surrounding solution, N/m

v = Molecular volume of the nucleus, m^3/mol

The nucleus formed is considered thermodynamically stable when the total free energy remains constant with increasing size, i.e. $\delta\Delta G/\delta r = 0$; the nucleus size at which this occurs is what is referred to as the critical radius (r_c). Using eq. (2.1) and eq. (2.2) to solve the differential equation gives eq. (2.3); it shows the relation of supersaturation with the critical size of the nucleus in that it reduces with increasing supersaturation.

$$\frac{\delta\Delta G}{\delta r} = 8\pi r\gamma - \frac{4}{v}\pi r^2\Delta\mu = 0$$
$$r_c = \frac{2\gamma v}{\Delta\mu} = \frac{2\gamma v}{kT\ln S} \quad (2.3)$$

Replacing r_c into eq. (2.2) gives the free energy at which a stable nucleus is formed (ΔG_{cr}):

$$\Delta G_{cr} = \frac{16\pi\gamma^3 v^2}{3(kT\ln S)^2} \quad (2.4)$$

Where k = Boltzmann constant (R/N_A), J/K

N_A =Avogadro's number, 1/mol

It has been established earlier that supersaturation is the driving force of crystallisation hence the rate (J) at which a stable nucleus is formed (per unit volume) is dependent on the level of supersaturation of the system; it is given as the equation below based on the Arrhenius expression for reaction velocity[18]:

$$J = K\exp^{\left(-\Delta G_{cr}/kT\right)}$$
$$= K\exp\left[-\frac{16\pi\gamma^3 v^2}{3k^3T^3(\ln S)^2}\right] \quad (2.5)$$

Where K = Nucleation rate constant, 1/s

Eq. (2.5) confirms that the nucleation rate is dependent of the level of supersaturation of the solution, absolute temperature of the system, and the interfacial tension between the nucleus

surface and the solution. If the critical size of the nucleus reduces due to increasing level of supersaturation, more nuclei will become stable hence increasing nuclei count which implies increased nucleation rate.

$$S \uparrow \rightarrow \quad r_c \downarrow \quad \rightarrow \quad J \uparrow$$

Previous works[19] have examined that the effect of supersaturation on nucleation rate as a function of the initial concentration of the solution (*c*); results showed that increasing the initial concentration increased the nucleation rate (inversely proportional to the *induction time*; time at which a stable nucleus was formed and observed after the solution had become supersaturated) until a critical supersaturation was reached where induction time approached zero and nucleation became spontaneous (homogeneous nucleation). The results also showed that increasing the rate at which supersaturation was generated within the solution caused an increase in the metastable zone width that was the supersaturation at which a nuclei was observed was increased. By numerical manipulation based on the interfacial tension (γ) in eq. (2.5), it was discovered that materials with higher solubility had lower surface tension and therefore a lower critical supersaturation[20]. Evaporation with solvent loss was used to attain supersaturation in this work.

The kinetic model above is based on the assumption that nucleation occurs in the absence of any solid materials that is primary, homogenous nucleation. However, this is rarely the case in reality due to the presence of foreign bodies and/or surrounding environment; the *real* free energy barrier required for nucleation is lower than that ideal value derived from the theoretical model, hence heterogeneous nucleation occurs at a lower supersaturation than homogeneous and to account for this, parameters such as impeller speed and contact angle, are incorporated into the kinetics equation[21]. However the general expression for overall nucleation rate that takes into account the possibility of heterogeneous nucleation is given below based on the Becker-Doering relationship:

$$J = k_N \Delta c^n \qquad (2.6)$$

Where *kN* = overall nucleation rate constant, 1/s

n = apparent order of nucleation

It was reported that the probability of heterogeneous nucleation taking place within a system which determines the crystal count from the solution is dependent on the degree of supersaturation and size of the facilitating surface (presumed to be in the nano-scale); this inference was a result of experiments based on liquid-gas systems[22, 23]. In a related previous work24], it was observed that at low supersaturation (close to the solubility curve), nucleation rate is a function of the surface area of the nucleating surface and this brought about the term *surface area-controlled nucleation*. This phenomenon was said to occur within a narrow range of supersaturation, hence not easily detected; beyond this region, full heterogeneous nucleation takes over.

2.1.2 Crystal Growth

This is the progressive adjoining of growth units to stable nuclei surfaces by intermolecular interactions in a supersaturated solution. Two mechanisms are involved in crystal growth[24]; diffusion of the growth units (ion, atom, molecules or clusters) from the bulk solution and integration onto the nuclei surfaces, the slowest of which determines the rate and direction of the growth process; this is also driven by the degree of supersaturation and it is proportional to the concentration difference between the bulk solution and nuclei surface.

According to literature, it is said that growth units tend to bind with a crystal surface at locations of the highest attractive force (highest binding sites) which means filling up an existing layer before starting a new layer. This is what brought about the theory that says crystal growth occurs stepwise in layers[25]. In view of the two mechanisms mentioned above, it is assumed that there is an interface layer between the bulk solution and the crystal surface which then brought about the below concentration-dependent growth rate equations, a function of the rate of increase in mass (m) of deposited growth unit with time (t);

$$\frac{1}{A}\frac{\mathrm{d}m}{\mathrm{d}t} = k_d\left(c - c_i\right) \qquad \text{(Diffusion)}$$

$$\frac{1}{A}\frac{\mathrm{d}m}{\mathrm{d}t} = k_r\left(c_i - c_*\right) \qquad \text{(Integration)}$$

Where *kd*, *r* = rate constant of diffusion and surface integration respectively, g/m2s

ci = solute concentration at the interface, g/g

A = surface area of the crystal, m2

However because it is difficult to determine the interfacial concentration (*ci*) experimentally, the above two equations are merged together to give an overall growth rate:

$$R_G = K_G\left(c - c_*\right)^g \quad \text{(Mass growth rate, kg/m}^2\text{s)}$$
$$G_r = k_G\left(c - c_*\right)^g \quad \text{(Linear growth velocity, m/s)}$$
$$K_G = \frac{3\alpha}{\beta}\rho k_G \qquad (2.7)$$

Where K_G = overall growth rate constant, 1/s
α, β = volume and surface shape factor respectively
ρ = crystal density, g/m^3
g = order of growth process

The rate of crystal growth which is similar to mass transfer can be measured in a different ways depending on the parameter of interest. In terms of the shape, it is measured as the speed of movement in the direction perpendicular to the face of interest[26]; in terms of size, it is the change in the characteristic dimension of the crystal with time; and in terms of weight, it is the change of the crystal mass with time; the last two are referred to as linear growth rate[21]. Eq. (2.7) confirms a relationship between growth rate and the supersaturation of the solution; previous works have shown these effects and that of solution flowrate (u); in an experiment involving single-crystal growth cell[27], it was observed that growth rate of the crystals increases with increasing driving force (supersaturation) and with increasing solution flowrate. Also at high flowrates ($u \to \infty$), surface integration becomes the controlling mechanism but when the crystals are allowed to grow in a stagnant solution ($u \to 0$), crystal growth becomes diffusion-controlled; it was however concluded that though the transition between the two rate-controlling region is not as continuous as depicted, results confirmed limiting factors to growth rates.

In another work involving an mixed-suspension-mixed-product removal (MSMPR)[28], results confirmed the aforementioned effects. The results also showed that an increase in the initial solute concentration causes a decrease in the growth rate and these was attributed to increased nucleation rate (both primary and secondary) which impedes crystal growth. Furthermore, it was confirmed that increasing mean crystal size increases the growth rate and

this brought about the *size-dependent growth* (SDG) model; however a point is reached where the growth rate becomes unchanged with size; this is referred to as *size-independent growth rate*; however until a minimum size is reached, growth rate is significantly low and this was attributed to the higher terminal velocity of the larger crystals which favours surface integration[29], consistent with the earlier-mentioned effect of solution velocity (u). This implies that nuclei which were of the same size, exposed to the same conditions tend to grow at different rates and this was attributed to secondary nucleation brought about by attrition or other mechanical stress; this then led to the *growth rate dispersion* (GRD) model[30].

From the findings highlighted above, a strong relationship can be observed between nucleation and crystal growth as they are both driven by the degree of supersaturation of the solution amongst other similarities. It can therefore be concluded that the control of these two steps contribute majorly to the characteristics of the crystal products of which include purity, size distribution and shape.

2.1.3 Metastable Zone Width

A major part of process control for a crystallisation process is the ability to control the occurrence and rate of nucleation and subsequent crystal growth, and a common way of achieving this is by designing the process such that the crystallisation is induced within the metastable zone width (see Error! Reference source not found.); an example is the seeding process highlighted above. Seeds (small particles of the material to be crystallised) are often introduced just when the solution becomes supersaturated, and their primary aim is to act as the nuclei thereby suppressing primary nucleation while promoting crystal growth at a controlled rate[6].

It is therefore essential to have a fundamental knowledge of the supersaturation condition at which a solution is likely to nucleate spontaneously, likely or not at all; the metastable zone width (MSZW) provides this information. In a cooling process, it is defined as the difference between the saturation (dissolution of last crystalline particle) and nucleation temperature (appearance of first crystalline particle) provided a steady cooling rate is maintained[31]. It could also be defined simply as the maximum allowable degree of supercooling (supersaturation) for a particular system (ΔT_{max}); it is specific to the particular system hence

not based on thermodynamic calculations but a function of the operating parameters such as temperature profile, initial concentration and rate of supersaturation[32]. An adopted expression used for calculation of MSZW is given below; where dc*/dT represents the concentration change with temperature:

$$\Delta c_{\max} = \left(\frac{dc^*}{dT} \right) \Delta T_{\max} \tag{2.8}$$

From the data on the MSZW (ΔTmax) as a function of cooling rate $\left(\dot{T}\right)$ for a particular system obtained through experiments, the nucleation rate constant (kN) hence nucleation rate (J) can be determined by taking the logarithm of eq. (2.6) and the resulting expression is given below eq. (2.9) where ε is the concentration correction factor in case of hydrate formation[33]; plotting a graph of $\log\left(\dot{T}\right)$ against $\log(\Delta Tmax)$ gives a straight line with a slope equal to the nucleation order (n) and the rate constant (kN) can be calculated from the intercept.

$$\log\left(\dot{T}\right) = (n-1)\log\frac{dc^*}{dT} - \log\varepsilon + \log k_N + n\log\left(\Delta T_{\max}\right) \tag{2.9}$$

This analysis however assumes that nucleation rate is a direct function of the supersaturation rate, which is not always the case as nuclei after being created undergo a growth process to the critical size before being detected. This therefore reduces the reliability of the above expression and brought about its modification[34]. For melt crystallisation, the term *cloud point* and *clear point* are used to represent the temperature at which the first nuclei is observed during the cooling process and when the last crystal melts during the heating process respectively; the difference between these points is the MSZW and it has been proven to greatly influence the type of crystal formed from the crystallisation process[9]. A typical profile is shown (**Fig 2.3**).

A common technique used for this analysis is ***turbidimetry***, where light transmittance of the solution is measured against temperature during a consecutive cooling and heating process, using fibre-optic signal. The transmittance reduces as the solution becomes cloudy indicating crystals formation; during subsequently heating, the transmittance increases as the crystals are re-melted[35]. However, the signals recorded are un-calibrated and often affected by crystal size, system temperature and composition, etc.; hence they are taken as approximate, relative

values of solid concentration[36]. It should however be noted that the notice of the cloudiness in solution is the post-nucleation event, the exact detection points are dependent on the sensitivity of the technique for the detectable crystal size[37]. Other measurement techniques that have been used to acquire crystallisation information related to MSZW include infrared spectroscopy (solute concentration)[38] and FBRM (chord length distribution)[39].

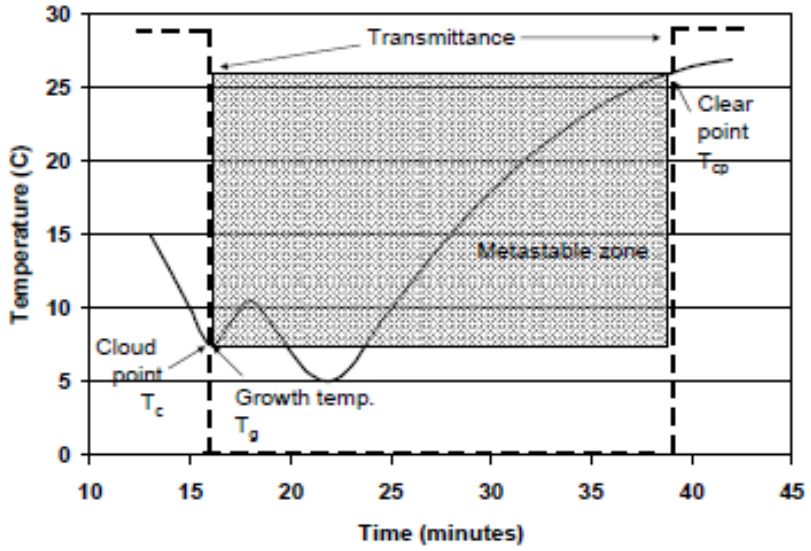

Fig 2.3: A typical transmittance vs. temperature profile for MSZW determination[40]

Previous studies have shown that increasing cooling rate increases MSZW and this was attributed to a higher rate of supersaturation and the longer time required for a stable nuclei to be formed & observed[41, 42]. It was also confirmed that the mixing intensity of the solution has an effect; since mixing is aimed at minimising concentration gradient within the supersaturated solution hence increasing the mixing intensity takes the solution closer to the equilibrium position (solubility curve) thereby reducing the MSZW[6, 43]. According to a previous study based on palm oil solid fractions (POP and PPP), it was reported that ΔTmax showed relatively more dependence on cooling rate, and was higher at lower concentrations of PPP; turbidimetry was also used to confirm rapid crystallisation of bulk of the palm solid fractions by primary nucleation due to the rapid reduction in the light transmittance[44].

In addition, it is established that MSZW is also a function of the temperature history the solution has been subjected to; in that the farther and longer a solution is kept above its saturation condition, the longer the induction time thereby widening the MSZW and reducing

the solid density of the resultant slurry[44]. It is therefore essential that the adopted process operation is carefully designed to facilitate a balance between process control and throughput.

2.2 Crystallisation from Melt (CfM)

As described in the *introduction* section, a *melt* is a multicomponent liquid mixture that solidifies on cooling (to room temperature). It is differentiated from a *solution* based on the dominating influence during the phase-change process – mass transfer (diffusion) and heat transfer for solution and melt respectively[45]; this is related to the two rate-determining mechanisms of crystal growth highlighted above. CfM is a controlled-cooling process by which these components are separated into their pure forms – it is referred to as ***Fractionation*** in the industry which is quite apt for the model compound on which this research is based on; this should however not be confused with ***fractional crystallisation*** which is basically a repetitive crystallisation process aimed at improving the purity of the product. It is considered advantageous in comparison to related separation processes; some of these advantages include:

- *Lower energy consumption*: When the energy required for phase change (liquid/solid) is compared to that of distillation (liquid/vapour), it is considerably lower; this was concluded based on the fact that the heat of fusion is lower than the heat of vaporisation for a particular compound (e.g. 334 kJ/kg and 2260 kJ/kg for water[6])
- *Lower running cost*: From a comparison with high-pressure extraction, based on the fractionation of milk fats, it was discovered that the extraction plant cost three times more for investments, and eleven times more for running costs[46].
- *Lower operating temperatures*: Operating at these conditions minimises the risk of chemical corrosion brought about by high temperatures; also the low melting points of most organic chemicals favours the use of low-level heat sources[47]

2.2.1 Mechanism

Equipment design for a crystallisation from melt process is based on two types of process mechanism; ***suspension*** and ***layer*** crystallisation[3].

- ***Layer***: Layers of crystals are deposited from the melt onto cooled surfaces; crystal growth is perpendicular to cooled surface. Phase separation is also taking place as the layers are being formed there, product purity is enhanced through controlled heating and partial melting. The models discussed above are all based on this mechanism. Minimal

encrustation issues, easy equipment handling and controllably high crystal growth rate are some of the reported advantages[4]. There are however also reported limitations:

- Limited surface area for heat transfer
- Reducing production rate due to increasing layer thickness; increased temperature driving force would be required to counter this
- High energy consumption (due to heating) is required to recover encrusted product from cooled surface
- Recurrent heating and solidification of product can be deleterious to both the product and equipment

- ***Suspension***: Melt is continuously converted to a crystal suspension through a cooling process; separation of the solid phase from the suspension is often carried out through a mechanical process (e.g. filtration, centrifugation). A large interfacial area due to the suspended small particles is considered advantageous for the separation process; another being the absence of the need for re-melting to recover product – this reduces the energy consumption and operation time. The reported drawbacks to this mechanism include:
  - More *complicated* equipment operation, e.g. slurry handling, moving parts and encrustation issues.
  - Additional unit operations required to separate product from slurry
  - Limited growth rate due to isothermal conditions
  - High system viscosity and close density between feed melt and product

Based on these mechanisms and other considerations like mode of operation, equipment for CfM can be grouped into the categories below[4]:

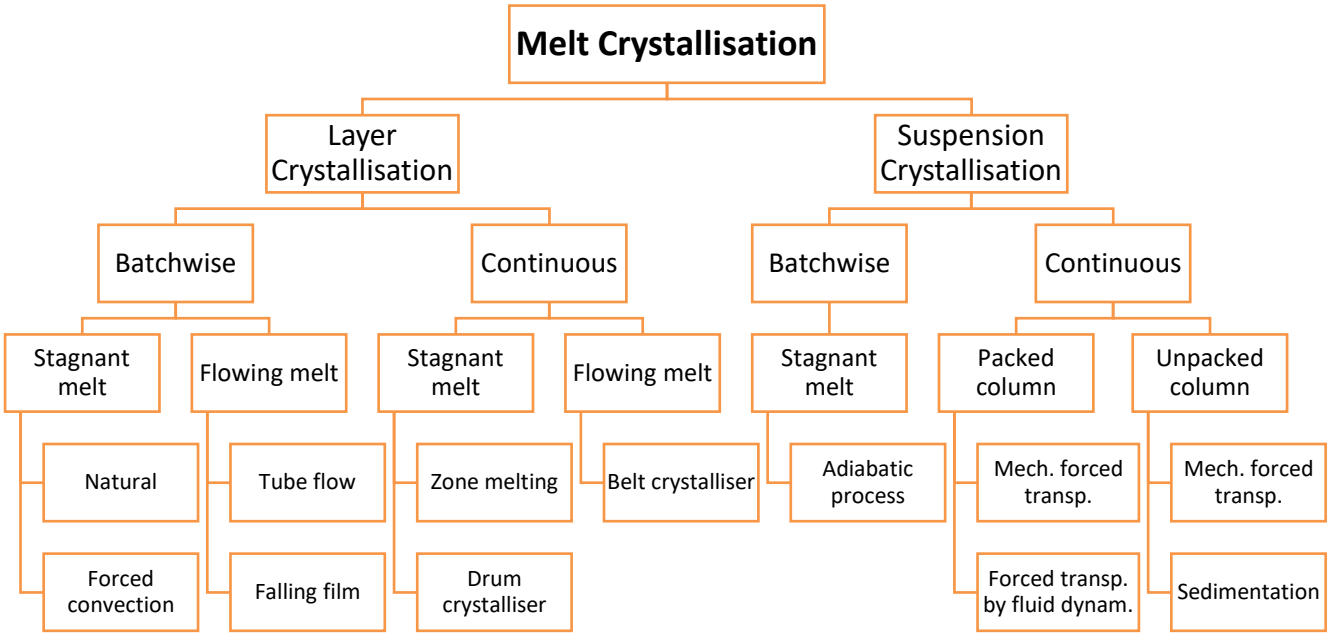

Fig 2.4: Different categories of melt crystallisation process based on the equipment used

For the purpose of this research work, the focus will be on ***suspension crystallisation***. In general, the cooling process can be achieved through two types – jacketed systems and direct cooling (using inert gases)[48]. After the crystallisation process has been completed, downstream processes are then required to recover/purify the resultant product. Some of these include[49]:

- *Sweating*: This is the partial melting of the formed crystals (or crystal layers) through heating with the aim of enhancing the product purity – it is expected that residual impurities and entrained liquid within the crystal surfaces are melted along with some of the product thereby increasing the product purity at the reducing process throughput[50]; the benefits are more applicable for layer-type crystallisation mechanism.
- *Washing*: This is a process by the which contaminants on the product surface are either washed off and replaced with a film of pure liquid (rinsing) or are diffused into the wash liquid and drained out (diffusion washing); benefits are more applicable to suspension-type crystallisation mechanism.

In conclusion, the eventual separation efficiency of the crystallisation process is specific to the equipment set-up, process operations (and parameters) and the system being processed.

2.2.2 Kinetics

The kinetics of CfM has its basis on the two steps discussed above (nucleation and crystal growth) however with some *exceptions*. For instance, eq. (2.5) shows that increase in supersaturation increases the nucleation rate; however a maximum rate is reached after which it begins to decline. It was reported[51] that this is as a result of a sharp increase in viscosity (brought about by excess supercooling), a point where molecular movements become restricted thereby obstructing the formation of crystalline structure (**Fig 2.5**); the temperature at which this occurs is referred to as the *optimal* temperature.

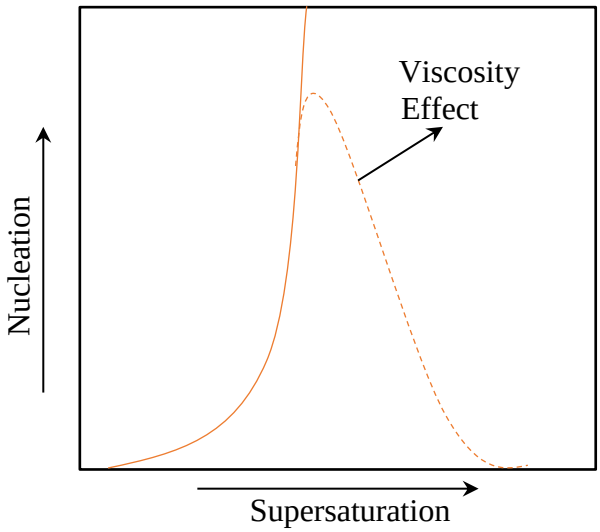

Fig 2.5: Effect of sharp increase in viscosity on Nucleation rate

This phenomenon brought a modification to eq. (2.5) by including an additional term ($\Delta G'/kT$) that takes into account the viscosity effect, and this is shown in the eq. (2.10)[52]. This term is the activation energy required for the molecules to move across the solid/liquid interface; it is relatively large in comparison to the other term within the exponential (since the supersaturation, *S* at this point is high) thereby reducing the nucleation rate with increasing *S*. It should however be noted that this exception is not exclusive to melts, but also for highly viscous aqueous solutions as reported for citric acid[53].

$$J = K' \exp\left[-\frac{16\pi\gamma^3 v^2}{3k^3 T^3 (\ln S)^2} + \frac{\Delta G'}{kT} \right] \tag{2.10}$$

Crystal growth from melts can be categorised into four steps[4]:

1. Transportation of crystalline molecule from the bulk of the melt to the vicinity of the crystal surface
2. Surface integration of this molecule into the crystal lattice
3. Transportation of impurity from the crystal vicinity into the bulk of the melt
4. Transportation of the dissipated heat to facilitate the solidification process

The dominant effect of heat transfer over mass transfer during crystal growth is what differentiates CfM from crystallisation from solution. A maximum permissible growth rate for which the inclusion of impurity is minimised thereby enhancing the recovery of pure product was predicted from a previous work[54] based on the layer mechanism; this prediction (referred to as the *v/k*-criterion) then led to the development of an equation for the effect of the system properties and process parameter on the separation efficiency as shown below[55]:

$$k_{eff} = 1 - \frac{c_i - c_\infty}{c_\infty \left(e^{\frac{v_{cr}}{k} \cdot \frac{\rho_s}{\rho_l}} - 1 \right)} \qquad (2.11)$$

$$k_{eff} = \frac{c_{cr}}{c_\infty}$$

Where: k_{eff} = effective distribution coefficient

c_i = concentration at solid/liquid interface, g/g

c_∞ = concentration in the bulk, g/g

v_{cr} = velocity of interface normal to crystal surface, m/s

k = mass transfer coefficient

ρ_s = solid density, g/m^3

ρ_l = liquid density, g/m^3

However, the property, *ci* is often difficult to determine experimentally as it changes with time ('moving boundary' problem); also, the effect of heat and mass transfer was not accounted in this equation thereby limiting its application to systems with negligible dependence on heat and mass transfer[56]. Subsequent study by other researchers developed different models to include the effect of the mass and heat transfer on the crystal growth process and referred to it

as the *gradient* criterion. Due to the slower rate at which impurities are transported into the bulk melt compared to the rate at which crystalline molecules are integrated into the crystal surface, a concentration gradient is formed within the system; this can reduce the actual temperature of the system (at the solid/liquid interface) below the equilibrium temperature (for the corresponding concentration) – this effect is referred to as *constitutional supercooling* (CSc) and reported to cause dendritic crystal growth an impure products[57]. Mathematical formula used to predict the optimum gradient to ensure pure products was also developed through this study;

$$\frac{\partial T_{eq}}{\partial x} = -m.\frac{v_{cr}}{D}.\frac{\rho_s}{\rho_l}.e^{\left(\frac{v_{cr}}{k}.\frac{\rho_s}{\rho_l}\right)}$$
$$\frac{\partial T}{\partial x} = \frac{\alpha}{\lambda}.(T_i - T_\infty) \qquad (2.12)$$

Where: T, T_i, and T_{eq} = Actual, interface and equilibrium temperatures respectively, K

x = distance from cooled surface, m

m = linear gradient in the phase diagram

D = diffusion coefficient, m/s

α = heat transfer coefficient, W/m^2-K

λ = heat conductivity, W/m-K

This model has also been modified and improved upon by subsequent related studies, some of which are highlighted below:

- It is possible to produce pure products despite the occurrence of CSc provided that a maximum supercooling was not exceeded[58]
- Impurity inclusion is due to the non-planar growth of the crystalline layer[59]
- The migration rate of liquid inclusions is significant and a function of process parameters[60]
- The liquid inclusions can be significantly large and change their shape while migrating[61]

Parameters Estimation

Although the terminology of crystallisation is used for all inorganic and organic compounds, while fractionation is applied to all melts, the essence of the process is the same, i.e. by cooling for all. In spite of the similarities in the processes, different model approaches have been used for crystallisation from solution (e.g. APIs) than from melts (e.g. fats). Taking palm oil as the model compound for melt, it consists of a wide range of triglyceride (TAGs) fractions based on their physical state at different temperatures. These are significantly different to crystallisation of paracetamol for instance. Some of the models that has been developed for melt crystallisation and also considered in this study are highlighted below.

Avrami model

This model deals the rate of phase change (i.e. the formation of solid phase from liquid phase per unit time) at isothermal conditions. It is a simplistic model that uses the *deterministic[62]* approach to evaluate the *overall* kinetics in relation to nucleation mode and crystal growth mechanism[63, 64] of the isothermal process. The original derivations by Avrami[63] have been simplified by Evans[65] and put into polymer context by Meares[66] and Hay[67]. Through probability derivations[68], the volume fraction of crystalline material, X, known widely as the degree of crystallinity, can be written as:

$$1 - X = e^{-E} \tag{2.13}$$

Where E represents the average number of fronts of all such points in the system. For low degrees of crystallinity, a useful approximation is X ≈ E. For the bulk crystallisation of polymers, X in the exponent may be considered the volume or volume fraction of crystalline materials, V_t, i.e.:

$$1 - X = e^{-V_t} \tag{2.14}$$

This has been the widely accepted and used equation in bulk crystallisation[69-72]. For either instantaneous or sporadic nucleation, eq. (2.14) can be written as:

$$1 - X = e^{-Kt^n} \text{ or } -\ln(1-x) = kt^n \tag{2.15}$$

Where x is the fraction of solid formed at a particular time (t); k the overall crystallisation rate constant; and n the index of crystallisation, also referred to as the *Avrami exponent*, the phenomenological index of crystallisation[73], depending not only on the structure of the crystal, but also on the nature of nucleation[64, 74]. For example, when $n = 1$, it corresponds to rod-like growth from instantaneous nuclei; whereas $n = 3$ or 4 refers to spherulitic growth from either sporadic or instantaneous nucleation[75]. However, fractional values of n also exist due to secondary crystallisation, e.g. lower n values (< 1) are caused by linear crystal growth[76]. The model was developed based on a few assumptions, one of which is that the growth rate is constant throughout the crystallisation process[63]; but this may not be the case for fat systems in practice due to their multicomponent property. Hence modifications to the Avrami model have been proposed by other researchers[77-79]; nevertheless the Avrami model, though simplistic, has widely and successfully been used to characterise the *overall* kinetics of fat crystallisation.[62]

Fisher-Turnbull (F-T) correlation

This is used in estimating the activation energy barrier required for the formation of stable nuclei by exploring the relationship between the degree of supercooling and the induction time needed for the formation of the nuclei[80]. This model which was originated by Becker[81] for condensed systems (liquid-solid or solid-solid transformations) links nucleation rate with the activation free energy required for the formation of a stable nucleus ($\boldsymbol{\Delta G_c}$) and the diffusion energy for phase change. $\boldsymbol{\Delta G_c}$ was estimated in the equations below:

$$\frac{1}{J_n} = \tau = \frac{h}{Nk_bT}\exp\left(\frac{-\Delta G_c}{k_bT}\right)\exp\left(\frac{-\Delta G_d}{k_bT}\right)$$
$$-\Delta G_c = \frac{16}{3}\frac{\pi\sigma^3 T_m^2}{(\Delta H \Delta T)^2} \qquad (2.16)$$

$$T\tau = \frac{h}{Nk_b}\exp\left(\frac{16}{3k_b}\frac{\pi\sigma^3 {T_m}^2}{(\Delta H)^2}\frac{1}{T(\Delta T)^2}\right)\exp\left(\frac{-\Delta G_d}{k_bT}\right) \qquad (2.17)$$

$$\Delta G_c = \frac{s \times N_A k_b}{(\Delta T)^2} \qquad (2.18)$$

Where h and k_b are the Planck (6.626×10^{-34} Js) and the Boltzmann (1.381×10^{-23} JK^{-1}) constants respectively; N and N_A are the Avogadro's number and constant (6.022×10^{23} and 6.022×10^{23} mol^{-1} respectively); ΔH is the enthalpy of fusion ($Jmol^{-1}$); T_m the melting point of the palm oil (K); ΔT the degree of supercooling ($T_m - T$) with T being the crystallisation temperature; *s* the slope of the plot of ln ($T\tau$) against $1/T (\Delta T)^2$ with the unit of K^3; ΔG_d the activation energy for molecular diffusion. Using the activation energy (ΔG_c) from this model, the nucleation rate constant (k_n) can be estimated based on the Arrhenius-type equation[82] shown below, where *R* is the molecular gas constant (8.314 $Jmol^{-1}K^{-1}$):

$$k_n = A\exp\left(-\Delta G_c \big/ RT\right) \tag{2.19}$$

If the rate of solid crystals formation (*dx/dt*) is an indication of the crystallisation rate (*J*), then the rate equation is given as:

$$J = \frac{dx}{dt} = A\exp\left(-\Delta G_c \big/ RT\right) f(x) = k_n f(x) \tag{2.20}$$

Assume $$f(x) = (1-x)^n \tag{2.21}$$

Where *f(x)* is referred as a function dependent on the kinetic model of the crystallisation process[83]. If homogeneous nucleation is assumed, the f(x) is taken as *(1 – x)n* where *n* is the nucleation order[82].

Similar to the Avrami approach, there are a few assumptions for the F-T model, e.g. induction time is a direct indication of nucleation event at a macroscopic level[84, 85]. This assumption is not unreasonable due to the negligibility of some of the inherent steps[18]. The activation energy would allow the nucleation rate constant at isothermal conditions to be determined. Although this method was originally designed for pure systems which is not the case for fat systems, it has widely and successfully been used to characterise the *nucleation* kinetics of fat crystallisation [86].

Classic Nyvlt model:

Since fractionation of fat is effectively a cooling crystallisation process, the *classical Nývlt nucleation theory* is also applicable where the nucleation rate is a function of supersaturation (ΔC) and the rate of supersaturation generation is a function of cooling rate.

$$J_n = k_n(\Delta C_{\max})^n \tag{2.22}$$

Where k_n is the nucleation rate constant on a number basis, and n the nucleation order. The unit of J_n is the number of crystals generated per volume and per time. For cooling crystallization, the rate of supersaturation generation is a function of the cooling rate (β):

$$J_n = \beta\left(\frac{dC_{sat}}{dT}\right) \tag{2.23}$$

Where dC_{sat}/dT is the slope of the solubility curve for a given saturation temperature. For the palm oil used in this work, the solubility curve of stearin/olein as a function of temperature (T in ^oC) is given by $C_{sat} = \mathbf{1\times10^{-6}e^{0.2695T}}$ (C in g/g_{olein}). At the point of nucleation, the maximum possible supercooling, ΔT_{max} (or metastable zone width), and the corresponding maximum supersaturation, ΔC_{max}, are given by:

$$\Delta C_{\max} = \Delta T_{\max}\left(\frac{dC_{sat}}{dT}\right) \tag{2.24}$$

Combining eq. (3.5) and (3.6) into eqtn (3.4) results in:

$$\beta\frac{dC_{sat}}{dT} = k_n\left(\frac{dC_{sat}}{dT}\right)^n(\Delta T_{\max})^n$$
$$\beta = k_n\left(\frac{dC_{sat}}{dT}\right)^{n-1}(\Delta T_{\max})^n \tag{2.25}$$

The Nyvlt model effectively relates the effect of cooling rate (β) with the metastable zone width (ΔT_{max}) at a particular operating condition as (see Nyvlt[33] and Sangwal[87] for full derivation of this model):

$$\ln \beta = +\ln(k_n) + (n-1)\ln\left(\frac{dC_{sat}}{dT}\right) + n\ln(\Delta T_{\max}) \tag{2.26}$$

2.3 Crystallisation of Palm Oil

2.3.1 Introduction

Palm oil is one of the most common edible oils, which is natural rich in triglycerides also known as triacylglycerol (TAG) – these are made up of three fatty acid (FA) molecules bound to a 3-carbon glycerol molecule, a typical example is shown in **Fig 2.6** It is the largest produced edible oil globally (38% out of 4 major ones) with Malaysia (36%) and Indonesia (51%) being the major producers; it is also the largest imported oil in Europe (73.4%), UK taking up 34% of the total European consumption in 2007[88].

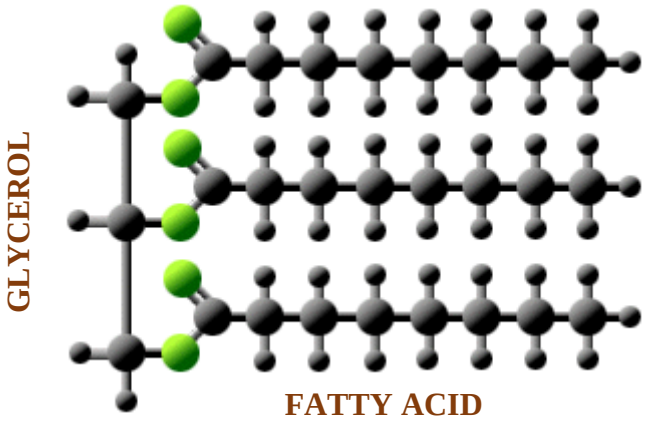

Fig 2.6: Typical triglyceride structure showing the bond between glycerol and fatty acid[89]

Palm oil consists of a wide range of TAG hence is considered as one of the most flexible vegetable oils; however, its composition can be categorised into three broad fractions based on their physical state at different temperatures[40]; the structural differences between them are based on their fatty acid chain length (long or short) and the type of bonds (saturated or unsaturated).

- **Olein**: This fraction is liquid at room temperature (i.e. has relatively low melting points); high in unsaturated fatty acids; called *oils* hence used as frying, cooking and salad oil
- **Mid-fraction**: This fraction melts sharply at about body temperature; high in di-saturated fatty acids hence used in the production of confectionary fats like chocolates. The main solid triglycerides that make up this fraction are referred to as Palmitate-Oleate-Palmitate (POP)
- **Stearin**: These are solid at room temperature (i.e. has relatively high melting points); high in saturated fatty acids; called *fats* hence used in the production of margarines and

shortenings. The triglycerides that make up this fraction are referred to as Palmitate-Palmitate –Palmitate (PPP) or simply put, *tripalmitin* – see **Fig 2.7**.

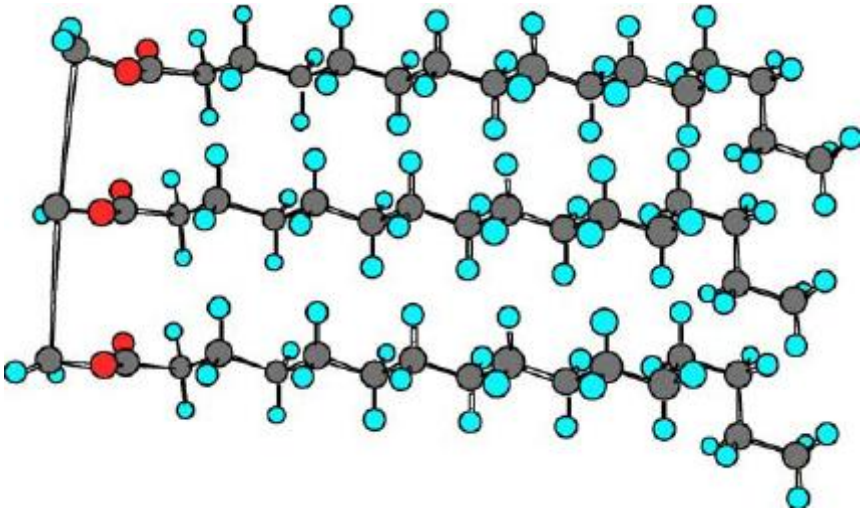

Fig 2.7: Sample structure of tripalmitin, a saturated triglyceride[90]

The presence of long-chain fatty acid is responsible for the high melting point (saturated) while the presence of double bonds in the fatty acid chain causes a drop in the melting point (unsaturation). As a short form, they are often represented by the number of carbons present on the FA chain and the type of bonds, e.g.

- C16:0 = palmitic acid (P) – depicting a 16-carbon length with 0 double bonds
- C18:0 = stearic acid (S) – depicting a 18-carbon length with 0 double bonds
- C18:1 = oleic acid (O) – depicting a 18-carbon length with 1 double bond
- C18:2 = linoleic acid (L) – depicting a 18-carbon length with 2 double bonds

The combination of these FA molecules bound to the glycerol molecules determines how saturated the TAG is, thus its melting point. For instance a TAG made consisting of PPP (tri-saturated) would have a higher melting point than that of PPO (di-saturated), a combination of POO (mono-saturated) and OOO (unsaturated) would have even lower melting points, in that order. It should however be noted that the actual combination of palm oil to be processed is usually more complicated due to the presence of minor fractions that are sometimes challenging to isolate thereby compromising the product purity.

2.3.2 Processing

Palm oil is gaining increased attention as it is made up of a wide range of fractions thereby making it a source for a wide range of applications from cooking oil to confectionaries and bakeries[7]. In view of this, separation of the fractions is an essential process and the conventional process by which this separation is carried out is ***Fractionation*** and this process steps are summarised below[91]:

- Complete melting (with or without addition of organic solvent)
- Controlled cooling to induce supersaturation hence nucleation
- Holding at low temperature for crystal growth and agglomeration
- Physical separation (mostly by filtration) of the phases (liquid and solid)

The process is primarily driven by temperature difference and dependent on the melting points of these fractions; its efficiency is therefore determined based on the phase behaviour of the liquid-solid mixtures - and this involves determination of the crystallisation temperatures for different mixture concentrations.

Fractionation is considered as a natural spontaneous phenomenon[92]; historically, during transportation of large volume of crude palm oil across the oceans (in ships), sediment of small solid crystals was often observed at the bottom of the barrels containing the oil; this process commonly referred to as *winterisation* which was said to be the natural occurrence of fractionation, with the ocean waves providing the required agitation[93]. The phase separation is therefore dependent on gravitational force to facilitate a settling effect. However, the inadequate control of the process results in poor yield and low product quality. Because of the wide spectrum of the palm oil compositions, each having different thermo-physical properties, the separation process is often carried in multi-stages and a typical example is shown below (**Fig 2.8**). The further processing of the palm olein is to increase its added value, while to have the highest yield. It can therefore be inferred that the holistic viability of the fractionation process is a largely dependent of the quality of the palm olein product[94].

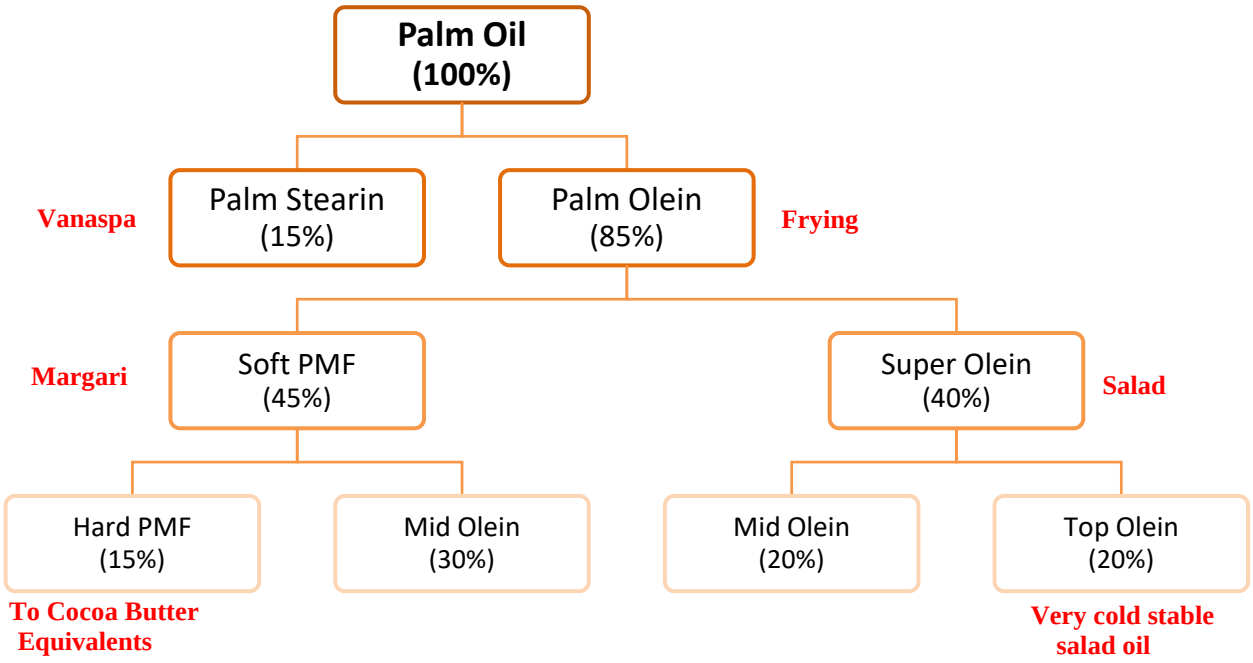

Fig 2.8: Multi-stage fractionation of palm oil, indicating fractions and yields

There are two major types of the fractionation process adopted in the industry:

2.3.3 Solvent Method

This involves the use of organic solvents to allow the high melting fractions to crystallise in a low viscosity medium; the crystallisation process is designed based on the solubility of these fractions in the chosen solvent. The choice of solvent used is dependent on properties such as polarity, flammability, toxicity, and energy requirement for recovery[95]. Three organic solvents have been reported in industries including acetone (Loders Croklaan, UK), hexane (Aarhus, Denmark) and 2-*nitro*propane (Glidden Durkee, USA). The properties of products obtained are different for each solvent due to the solubility parameters and other solution properties. Therefore the compatibility between the solvent and the target TAG fraction is necessary in the selection process; for instance hexane is preferred when olein is the target fraction while acetone for mid-fraction[91]. Some of the benefits of using the approach include:

- *Viscosity*: Since palm oil has high viscosity at low temperatures, the addition of solvents (which are typically low in viscosity) reduces the viscosity drastically thereby enhancing mass and heat transfer that speeds up the crystallisation process[96]
- A higher yield of purer product is obtained due to reduced solid concentration. This is also as a result of the low viscosity as highlighted above; filtration rate is known to be inversely

proportional to viscosity hence low viscosity favours high filtration rate thereby increasing product recovery[97]

However, limitations have also been reported for this method, some of which include entrainment due to higher liquid to solid ratio, higher production cost, increased risk due to the use of volatile/explosive substances, higher energy consumption due to solvent recovery and additional product purification. This is often only method considered for the production of high-value products where the added value offsets the production cost incurred.

2.3.4 Dry Method

This is essentially the crystallisation from melt (CfM) discussed earlier in the thesis. It is designed based on the different melting points of the constituent TAG in the oil; it is referred to as a thermo-mechanical process where high-melting fractions (HMF) are separated from low-melting fractions (LMF) by partial crystallisation thereafter by filtration[98]. The product morphology (shape and size distribution) which is a major determining factor of the product ***purity*** and ***yield*** is dependent on the cooling and mixing conditions[99, 100]. The process is considered[94] as:

- Simple – since it only involves a cooling operation in a controlled manner followed by a physical phase separation
- Safe – as there is no added chemical/solvents into the system
- Sustainable – it doesn't require extreme processing conditions and it's a fully reversible process.

Being a laborious, unpredictable and tedious process are some of the weaknesses reported for this method[92]. However, the attractive features highlighted above have made it a promising process, for which modifications and extensive research are being developed such that with expanded scientific understanding of the process and innovative technical developments, the process know-how and capability can greatly be improved specifically with regards to palm oil fractionation [101].

A comparison was carried out between solvent and dry method of fractionation based on the best possible operations for both methods, and the following results emerged[91]:

Table 2.1: Comparison between dry and solvent fractionation based on best possible operations

Process	Yield (%)	IV (of Stearin)	Entrained oil (% stearin)
Solvent method (acetone)	10 – 11	~8	~5
Dry method	~17	~32	~30

The *best possible operations* considered were:

- *Solvent* – Continuous tube crystalliser
  - Belt filter
  - Washing (with pure solvent)
- *Dry* – Batch crystalliser
  - Membrane filter press
  - 25mm chamber width; 30 bar squeezing pressure

As can be seen from the table above, it is confirmed that the solvent method gave product with a higher purity based on the IV value (to be explained later) and the % entrained oil; however, the dry method seemed to give a high product yield. Considerations for process improvement were also suggested in the study reported above and they are:

- Counter-current crystallisation
- Novel separation process
- New solvent choice

For the purpose of this research work, the focus will be on ***Dry Fractionation***. Historically, processes such as hydrogenation and inter-esterification (chemical or enzymatic) are often adopted (in place of dry fractionation) in the industry to obtain the useful oil/fat products. However, due to the growing pressure (mostly health-related) against partially hydrogenated

fats (often implies the presence of unwanted *trans*-fatty acids) and demand for saturated fat products, dry fractionation has attracted more attention[7].

2.3.5 Polymorphism and Crystal Morphology

The size and shape of the formed crystals have a considerable effect on the physical phase separation that follows the crystallisation process hence they are functions of how the nucleation and crystal growth were controlled. A crystal property that influences the size/shape of a crystal is ***polymorphism***, which is the property of a crystalline material to exhibit more than one physical form but with the same chemical properties and these forms are regarded as *phases*[102] of the material. Among the polymorphs of a particular material, there is one that is thermodynamically stable while the others are metastable, and have the ability to undergo transition into the stable form which can be reversible (enantiotropic) or not (monotropic) depending on the conditions[103]. Polymorphs of the same crystalline material often exhibit different shapes hence are easily differentiated through microscopic view[26]; other adopted technique includes x-ray powder diffraction (XRPD)[104], DSC[105]. A previous study demonstrated the use of online XRPD for real-time monitoring of polymorphism during a batch crystallisation process[106] – this will be useful in capturing *in situ* transformations, thereby enhancing process control.

Palm oil, like most triglycerides, has two reported major polymorphs, α (flat plate), and β (needle), the latter being the most stable having a higher melting point; some intermediate forms have however been documented – β'_1, β'_2, and β'_3 [107]. These polymorphs vary in thermal properties and structural packing (see **Fig 2.9)**; it was reported that the α-polymorph crystallises at rapid cooling condition, but a transition to the β' form occurs during its melting event, and this is inferred from the consecutive exotherm/endothermic peak observed in the thermal profile. X-ray diffraction pattern shows some differences in the short spacings for each polymorph (see **Table 2.2**).

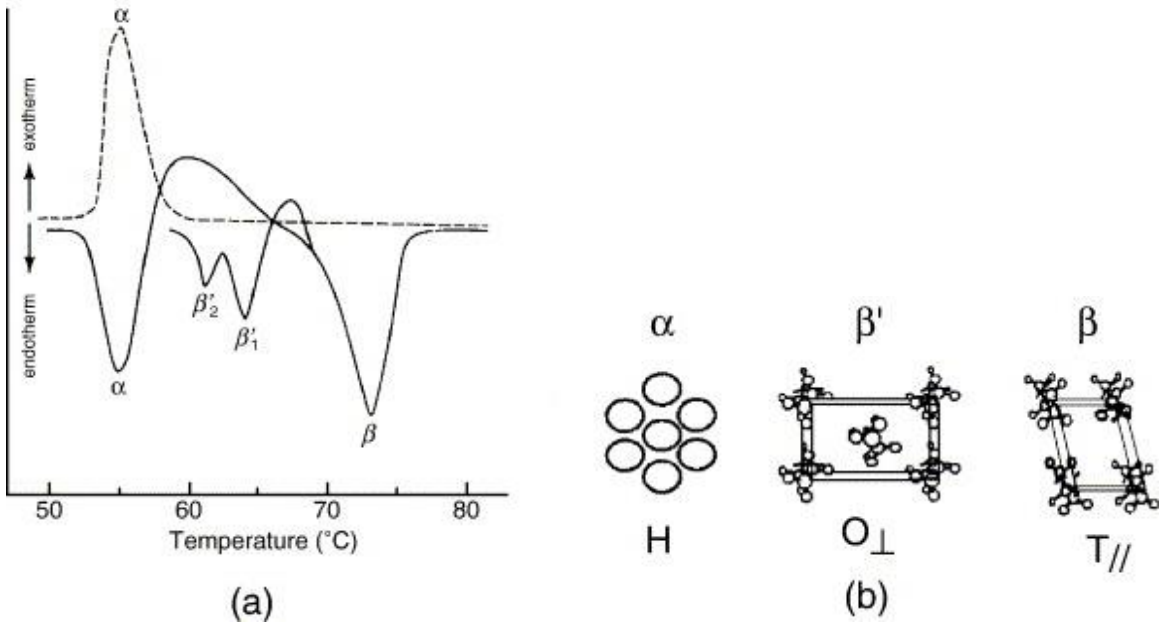

Fig 2.9: DSC thermograms (a) and sub-cell structure (b) of triglyceride polymorphs[108]

Table 2.2: X-ray diffraction short spacings for palm oil polymorphs[80, 104]

Polymorph	Short Spacing (Å)	Sub-cell Structure
α	4.13	Hexagonal (H)
β'	3.83 4.16 4.32	Orthorhombic/perpendicular (O⊥)
β	3.9 4.54	Triclinic/parallel (//)

The obtained form is strongly dependent on the constituent triglyceride and the cooling conditions adopted[80]. However, it is assumed that the operational boundaries of the fractionation process are sufficient to allow the formation of the (β'); hence polymorphism is often regarded as a secondary issue[92]. For size/shape analyses, different techniques have been adopted including polarised light microscope (PLM) fitted with hot-stage system and electron microscope. Images from previous works showed that palm mid-fractions (mainly POP) were generally spherulitic in shape (**Fig 2.10a**) while those of HMFs (mainly PPP) were more plate-like (**Fig 2.10b**)[40, 109].

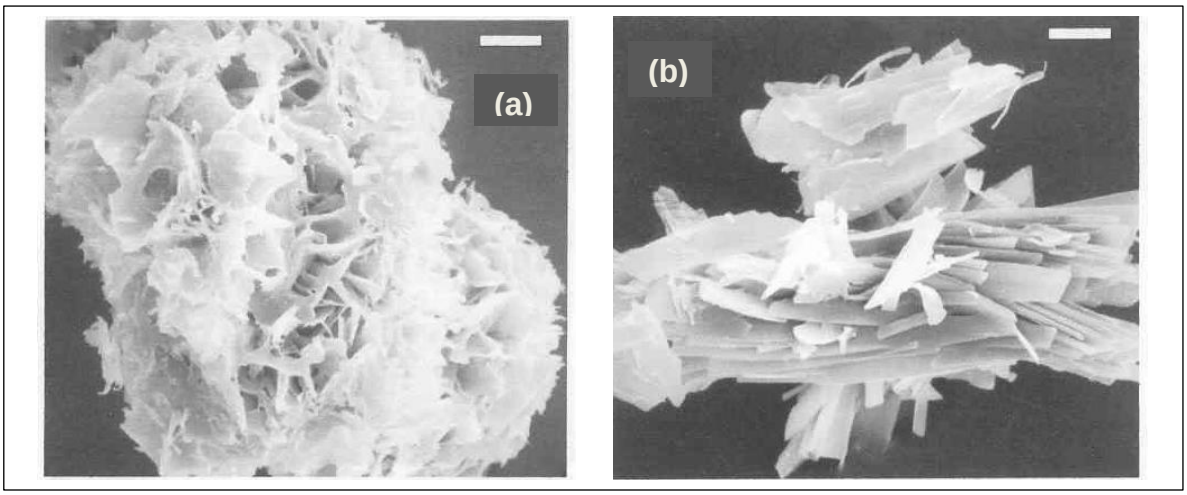

Fig 2.10: Electron micrograph of crystals of palm oil fractions; POP – spherulitic (a) and PPP – plate-like (b)[109]

The crystal sizes are a function of cooling rate and crystallisation temperature (hence slurry concentration)[110]; previous studies have shown that increasing cooling rate reduced the crystal size – an increase of about 6oC/hr can reduce the crystal size by approximately half, crash-cooling (very fast rate) has resulted in amorphous clusters[40, 109]. Previous works have also shown that crystal size increased with crystallisation temperature and this was attributed to aggregation hence crystal growth[111]. In comparing olein and stearin crystals, studies have shown different morphologies at the same temperature; stearin crystals appear smaller than the corresponding olein crystals[7].

Large, stable crystals are preferred for efficient phase separation; too low temperature could result in too high slurry viscosity which would then restrict mass/heat transfer within the system thereby impeding crystal growth; this condition has been reported to favour the formation of the metastable crystal form (∝)[112]. Therefore, cooling process should be designed such that a balanced effect of crystal size and stability is achieved.

2.3.6 Separation Process

It has been established earlier that after the thermo-phase separation created with the oil system due to the cooling process, a physical process is required to separate the formed solid crystals (stearin) from the liquid-solid suspension which is basically a filtration process; the efficiency of this step is crucial as it greatly impacts the result product yield and purity; the stearin quality is determined by the amount of entrained olein present within the solid cake

recovered (***purity***), while the olein quality is simply based on the amount recovered (***yield***) and crystal contamination (due to the shear-resistant property of some stearin crystals). The liquid fraction of the resultant slurry is reportedly distributed into three (3) locations[91]:

- Solid solution with solid fraction
- Un-crystallised fraction in bulk oil
- Un-crystallised fraction entrained in the solid crystals

To reduce the distribution into the third category, filtration process is addressed; therefore, the technology choice is based on minimising, as much as possible, the entrained olein in the solid cake. Three methods have been developed to this effect[91, 113]:

- Centrifugation: LipofracTM or Lanza process with a detergent solution to wet crystals in an aqueous phase or Nozzle centrifuges
- Vacuum filtration: Belt or belt filters
- Pressing: Vertical hydraulic press and filter cloth or automatic membrane press

These three methods have been categorised based on anticipated or desired process output as shown in the table below: (IV = *iodine value*, to be discussed later in the report)

Table 2.3: Some process outputs from different Separation techniques for palm oil fractionation[113]

	Centrifugation	Vacuum Filtration	Membrane Press
IV Palm Oil	52	52	52
IV Palm Olein	56 – 57	56 – 57	56 – 57
IV Palm Stearin	36	40 – 42	30 – 32
% Stearin Yield	-	46	65
% Olein Yield	76	72	82

From the above information, it can be inferred that the membrane press gives the best product quality, and this is why it is becoming the most preferred method for dry fractionation processes[114].

2.4 Technology

Over the years, processes have been designed to operate with pretty much the same approach except with the development of more sophisticated facilities (like implementing automation – see **Fig 2.11**). For instance, it was reported that the current mechanical advancement in tablet compression involving the use of die is still based on the process patented by William Brockedon in 1843 implying that long series of disconnected operations and extensive material handling is required[115]. In the UK today, a large percentage of the chemical productions are done in the *Batch* mode[116], which is basically mixing chemicals in a massive vessel at specified conditions, pouring out the product into another, to be purified, separated, and recovered. As can be imagined, this would involve largely sized equipment to meet up with the required production scale, hence leading to a large footprint which in itself is a challenge due to the increasing awareness (and cost) of environmental pollution.

Particularly, regarding the crystallisation process, many studies have been carried out, looking into the batch mode of operation and inefficiency has been reported on multiple accounts; some of which include long chain of operations, long process times, inconsistent product quality between batches, inadequate process control, scale-up difficulties, huge financial investment, large carbon footprints. Due to the batch-to-batch product variation, the particular batch that does not meet the desired product specifications is often discarded hence increased waste production becomes a concern. In other cases, additional downstream processes are often employed as corrective measures. Examples of such processes include milling, blending, and granulation, which are used to correct the particle size to the desired; these steps could be eliminated if the process was designed to meet product specifications the first time. Such processes are referred to as non-value added costs as they do not enhance the intrinsic quality of the product but simply incur additional operational cost to the production [1, 117, 118].

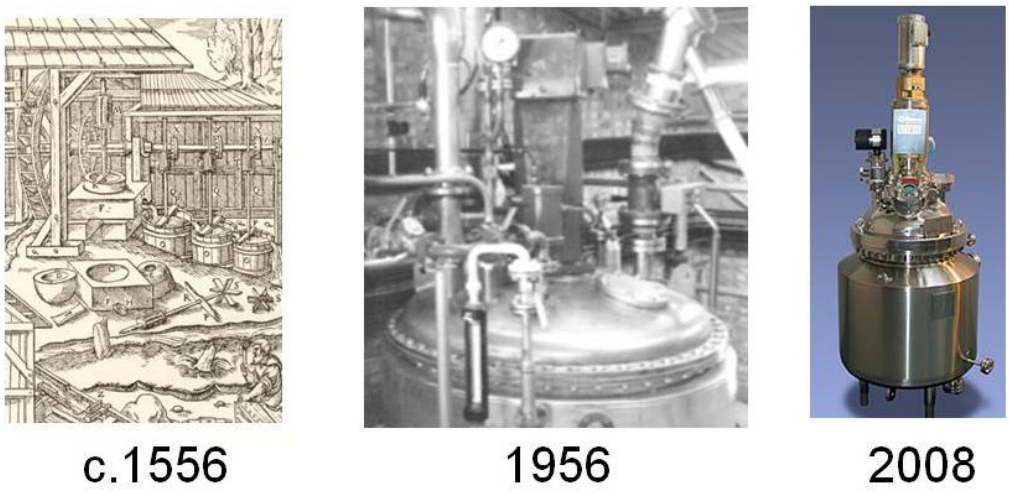

Fig 2.11: Process reactors indicating little technology advancement in 500 years[119]

Regarding palm oil crystallisation (or fractionation), the current plant set-up is multiple crystallisers connected in series, each serving the steps involved in the process – mixing, cooling, filtration, etc. The operation is designed such that every equipment in the set-up (particularly the filters) are in constant use, thereby minimising dead times. The crystallisation stage is said to the time-determining stage in the fractionation process due to its slow rate; it could take from 5 hrs to 3 days depending on the complexity of the triglyceride composition. High capital & production cost and long process times are few of the reported limitations to this multi-stage set-up. Though improvements to the crystallisers and separation technologies have been said to boost the product quality of dry fractionation products, the adoption of *plug flow* reactors have been highlighted as one of the technologies of interest due to its capability of enhance continuous operation, and reduce operation costs[92].

2.4.1 Mixing Mechanism

Mixing is very essential in a crystallisation process, in keeping the solid particles in suspension, avoiding concentration gradient along the crystalliser and enhancing mass & heat transfer as all these properties affect the crystallisation behaviour and eventually the crystal properties; hence a set-up that enhances uniform mixing is desirable.

For a **stirred tank crystalliser**, mixing is done by rotation of the impeller, the speed of which is controlled by an overhead stirrer; the rotations can either produce a *radial* or *axial*

flow patterns depending on the configuration of the impeller (**Fig 2.12**). Mixing in this set-up is considered effective when the fluid particles are evenly circulated through the entire vessel including the remote areas and turbulence is required for this – fluid motion at a velocity that fluctuates in time in all three directions in space, and a state when inertial forces becomes dominant over viscous force; this flow condition is characterised by high Reynolds number (ratio of inertial to viscous forces)[120]. Combination of three mechanisms are involved in a turbulent mixing process – *distribution* (material transportation to all parts of the vessel), *dispersion* (break up of bulk flow into smaller eddies) and *diffusion* (molecular movement within the small eddies formed); all these mechanisms contribute to homogeneity within the system, and the time taken to attain this (mixing time), is a parameter used in assessing the mixing efficiency; mixing time can be measured by tracer injection (concentration response) or addition of small quantity of heated liquid (temperature response). In a stirred tank, mixing time can be estimated experimentally using variables such as vessel and impeller size, fluid viscosity, and stirrer speed, and this is shown in the expression for Reynolds number (Re_i) below (the constant, *1.54* is specific to the Rushton turbine, different impeller types have different values)[121];

$$\mathrm{Re}_i = \frac{S_i D_i^{\,2} \rho}{\mu} \qquad S_i t_m = \frac{1.54V}{D_i^{\,3}} \tag{2.27}$$

Where Re_i = Reynolds number; S_i = impeller speed (s^{-1}); D_i = impeller diameter (m); ρ = fluid density (kg/m^3); μ = fluid viscosity (Pa.s); t_m = mixing time (s); V = tank volume (m^3).

Stirrer speed required to attain homogeneity ($S_i t_m$) increases with reducing Reynolds number (Re_i) but approaches a constant value at high turbulent flow where impeller Reynolds number ≥ 5000. Another parameter used to characterise mixing efficiency is the power required to drive the impeller at a given speed which is then dissipated into the fluid; due to frictional effect, the actual power dissipated is a function of the device efficiency[121]. This parameter is often expressed per unit volume of fluid in the tank hence giving the power density (P_d); it is a function of the tank & stirrer geometry, and fluid properties, this is shown in the expression below[122];

$$P_d = \frac{N_p S_i^{\,3} D_i^{\,5} \rho}{V_L} \tag{2.28}$$

Where N_p = power number; V_L = fluid volume (m^3)

It is can be seen from the expression above that the power consumption shows a significant dependence on impeller diameter (D_i) in that an 10% increase in diameter would increase the power requirement by over 60%. Power number is specific to different impeller types and is inversely proportional to the impeller Reynolds number (Re_i) in the laminar region where viscous force is dominant, but becomes independent when turbulence is reached ($\geq 10^3$) where inertial force is dominant. Therefore, the eq(2.26) above is more applicable for turbulent flow regime, and it has been modified for flow within the laminar regime where k_1 is a constant specific for different impeller types.

$$P_d = \frac{k_1 \mu S_i^{\,2} D_i^{\,3}}{V_L} \tag{2.29}$$

Though turbulence (relating to high impeller speed, eq(2.27) is necessary to achieve effective mixing for homogeneity, it should however be noted that too high speed could lead to the formation of vortex and/or bubble formation. Hence to enhance high enough power density at optimum speed, impellers with relatively higher power number are preferred. Also, vertical baffles are often fitted into stirred tanks to minimise swirling hence adequate allowance for this should be factored in. A major point of concern for mixing in stirred tanks is related to the scale-up capabilities as it involves too many parameters which are dependent on one another; hence though good mixing may easily be achieved in a lab scale set-up, it becomes more challenging with increasing processing scale. One of the contributing factors to this is the drastic reduction in specific surface per unit volume with scale as this poses deleterious effects on heat and mass transfer[43, 123]. Since STC cannot be linearly scaled up (for reasons earlier stated), unwanted occurrences such as concentration gradient are often observed in crystallisation processes (especially in large-scale productions); hence extensive research are being carried out to develop innovative solutions to the scale-up issues relating to stirred tank systems.

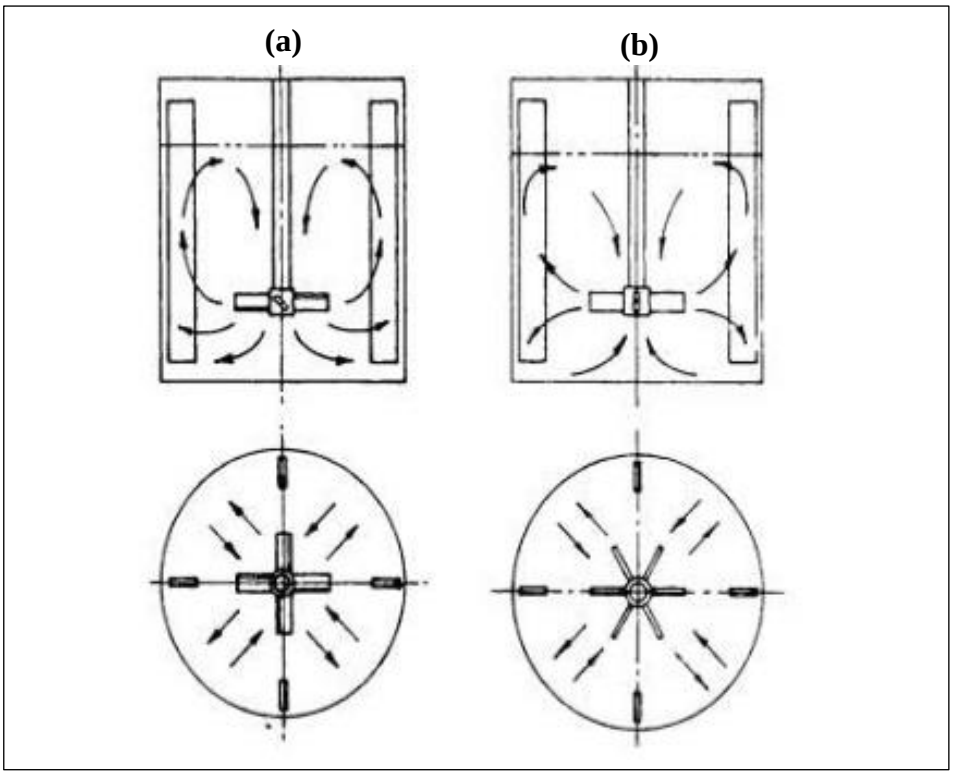

Fig 2.12: Modelled flow patterns in a stirred tank, axial (a) and radial (b)[124]

For an **oscillatory baffled crystalliser**, the interaction between the baffle movement and the oscillatory motion of the fluid in the crystalliser is what brings about the mixing effect; this is independent of the fluid net flow hence it is possible to maintain a good mixing even at low fluid flowrates thereby providing the capability to achieve near plug flow residence time distribution. This technology is considered innovative compared to related conventional systems such as the tubular reactor, where mixing is dependent on fluid velocity, and long tube lengths are required to achieve long residence times[125]. Extensive studies have been carried out regarding oscillatory flow patterns and transport behaviour involving different platforms such as furrowed channels[126], smooth-walled tubes[127], pulsed packed columns[128], but for the purposed of this research work, the focus will be on baffled column subjected to sinusoidal oscillation. The flow pattern (radial motion and axial dispersion) is shown in **Fig 2.13** below; the sharp edges of the baffles provide fully reversing fluid flow which accelerates and decelerates according to the sinusoidal velocity-time function; this leads to the formation of vortex rings that are swept through the centre of the column[129].

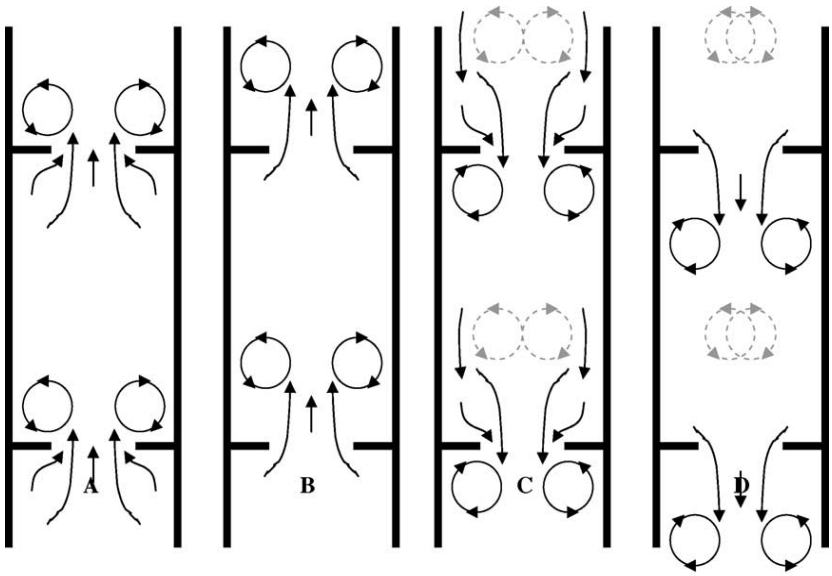

Fig 2.13: Modelled mixing mechanism in an oscillatory baffled column[129]

From previous studies carried out on batch oscillatory baffled reactors, the flow patterns observed were thought to be similar to that of a series of continuous stirred tank (CST) such that each cavity between baffles behaved like a stirred tank; when operated in the continuous mode where net fluid flow is incorporated, the flow patterns becomes closer to a plug flow[130]. The mixing in an OBC is controlled by regulating the amplitude (x_0) and frequency (f) of the oscillatory movement, and it is also a function of the system geometry (such as column diameter (D), baffle spacing, orifice diameter of baffles). Three dimensionless groups can be used to characterise fluid flow in an OBC, and these are listed below;

$$\mathrm{Re}_0 = \frac{2\pi f x_0 \rho D}{\mu} \qquad St = \frac{D}{4\pi x_0} \qquad \mathrm{Re}_n = \frac{\rho u D}{\mu}$$

The net flow Reynolds number (Re_n) is only applicable where fluid is being pumped at a net velocity (u) through the column; the oscillatory Reynolds number (Re_o) describes the mixing intensity while the Strouhal number (St) is the ratio of the column diameter to the stroke length, giving information on the eddy propagation[131]. For design purposes, the optimum oscillatory Reynolds number (Re_o) is estimated with respect to the net flow Re, using a term called velocity ratio (V_R) which is the ratio of Re_o to Re_n; from this, the optimum operating amplitude and frequency can also be estimated. It is preferred that V_R is always > 1 (i.e. $Re_o > Re_n$), to ensure that the oscillation dictates the mixing regime, not the fluid net flow. As is the case for stirred tank systems, turbulence is required here also to ensure good mixing, values of $Re_n > 50$ and

$Re_o > 100$ is considered the requirement to achieve proper mixing[132]. In stirred tank systems, plug flow is attained by using multiple stirred tanks connected in series, and the higher the number of tanks (N), the closer the system is to plug flow (*tank-in-series* model); and it was earlier stated that flow patterns in an OBC is observed to be similar to that a CST; hence N will be equivalent to the number of baffle cavities when the residence time distribution (RTD) gives a plug flow system. A previous study showed how V_R can be used to examine RTD in an OBC using the tank-in-series model; it was reported that optimal RTD was attained at $V_R = 2.5$ and a range of $2 \leq V_R \leq 6$ was the recommended range for close approach to plug flow[133].

It was reported in the study referred to earlier that operating at amplitude greater or equal to a value that gives a minimum value of D/uL (a group developed for the analysis of residence time distribution for plug flow with axial dispersion where D = dispersion coefficient, u = mean net flow velocity, L = length of vessel[134]) enhances good mixing while amplitude that gives the minimum D/uL facilitates plug flow condition[130]. It was also reported that at high amplitudes, eddies generated are large enough to cause strong axial dispersion thereby making radial flow pattern negligible.

For design purposes, power requirement is a parameter used to rank column configurations and also used as a basis of comparison with other mechanisms (in this case, the stirred tank). The power density of an OBC is based on the pressure drop due to the net fluid flow through the baffled tube (standard equation for flow through an orifice) and due to the oscillatory flow (pressure enhancement ratio). Therefore, the overall power dissipated is a sum of the two flow equations; when expressed as a quasi-steady state condition where the power is averaged over time, it gives the below equation[135]:

$$P_d = \frac{2\rho N_b}{3\pi C_D^{\ 2}} \left(x_0 2\pi f\right)^3 \left(\frac{1}{S^2} - 1\right) \qquad S = \frac{d^2}{D^2} \tag{2.30}$$

Where N_b = number of baffles per column length (calculated as 1/baffle spacing); C_D = orifice coefficient (taken as 0.6); S = baffle free area ratio; D and d = column and orifice diameter respectively (m)

2.4.2 Continuous Oscillatory Baffled Crystalliser (COBC)

In addition to mixing, another key challenge in crystallisation processes is the ability to control the quality of product obtained; hence a major motivation in adopting a continuous process is the ability to control both mixing and heat transfer simultaneously; ensure consistent fluid mechanical conditions for reaching a steady state, which is when the properties of the process and product remain unchanged with time thereby ensuring consistency in the product quality, and in shorter time. In a crystallisation process, some of the properties that indicate steady state include solute concentration (i.e. supersaturation), size distribution and crystal yield. It was estimated that a typical crystallisation process attains steady state after about 7 – 10 residences time in a mixed-suspension mixed-product removal (MSMPR) set-up [28].

To address these issues, a plug flow situation where all the components within the system are undergoing same condition at the same time is often desired; this is typically accomplished with the use of a continuous stirred stank reactors (CTSR) which is basically a series of stirred tanks of same size connected either in series or parallel. Another is the use of tubular reactors operating under turbulent flow conditions. These two methodologies are associated with high capital investments and deleterious process conditions.

In view of this, the COBC is a typical example of the innovative technology developed to highlight the benefits of continuous processing as it concerns product quality and cost of production. It is a tubular system with series of inserted (or inbuilt) orifice baffles positioned at regular intervals (**Fig 2.14**); oscillatory motion of either the baffles or the fluid (depending on the set-up) is used to stimulate a uniform flow conditions through interactions between the fluid flow and the baffles. This movement is independent of the net fluid flow through the column; hence it is possible to operate at a low flowrate (i.e. longer residence time) while still maintaining uniform mixing through oscillation. This property enhanced by its unique configuration is what makes the COBC an attractive technology compared to its counterparts – CSTRs and tubular reactors – especially in the pharmaceutical and food industries where efficient production of consistent product quality is always a desired outcome.

Studies have been carried out to examine the capability of this technology in providing solutions to the pressing challenges with conventional batch processing. Results (which were

later validated) were obtained using a jacketed OBC – this is the batch-based set-up but with the same mechanism as the COBC; a comparison with the conventional stirred tank was made and the following was reported[1]:

- 20% reduction in capital cost – for a new build
- 33% reduction in operating (labour) cost
- Unit operation reduction (milling eliminated) – 50% reduction in capital cost
- Much shorter process time – 12mins vs. 9.67hrs
- 10% reduction in solvent consumption
- Higher productivity – to meet demand driven by *lean* production
- Better process control and reduced space usage
- Efficiency of downstream processes (filtration) is not compromised

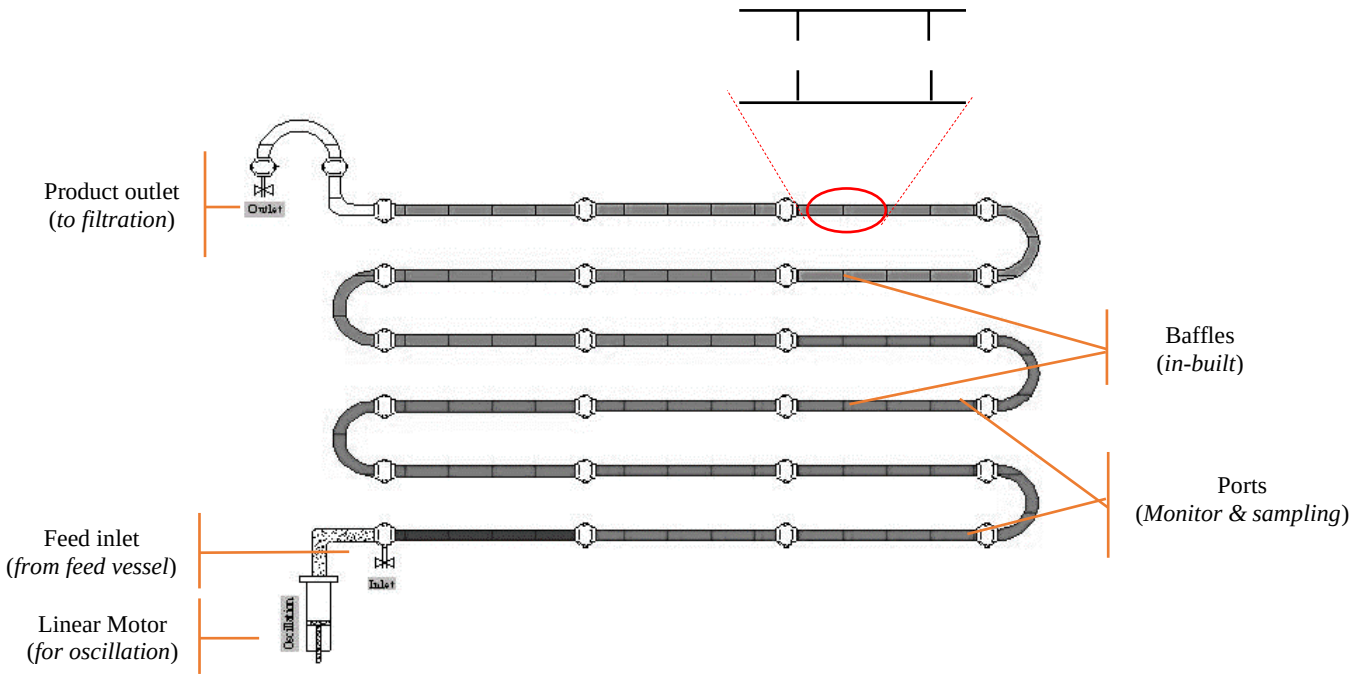

Fig 2.14: Schematic showing a typical horizontal configuration of a COBC

Due to the restricted cross-sectional area, real-time process monitoring, and control is often a challenge in the operation of crystallisers; hence process analytical techniques (PAT) are continuously being developed and modified to address these challenges. A review carried out by Nagy *et al* outlined the application of modelling and statistical approaches to crystallisation process monitoring and control[136]; areas where significant advancements have been made include particle imaging, turbidity (solids concentration), FBRM (particle size distribution),

PVM (particle imaging) and FTIR (solute concentration). Some of these will be used in this thesis study.

2.5 Material and Process Analytical Techniques (PAT)

The desired objective of a fractionation process is to efficiently isolate as much of the unsaturated TAGs as possible in the liquid phase (olein) leaving the solid phase consisting mainly of saturated TAGs (Stearin).

Having highlighted the complexity associated with the (dry) fractionation process and the palm oil system itself, it is imperative that adequate analytical tools are available to enhance appropriate monitor and control for process and product optimisation. An overview of some of these analyses tools is shown below in **Table 2.4**. A knowledge of some properties/issues is essential in designing a viable process, some of these are explained below.

Table 2.4: Some essential analyses required for the robust design of a palm oil fractionation process

Analysis	Information	Method
Fatty acid (FAC)	Compositional analysis	Gas chromatography (GC)
Triglyceride (TAG)		High performance liquid chromatography (HPLC)
*Melting profile	Thermal analysis	Differential scanning calorimetry (DSC)
Iodine value (IV)	Measure of saturation	Titration/IR spectroscopy
Solid fat content (SFC)	Purity and yield	Nuclear magnetic resonance spectrometry (NMR) Differential scanning calorimetry (DSC)
Crystal morphology	Shape, size and polymorphism	Polarised light microscope (PLM) Malvern Mastersizer

2.5.1 Compositional Analysis - Chromatography

Palm oil (RBD) is a large and complex material, and its exact composition varies from one batch to another, based on the source and the preparatory processing it had gone through. For this reason, information on the triglyceride (TAG) and fatty acid (FA) composition of the particular system to be fractionated and its products is necessary for process design. The

technique used to determine the FA composition is by conversion them to their corresponding methyl esters using direct methylation with sodium methoxide and methanol[137]. The formed methyl esters are then analysed in a gas-liquid chromatograph (GLC); *peak retention times* are used to identify the FAs while their concentrations are determined based on the percentage area under the peaks. Depending on the temperature program used for the analysis, the retention time could either increase or decrease[138] with increasing number of double bonds (double bond ≡ unsaturation), and the result obtained is reported based on the carbon number (CN) of the constituent fatty acids; sample results are shown in **Fig 2.15** below. In addition, the TAG composition can be analysed with a high performance liquid chromatograph (HPLC) which uses similar technique as the GLC but with different reagents and accessories[139]; it separates the constituent triglycerides with the elution sequence based on the equivalent carbon number (ECN) and number of C = C double bonds – the triglycerides with the lowest ECN and highest number of double bonds are eluted first[140]. Alkyl bonded-phase column and non-aqueous mobile phase are often used in chromatography analysis of triglycerides; the latter is the due to lipophilicity of TAGs eliminating water-based solvents as options; acetone, acetonitrile, tetrahydrofuran, and methylene chloride are some of the considered options for mobile phases[141]. The particle size of the column packing, column length, mobile phase composition, injection volume, analysis time & temperature are some of the important considerations in liquid chromatography. For palm oil triglycerides, mobile phase of acetone/acetonitrile (62.5:37.5 v/v%) at 50 °C were reported to give the best separation results[142].

These compositional analyses are carried out using standard procedures such as PORIM's test[143] and AOCS official method Ce 1-62[144].

TABLE 2
Glyceride Composition of CPO, RBD Palm Oil, RBD Palm Olein, RBD Palm Stearin, and Superolein

	Glyceride composition (%)				
Fatty acid	CPO[a]	RBD palm oil	RBD olein	RBD stearin	superolein
Diglyceride	6.32	5.20	5.55	5.15	6.24
Triglyceride	93.60	94.80	94.45	94.85	93.76
Triunsaturated					
OOO	3.90	4.40	4.61	2.14	5.25
OOL	1.22	0.58	0.66	1.81	0.77
Total	5.12	4.98	5.27	3.95	6.02
Monsaturated					
PLO	10.02	9.68	10.63	4.53	12.56
POO	21.39	23.26	25.60	9.40	29.13
OOS	2.78	2.24	2.58	2.47	3.17
Total	34.1	35.18	38.81	16.40	44.86
Disaturated					
MPL	3.03	2.20	2.52	2.22	2.99
PPL	9.37	9.23	9.61	7.18	10.14
PPO	27.39	29.62	29.64	23.36	22.46
POS	5.29	4.90	5.11	3.85	3.97
SOS	1.36	—	0.68	—	0.51
Total	46.43	45.95	47.56	36.61	40.07
Trisaturated					
MMM	0.76	0.42	0.46	0.93	0.54
MMP	2.38	1.70	1.85	2.05	2.27
PPP	4.81	5.51	0.50	27.16	—
PPS	—	1.06	—	5.06	—
Total	7.95	8.69	2.81	35.20	2.81
Unknown	—	—	—	2.69	—

[a]See Table 1 for abbreviations. Retention time of unknown peak lies between PPL and OOO.

Fig 2.15: A sample of glyceride composition of RBD Palm oil and its fractions determined by HPLC analysis [107]

Table 1.
Fatty acid composition of RBD palm oil, and olein and stearin fractions at different crystallization temperatures

Sample	Fatty acid composition (%)								
	12:0	14:0	16:0	16:1	18:0	18:1	18:2	18:3	20:0
RBDPO	0.3	1.1	44.2	0.1	4.0	40.4	9.8	0.3	–
St18 (°C)	0.5	1.4	51.0	0.2	30.8	3.7	7.4	0.3	4.7
St15 (°C)	0.2	1.2	54.3	0.2	32.0	4.5	7.6	0.2	6.5
St13 (°C)	0.3	1.3	54.4	0.1	32.3	3.7	7.5	0.3	–
St11 (°C)	0.2	1.1	50.0	0.1	35.3	4.5	7.9	0.4	7.5
St9 (°C)	0.2	1.1	48.9	0.2	36.0	4.6	8.2	0.4	0.4
Ol18 (°C)	0.4	1.0	37.9	0.1	3.7	44.0	11.1	0.3	0.7
Ol15 (°C)	0.4	1.0	37.0	0.1	3.6	44.5	11.4	0.4	0.7
Ol13 (°C)	0.4	1.0	36.5	0.1	3.4	45.4	12.3	0.3	0.4
Ol11 (°C)	0.4	1.1	34.4	0.1	3.3	45.3	12.2	0.1	1.0
Ol9 (°C)	0.4	1.1	34.4	0.1	3.2	46.1	12.9	0.7	0.3

All the readings were based on means of three measurements (RBDPO, refined bleached and deodorized palm oil; St, stearin fraction; Ol, olein fraction).

Fig 2.16: A sample fatty acid composition of palm oil and its products obtained from GLC analysis [145]

Fig 2.15 shows that palm olein has more di-saturated than tri-saturated FAs while the palm stearin has more tri-saturated than monosaturated FAs. It can also be seen from **Fig 2.16** that with decreasing crystallisation temperature (18°C → 9ºC), the olein fraction became more unsaturated as shown by increasing percentages of C18:1 (44.0% → 46.1%) while the stearin fraction became more saturated as shown by increasing percentage of C18:0 (30.8%→36.0%). This confirms that low operating temperatures favour high solid (saturated fat) content which could then imply higher stearin yield; however issues like high slurry viscosity could become a point of concern. All these inferences demonstrate to the importance of compositional analysis on process/product design.

Minor components

Besides the TAGs that make up the bulk of palm oil fractions, palm oil may also contain some diglycerides (DAGs, **Fig 2.17**); they contribute to the impurities of the end products (often end up in the olein fraction), and also affect (negatively) the crystallisation process - reduced crystal growth rate and increased process time. The presence of DAGs in palm oil reduces its melting point which then causes a reduction in the solid fat content; however these effects were not generic as opposite observations were made for some other oil types. It was then concluded that the eventual effect of DAGs on the crystallisation process and the products is greatly dependent on the type (and amount) of DAG present in the system in use[146, 147]. However, they have been reported to have better metabolic characteristics than TAGs that are beneficial in the prevention and management of obesity[148] – a metabolic disease resulting from increase in body fat[149]. An *enzymatic decomposition* reaction using filamentous fungus of the Genus Penicillium (Lipase G "Amano" 50) has been reported to be able to decompose DGA into fatty acids and glycerol thereby causing an increase in the TAG concentration[150]; this however nullifies the benefit of having no chemical/solvent in the system for dry fractionation.

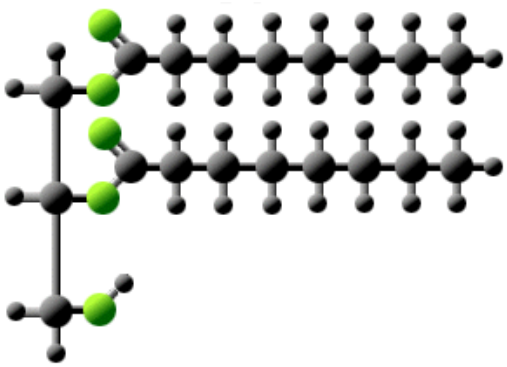

Fig 2.17: A typical structure of a diglycerides showing the bonds between glycerol and fatty acids[151]

2.5.2 Thermal Behaviour - Calorimetry

It has been established that the property on which the operating temperature range for fractionation process is based is the melting points of the different fractions within the system; hence a prior knowledge of the melting profile of the system is useful in designing the cooling process. A *differential Scanning Calorimetry* (DSC) is a thermo-analytical technique used to monitor the phase transitions of a material as a function of temperatures by detecting the associated heat changes[152] i.e. the difference in the heat flow to the sample and a reference (usually an empty aluminium pan comparable to the sample pan). The sample and reference are maintained at almost the same temperature throughout a measurement such that when the sample undergoes a phase transition, more (or less) heat will flow to the sample in order to bring the sample back to the reference temperature. The temperature program records the changes of sample temperatures linearly with time.

This difference in heat flow corresponds to enthalpy change (dH/dt) since pressure is constant; its direction is an indication of the nature of the process involved. In an *endothermic* process (e.g. melting), energy is absorbed by the sample hence more heat flow to the sample is required to maintain the same temperature increase as that of the reference – enthalpy change (dH/dt) is positive; the opposite is the case for an *exothermic* process (e.g. crystallisation) where heat is released by the sample, hence less heat flow to the sample is required to maintain its temperature same as the reference's – dH/dt is negative. The analysis output is a thermogram, a heat flux – temperature (or time) profile, a thermal curve (peak) that can be used to quantify the actual enthalpy required for the given transition by integration. The generic expression used for this calculation is given as $\Delta H = kA$ where ΔH is the enthalpy of the

transition, *A* is the area under the curve, and *k* is the calorimetric constant which is dependent on the instrument[153].

In addition to melting and crystallisation processes, DSC can also be used to detect other events such as amorphous formation, glass-transition, polymorphism, etc. In addition to being useful in characterising phase transitions (temperature and enthalpy), other benefits of this technique are its high sensitivity allowing analysis of a small amount of sample (down to *micro* – scale), and fast measurement rates. The benefit of micro-scale analysis could also be seen as a limitation where larger scale sample representation is desired, so additional analyses such as x-ray scattering and microscopy are recommended as complementary techniques.

A sample thermogram for palm oil is shown below in **Fig 2.18**; the oil sample was crash-cooled to –30°C at 40 °C/min, held for 10 min and then heated to 80°C at 5 °C/min to obtain the melting profile; for the cooling profile, the sample was again cooled to -30°C at 5oC/min. the downward (exothermic) peaks represent temperatures at which the corresponding fractions crystallises; the first sharp peak at about 18°C indicates the crystallisation of high-melting fraction (H_m) while the second broader peak at about 0°C denotes the crystallisation of the low-melting fraction (Lm). Previous works have shown that the exothermic peaks were only dependent of the chemical composition of the oil sample, not the cooling process[154, 155]. Broad peaks suggest a broad distribution of TAGs within the sample. The analysis could also be carried out in the reverse order, i.e. a heating process to analyse the melting profile of the oil sample first, also seen in **Fig 2.18**; the endothermic (upward) peaks are broader and more complex than the cooling thermogram which is again due to the wide distribution of TAGs present in the sample. Sometimes, exothermic peaks could also be present on a melting thermogram, and this is attributed to polymorphic transformation[156, 157].

The actual peak temperatures on the thermograms are of little relevance to the fractionation process; the focus is more on the energy–temperature relationship that results from the observed profiles[94]. Effect of cooling rates on DSC crystallisation profiles was studied by varying the scanning rates used for the analysis; it was observed that the position of the exothermic peaks was dependent on cooling rate while the amount of heat flow (peak height) remained the same for all cooling conditions. It was also observed that the peaks shifted to

lower temperatures and widened with increasing cooling rate[7]; this was attributed to increased crystallisation rate and longer *lag period* required for the formed crystal to stabilise[158].

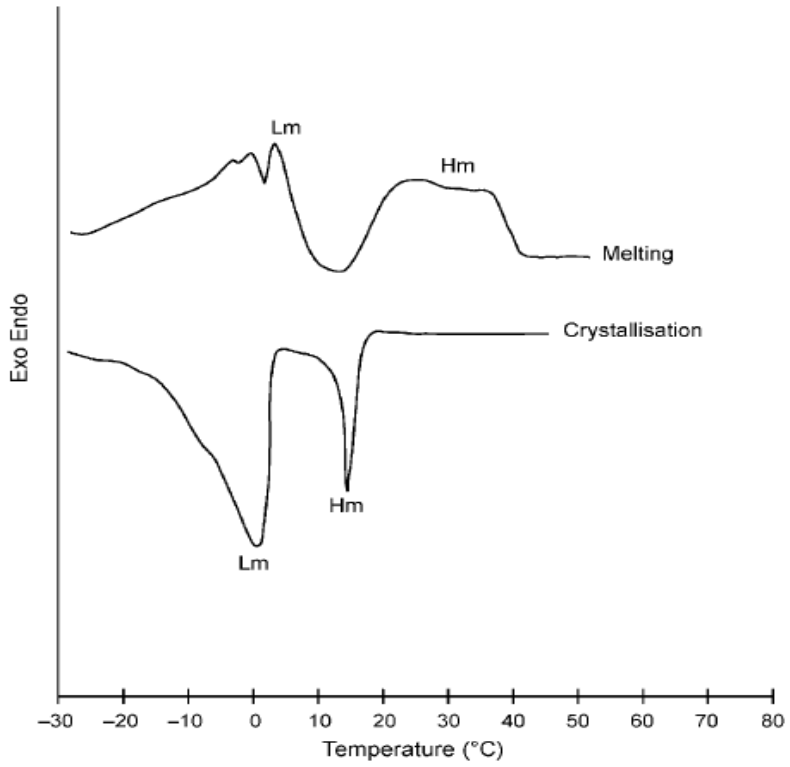

Fig 2.18: DSC melting and cooling thermograms of palm oil between -30°C and 80°C [159]

2.5.3 Iodine Value

Iodine value (IV) is defined as the number of grams (g) of iodine absorbed by a 100g of fatty acids; it is used to represent the measure of unsaturation (presence of C = C double bonds) of edible oil & fats and forms an important parameter used for product quality control[160] in that ***the higher the IV*** *of a fat or oil sample,* ***the more unsaturated it is***. Increasing interest in the health benefits of polyunsaturated fat consumption has driven the development of the analysis of fat unsaturation[161]. Besides its relevance in edible oil processing, IV values have also proven useful in other fields such as;

- Oil quality of plant species[162, 163]
- Insecticides effects on plants[164]
- Quality of biodiesel sourced from vegetable oils[165]

Historically, the experimental methods used for IV analysis are titration-based methods such as Wijs[144], Hanus-Hubl[160], Hofmann-Green[166] and Rosenmund-Kuhnhenn[167]; all of these methods are based on the reaction of halogens with unsaturated fatty acids but vary in the reagents and catalysts involved in the reactions. The most widely used of these methods is the *Wijs* method and has been endorsed by AOCS as a standard method; it uses iodine monochloride (ICl) as its halogen source, which reacts with the fatty acid at the C = C site; the amount of iodine consumed by the halogenation reaction (1) is determined by adding potassium iodide solution to the product mix, which then reacts with the remaining unreacted ICl to form free iodine molecule (2); the iodine molecule is then titrated with standardised solution of sodium thiosulphate (3); the end point of the reaction is detected by a colour change from brown to a colourless solution. See reaction steps below:

(1) 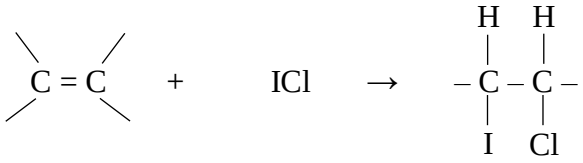

(2) $ICl + KI \rightarrow KCl + I_2$

(3) $I_2 + 2Na_2S_2O_4 \rightarrow 2NaI + Na_2S_2O_4$

However, there are many health & safety concerns associated with it, mainly because it involves the use of highly toxic and environmentally-unfriendly chemicals such as iodine trichloride (ICl_3) which is referred to as *Wijs reagent*; other downsides with this method include:

- Time consuming procedures
- High consumption of costly solvents
- Highly dependent on the skill of the analyst

Consequently, efforts have been made to discourage its continuous use by developing alternative analytical methods and correlations; for instance, a previous work developed a calculation-based method based on the quantitative determination of the methyl esters of the constituent FAs of the oil sample – similar to the empirical method described above. When the

results were compared with that obtained from Wijs method for a number of oil types, a good correlation was observed[168]. Other methods that have been considered involved calibrating instruments such as Fourier Transform Infrared (FTIR) spectroscopy[169], differential scanning calorimetry (DSC)[170], nuclear magnetic resonance (NMR)[171] and etc.

The spectroscopy technique involves the absorption of infrared radiation by the molecules being analysed which causes them to vibrate; vibrations that lead to a change in electric dipole moment are those that cause IR light absorption, and the absorption intensity is proportional to the square of the change in the dipole moment[172]; the results obtained from this technique are absorbance (or a transmittance) spectra, the peak position and height are corresponding to specific bonds and its concentration within the sample respectively.

A number of studies have been done based on using this technique for oil & fats analyses; a study has used the absorbance ratio of *oleifinic* (assigned to 3030 cm-1) and *aliphatic* (assigned to 2857 cm-1) C-H stretching to determine the degree of unsaturation of fats and oils[173]; another study has used pure triglycerides to calibrate an IR spectrometer for IV determination, using peak regions of 3200 – 2600 cm-1 and 1600 – 1000 cm-1, corresponding to the C-H stretching and CH2 scissoring respectively[174].

Analysis with IR spectroscopy is rapid, simple and cost-effective making it a promising and attractive technique[169]. Using the spectral region that corresponds to the presence of double bonds (which depicts unsaturation) as a reference, IR spectroscopy is a useful tool for qualitative and quantitative analysing of palm oil and its fractions; the greater the absorption in this region, the higher the IV value hence the more unsaturated the oil sample.

2.5.4 Solubility

As part of the considerations required for an optimum crystallisation process design, understanding of the temperature-concentration equilibrium relationship is essential, and this information can be obtained from a phase diagram, also referred to as *solubility curve*. As stated earlier, the solution system formed by palm oil melt is such that the high-melting fractions (HMFs) form the *solute* that is dissolved in the low-melting fractions (LMFs) which form the

solvent; this, coupled with its complex compositions, has led to a deviation from an ideal situation for palm oil[175]. Most previous related solubility studies were based on pure TAGs and made-up system compositions; only a few have focused on natural-occurring fat systems, for instance, solubility results using dilatometry technique have been reported for hardened groundnut oil in linseed oil[176]; also the solubility of milk fat in liquid oils using DSC technique has also been reported[177]. Hence, techniques for determining the solubility of fats include thermal methods (e.g. involving the use of DSC as highlighted above); another involves compositional approach[178] and pulsed NMR[175].

An equation has been developed for the determination of the solubility of HMFs in LMFs, with the assumption that they form an ideal solution[179]:

$$\ln x = -\frac{\Delta H_{fus}}{R}\left(\frac{1}{T} - \frac{1}{T_m}\right) \tag{2.31}$$

Where x = solubility of HMF in LMF (mol/mol)
ΔH_{fus} = heat of fusion of HMF (kJ/mol)
T, T_m = experimental and HMF melting temperature (K)
R = gas constant (kJ/mol-K)

This equation is referred to as *Hildebrand* equation and is used to depict ideality by plotting a graph of ln(x) against *1/T*. This equation bears a resemblance to the Van't Hoff equation which was developed to establish the linear relationship between solute concentration (logarithm of mole fraction, *log x*) and the inverse of equilibrium temperature (1/T); Hildebrand's approach was the argument that *log x* against *log T* gives better correlation[180, 181]. However the equation above is based on the linear relationship between *ln* (or *log*) *x* and 1/T so it can be inferred that it takes its root from a combination of these two basic models (Van't Hoff and Hildebrand).

a linear relationship verifies ideal mixing behaviour (enthalpy of mixing is zero, and the volume remains unchanged with mixing[182]); the melting temperature (T_m) can be determined from the *y*-intercept of the graph. This equation has been used in a previous work on lipid systems; solubility (x) was determined using the compositional approach[175]. In conclusion, as there are no generic theoretical correlations, solubility analysis for a multicomponent melt is done experimentally, with little or no literature source for verification.

For this research work, calorimetry and turbidity analyses were considered, more detail is found later in the thesis.

Inter-solubility

Since dry fractionation process involves the absence of other chemicals/solvent, the solution being crystallised is just the palm oil melt composed of mainly triglycerides, i.e. both the *solute* and the *solvent* are TAGs having similar structural properties but differing in thermo-physical properties (such as melting points); this is very different from the *solution* involved in a basic cooling crystallisation where the solute is dissolved in an inert solvent, both varying widely in structural and other properties. This therefore constitutes to a deviation from the solution crystallisation and makes it often challenging to determine its solubility profile (temperature–concentration equilibrium relationship). Due to the wide range of TAGs in palm oil, it is a common occurrence for some of the fractions (especially the HMFs) to have close melting points, and therefore crystallise together as one phase – this is referred to as a *solid solution*, some even crystallise as co-crystals (a unique crystalline structure formed by two or more components which could be ions, atoms, or molecules[183]) when formed as a metastable polymorph[94]. This occurrence is what is referred to *Inter-solubility*. The solid solution formed cannot be separated by a physical filtration process thereby compromising the product quality; it could also alter the crystal structure such that the slurry's viscosity is considerably high enough to compromise the efficiency of the downstream (filtration) process. This constitutes one of the major challenges associated with the fractionation process since its primary aim is to separate the melt into its constituent fractions[92, 94].

Therefore, the cooling process adopted for a CfM must carefully be designed based on a compositional analysis of the melt and hence the triglyceride products of interest, for instance, to ensure that fractions with close melting points selectively crystallise, a slow cooling rate should be considered[92]. It is has been reported that a high (and higher degree of) supercooling increases the probability of inter-solubility[94]; hence an obvious preventive measure would be operating at a low supercooling condition, i.e. higher crystallisation temperature and/or slow cooling rate. This would however be at the expense of long process times; some alternative solutions to counter inter-solubility are discussed below:

- Seeding with PPP– this can facilitate crystallisation to occur within the metastable zone (see **Fig 2.1**) thereby enhancing a better control over nucleation and crystal growth rates. Since the process can then be carried out at a relatively higher temperature, the viscosity of the process fluid would be reduced hence improving the filtration efficiency (i.e. better olein yield and stearin purity). However, a shortcoming of this solution is that the now higher concentration of PPP in the melt would increase the percentage of PPP recovered with the mid-fractions (POP)[184].

2.5.5 Solid Fat Content

Solid fat content (SFC), as the name suggests is the percentage of a fat/oil sample that is in the solid phase at a particular temperature; it's a property that changes consistently with temperature and determines the suitability of the sample for specific applications as it influences some physical properties of the product such as texture, firmness, mouthfeel, etc.[185]. *Pulsed* NMR spectrometry is currently the most common technique used for this analysis[186]; the *direct-method* measurements are based on the ratio of the magnetisation signal from both the solid and liquid phase of the sample. A pre-set heating/cooling/holding program is applied to the sample before the measurements are taken, and obtained results are based on calibration with three measurements (usually 0, 30, and 70%)[175]; selected programs are in accordance to official methods such as IUPAC 2.150[187], PORIM tests[188], MPOB p4.8[189]. The result obtained from this technique can either be reported as a SFC/time or SFC/temperature relationship, and it is closely related to the melting behaviour of the analysed sample.

Previous related studies on palm oil and its fractions have confirmed a higher %SFC and melting temperature for palm stearin compared to the olein fraction; and this was attributed to the higher amount of saturated fat in the stearin fraction[145]. In another work based on isothermal crystallisation process, higher %SFC was observed at lower temperatures due to rapid nucleation rate brought about by a higher degree of supersaturation[7]. SFC can also be used to determine equilibrium conditions of a particular sample; this is taken as the temperature at which %SFC becomes zero; however, NMR measurements are reportedly inaccurate at low %SFC hence interpolations of readings at higher %SFC are employed to determine the temperature at which SFC is zero[190]. Since solubility information can be extracted from the

equilibrium conditions, it was reported that extrapolation of NMR data gave lower solubility values, compared to those obtained from using the compositional approach[175]. Besides the melting behaviour, NMR data can also be used to examine compatibility/miscibility of fat blends through the construction of iso-solid diagrams[191, 192]. Another common technique that is adopted for SFC analysis is calorimetry (i.e. DSC) and this was the adopted method in this research work. Here, the solid-liquid ratio of a fat sample is determined from the melting thermogram by partial integration of the curve[193]. More details regarding this method will be discussed later in the thesis.

2.5.6 Crystal Size Distribution

Besides the crystal morphology, the crystal size distribution (CSD) within the system is also important and should closely be monitored as it has been reported that separation efficiency hence product yield and quality are directly affected by CSD[194]. Various devices have been used to analyse the size distribution of fat crystals, most of which is based on either laser or optical techniques[195]; previous studies on palm oil crystal analysis have reported the use of Malvern master sizer (based on laser light diffraction)[196] for CSD and crystal count, laser particle counter (based on laser light scattering) for crystal size of vegetable shortenings[197], scanning electron microscope (SEM) for form and CSD of PPP crystals[198], etc. Other reported techniques include *p*NMR[199], rheo-optics[200], and optical thermal analysis[201]. However precise the measurements obtained from the analysis are, it is still not a good representation of the actual system if the analysis was not conducted *in situ*; hence for real-time crystal study, online measurement techniques are preferred; a common technique adopted for this purpose is the focused beam reflectance measurement (FBRM) which is based on laser backscattering; it obtains information of crystal count, distribution[202], and also kinetics estimation[28]. It is reported to have the capability of detecting onset nucleation, *in situ* change in dimensions, concentration, and population[203]. Size Analysis with FBRM are reported as chord lengths[204].

Previous studies have shown that total palm oil crystal count increased with reducing process temperature and increasing process time, suggesting rapid nucleation rate and/or attrition of agglomerates[111]; whereas crystal growth was favoured at higher temperature due to less crystal count[205]. Mean chord length was also reported to increase with increasing

crystallisation temperature to an extent after which it began to decrease with temperature increase; this subsequent decreasing at high temperatures was said to be due to the increased breakage/attrition of the crystals while the initial reduced mean size at low temperatures was attributed to the increased nucleation rate of small nuclei[195]. In this same work, crystal melting was also analysed with FBRM, and a simultaneous decrease in fine particles and increase in coarse particles was observed; however, a sudden increase in fine particles was observed within a particular temperature range, and this was attributed to de-agglomeration of the HMFs by melting of the LMFs that supposedly links the agglomerated HMFs[206].

In conclusion, exploiting the physical and chemical properties of palm oil through well-designed cooling profile and separation process, good quality products can be obtained. Though all these techniques provide useful monitoring information for optimum process development, the adoption of multiple tools is however essential in order to verify detections thereby minimising uncertainties.

CHAPTER 3- EXPERIMENTAL WORK

This chapter provides detailed description of the methodologies adopted in the different studies carried out in this research. An overview of the experimental plan designed for this research is therefore shown below:

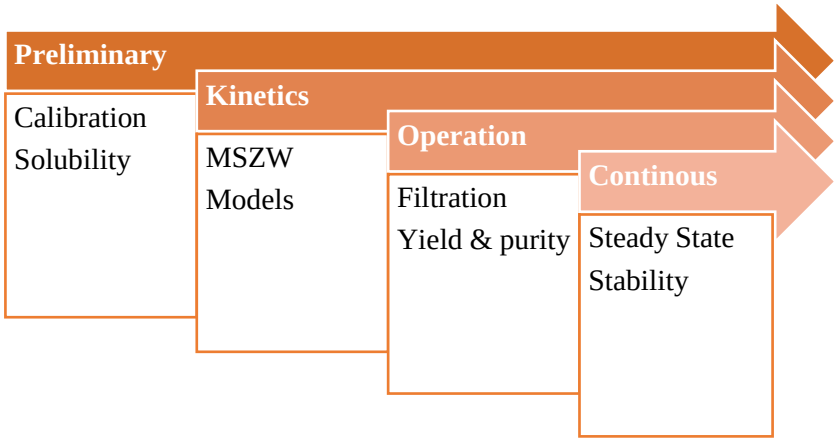

Fig 3.1: An overview of the experimental plan followed during this research

3.1 Initial Characterisation

3.1.1 Composition

The model compound, ***refined, bleached, and deodorised (RBD) palm oil*** used for this research work was sourced from AarhusKarlshamn (AAK) based in Hull, UK. The compositional analysis (fatty acids) provided by the company is shown in **Table 3.1**; from this data, it can be deduced that the saturation/unsaturation ratio of the oil sample is almost 50:50 with palmitic acid (C16:0) constituting most of the saturated fats (44%) and oleic acid (C18:1), the unsaturated fat (38.4%). However, the triglyceride composition analysis of the palm oil was determined by *liquid chromatography* (see **section 2.5.1** for more information regarding this technique). The HPLC system used (HP Agilent 1100 Series) was equipped with vacuum degasser (Model G1379A), a binary pump (Model G1312A), an autosampler (Model G1313A), and a UV (variable wavelength) detector (Model G1314A). The column used was a Nova-Pak C_{18} (3.9 x 150 mm) Waters packed with a particle size of 5 µm. The mobile phase was a mixture of acetone/acetonitrile in the ratio 63.5:36.5 and the flowrate was set at 1 ml/min. The injection volume was 10 µL of 5% (wt/vol i.e. 5g/100ml) oil in acetone. TAG peaks were identified based on the retention times of standards according to the results of Swe *et al*[207] and Haryati *et al*[208]. The percentage peak area was used to quantify the TAG components. The UV

wavelength of the detector was however set to 211 nm which is the characteristic wavelength for triglycerides[209, 210].

Table 3.1: Compositional data of RBD palm oil as received from the supplying company, AarhusKarlshamn (AAK)

Composition	%
Fatty Acids	
C12:0	0.2
C14:0	1.0
C16:0	44.0
C17:0	0.2
C18:0	4.5
C18:1	38.4
C18:2	10.7
C20:0	0.8
C22:0	0.1
Total	**99.9**
Triglycerides	
trisaturated (*SSS*)	50.8
Monounsaturated (*SUS*)	38.4
Polyunsaturated (*SUU*)	10.7
Other	0.1
Total	**100**

3.1.2 Thermal Profile

To further analyse the feed sample, a cooling and melting profile (called *thermograms*) was obtained using a NETZSCH differential scanning calorimeter (model DSC 214 Polyma, NETZSCH, Germany) equipped with an intracooler cooling system operating between a temperature range of -70 to 600°C. Compressed air at a flowrates of 40 mL/min and 20 mL/min were used as the purge and protective gas respectively. 10–15 mg of sample was weighed into an aluminium pan and sealed with a pierced lid; an empty and sealed pan was used as a reference. The system was interfaced with a PC operating under Windows-based Netzsch Proteus© thermal analysis program version 7.0.1 for data acquisition and analysis. The sample was heated to 353K for 5 min, then cooled to 223K at the rate of 10 K/min; it was held at this

temperature for 5 min to allow complete crystallisation. The sample was then heated again to 353K at the rate of 10 K/min to obtain the melting curve; the melting point (T_m) of the palm oil sample was taken as the temperature at the end of the curve, i.e. when melting is completed. Average of two measurements was determined.

3.1.3 Iodine Value

Here, relationship between different blends of olein/stearin system and iodine value was examined. A 785 DMP Titrino (from Metrohm UK Ltd) fitted with a 6.0451.100 Combined Pt electrode, a 6.2104.020 electrode cable, and a 6.3026.220 Exchange Unit was used for the titration experiment; it was interfaced with a PC which operated under Windows-based Metrohm Vesuv DL version 3.0.0.10 software for data acquisition. The method adopted is in accordance to the AOCS official methods.

The titrant used was 0.1M sodium thiosulfate ($Na_2S_2O_3$), the *Wijs* solution used was 0.1M iodine monochloride (ICl) in glacial acetic acid solution. All chemicals were ACS reagent grade, purchased from Sigma Aldrich, UK with purity of 95 – 99.7% and were used without further purification. The titrant was initially standardised with 0.625 g/l potassium iodate (KIO_3) solution; the titre value obtained was then used in subsequent calculations for the IV determination. Also, blank values for the reaction solution (ICl) were determined before each sample was analysed, and these values were also used for subsequent calculations. Detailed information of the titration methods adopted is located in the appendices.

Samples of olein (IV = 54.7 g/100 g Iodine) and stearin (IV = 36.0 g/100 g Iodine) were sourced individually from the supplying company, AAK. The two were blended in different proportions, to make up six blends of different, but known stearin/olein concentrations ranging from 0 to 100 wt% olein. The IV of each blend was then determined with the titration method; the formulas programmed into the titrator for IV determination are shown below:

Titrant standardisation $$Titre = \frac{C00}{C01} \times \frac{1}{EP1}$$

Where: C00 = Weight of KIO_3 (mg); C01 = 3.567 (equivalent weight of iodine); EP1 = Titration endpoint (mL of $Na_2S_2O_3$ solution up to endpoint).

Iodine Value of sample $$IV = [C31 - EP1] \times C01 \times \frac{C30}{C00}$$

Where: C31 = Blank value (mL of titrant); EP1 = Titration endpoint (mL of titrant); C01 = 1.269 (equivalent weight of iodine); C30 = Titre value (from titrant standardisation); C00 = Oil sample weight (g).

In addition, the iodine value of the feed palm oil was also determined using the titration method and the resultant *conc – IV* curve obtained from the above was then used to estimate the olein (and stearin) fraction of the palm oil feed.

3.1.4 Solubility

Due to the complexity and wide variations of the compositions of palm oil, it is essential to establish a concentration– temperature relationship of the fractions (broadly classified into olein and stearin). A solubility is relevant in providing useful information for the design of the crystallisation process with respect to supercooling. In this study, multiple techniques were considered and the resulting curves were compared with that reported in a previous study involving palm oil of similar compositions. The curve that was relatively most similar to the reported one was taken forward and used for further studies. The techniques considered were calorimetry (DSC) and turbidimetry.

Calorimetry

The Hildebrand equation was used as explained in ***section 2.5.4***. The thermal profile of the palm oil sample was analysed with DSC system to obtain the endothermic peak for the melting process (see ***section 3.1.2*** for detailed description of the thermal analysis). The melting temperature (T_m in K) of the stearin fraction and the corresponding enthalpy of fusion (ΔH_{fus} in J/mol) were used to determine the solubility (mol/mol) at different temperatures. The latter corresponded to the area under the melting curve which was calculated by integration on the interface software.

Turbidimetry

Here, blends of known olein/stearin concentrations were made up (same blends used for the iodine value determination) and a cooling/heating process was carried out consecutively on each blend at a constant cooling and heating rate of 0.5 ^{o}C/min from temperatures 60°C to 20^{o}C. The process was carried out in a 250 mL jacketed beaker, which was connected to a water bath (see details below in section **3.2.1**) to control the jacket temperature; the experiment was stirred using a magnetic stirrer bar. Turbidity and temperature probes (HEL Group, UK) interfaced with a Windows PC were used to determine the *cloud* and *clear point* for each blend. The *clear point* of each blend was taken as the apparent solubility temperature of the stearin concentration in the blend.

3.2 Kinetics Study

This study is in the following two parts.

3.2.1 Metastable Zone Width

The objective here is to examine the effect of cooling rate and mixing intensity on the nucleation properties of palm oil crystallisation with respect to the metastable zone width (MSZW) on a batch platform. Comparisons were also made between a stirred tank (STC) and an oscillatory baffled (OBC) crystallisers.

The STC set-up (manufactured by Scott Glass, UK) consists of a 500 mL jacketed round-bottom glass vessel of 100 mm internal diameter (ID), and using a stainless steel O-ring clamp, a 5-port glass lid was fitted on top of the vessel; the ports include a centre port which has an ID of 2.5 cm through which the stirrer shaft was fitted; the other ports are access for tools such as thermocouples, and other analytical probes. The stirrer shaft used for this set-up was a PTFE anchor stirrer with shaft and rotor diameters of 6 mm and 75 mm respectively; this was positioned into the vessel through the lid with a PTFE universal stirrer guide. The whole set-up was mounted on a 65 cm long metal clamp stand, and held in place with a nickel-plated chain clamp; a heavy-duty metal bar was an additional support in order to offset the downward weight of the overhead stirrer.

The overhead stirrer used to control the stirring speed was a Eurostar DS2 digital device (IKA-Werke®, Germany) fitted with a control dial of speed between 50 – 2000 rpm; this was connected with the stirrer shaft with a chuck key, and clamped in place above the vessel. In order to minimise vortex formation especially at high stirring speed, a four-leg stainless steel baffle ring, 9.5 mm wide and 165 mm long, was fitted into the vessel such that they were mounted against the wall; these baffles posed a restriction hence the stirrer shaft was positioned to allow a clearance of just about 10 mm from the bottom of the vessel. The schematic of the set-up is shown in **Fig 3.2** below.

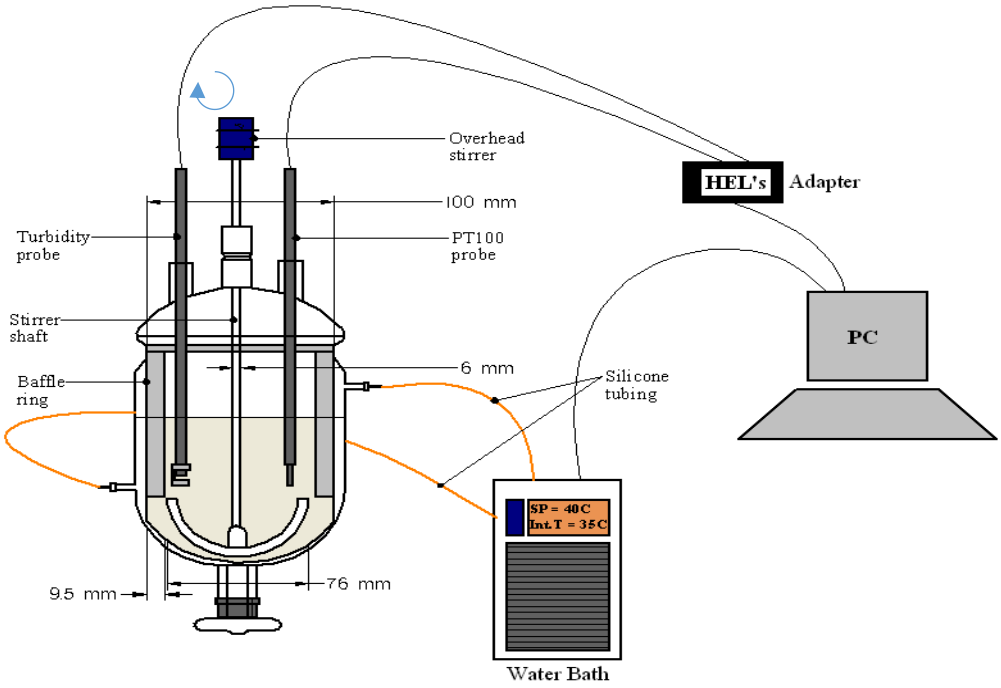

Fig 3.2: Schematic of STC set-up used for MSZW measurements

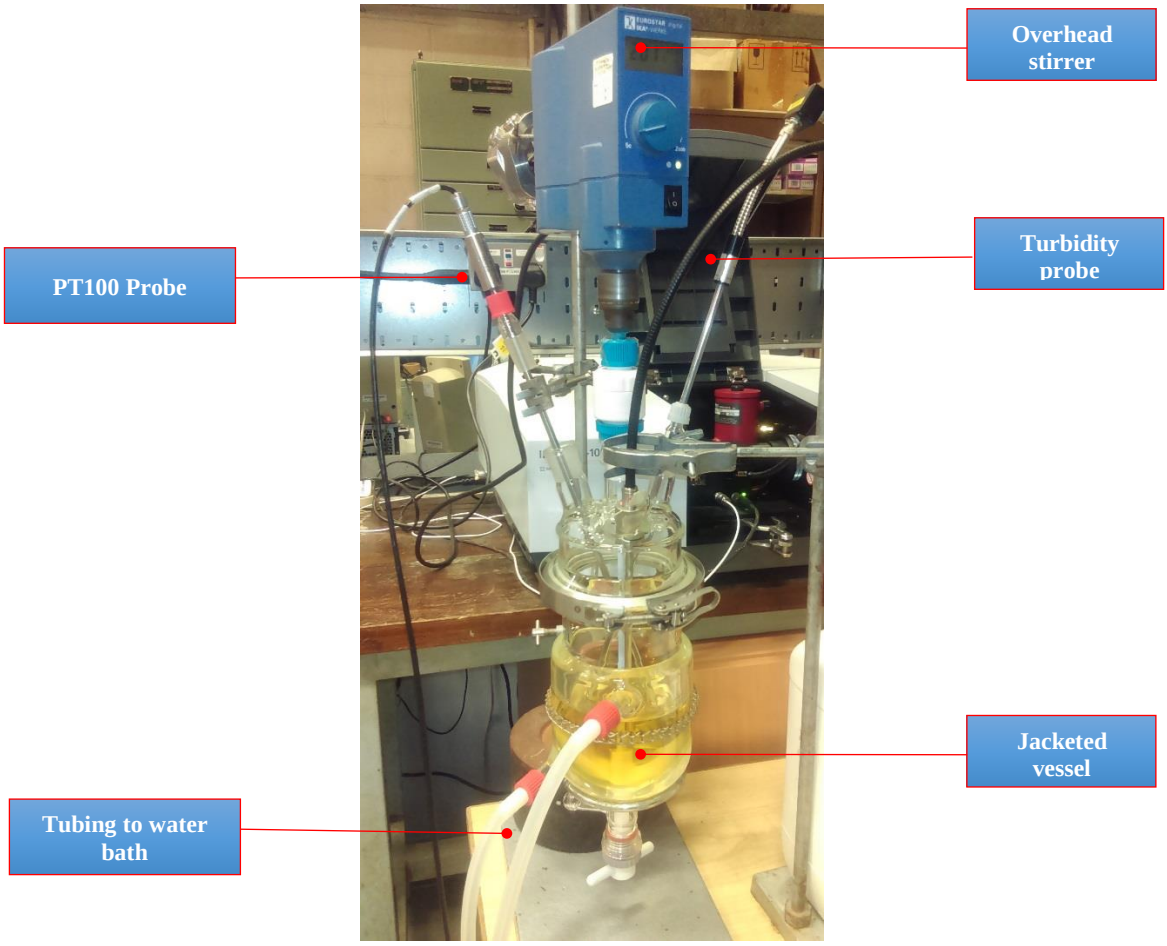

Fig 3.3: Picture of the STC set-up used for MSZW measurements

The OBC set-up consists of a 500 mL jacketed glass column of 50 mm ID and about 25 cm length, with three neck side ports which was supported in a PTFE frame structure to minimise the effect of mechanical vibrations. A set of four PTFE orifice plate baffles joined together by stainless steel rods was fitted into the glass column; each baffle has an outer and orifice diameter of 46 mm and 24 mm respectively, and spaced 65 mm from one another. A XTA3806 ServoTube linear motor (SCS Ltd) was used to effect an up-down movement of the baffles such that the content in the column moves in an oscillatory motion; the motor movement was regulated with a control box containing a XTL 230-18 amplifier and built-in functions to control the frequency (range 0 – 10 Hz) and amplitude (range 0 – 60 mm) of the oscillatory motion. The motor was mounted on a metal stand above the column, and connected with the baffles through a threaded aluminium rod. The schematic of the set-up is shown in **Fig 3.4** below.

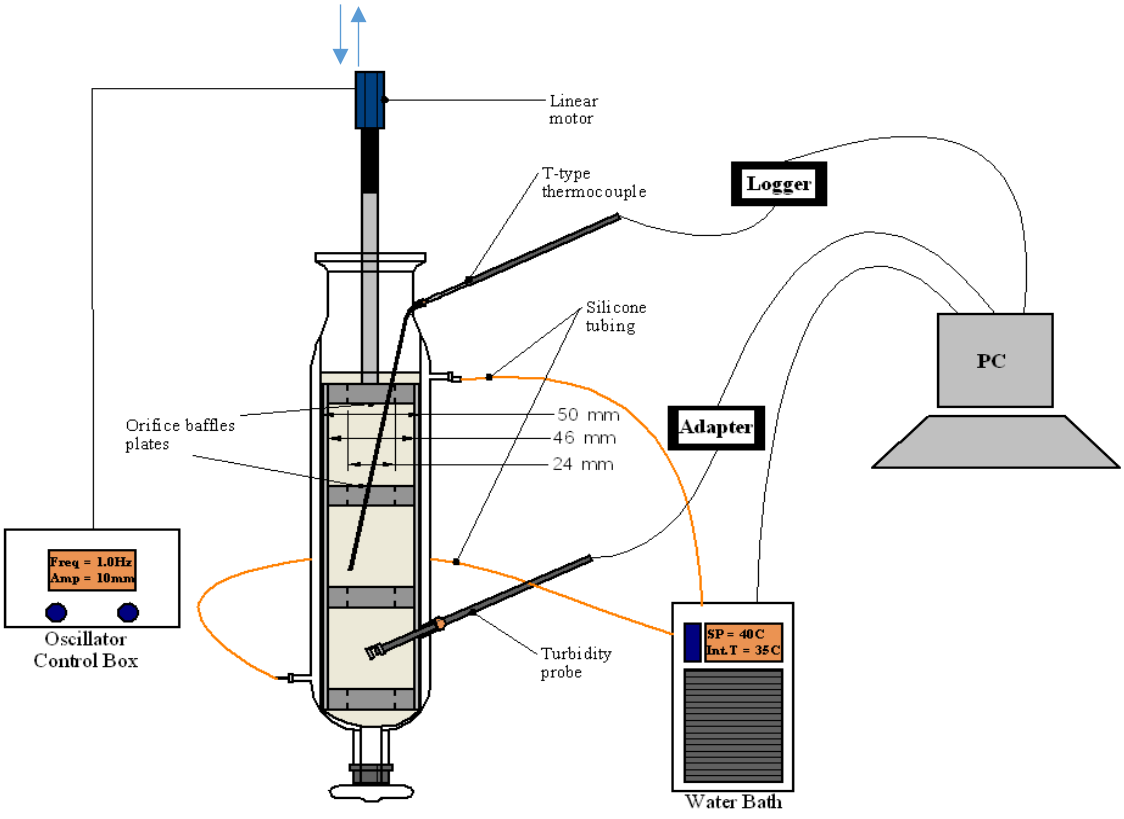

Fig 3.4: Schematic of OBC set-up used for MSZW measurements

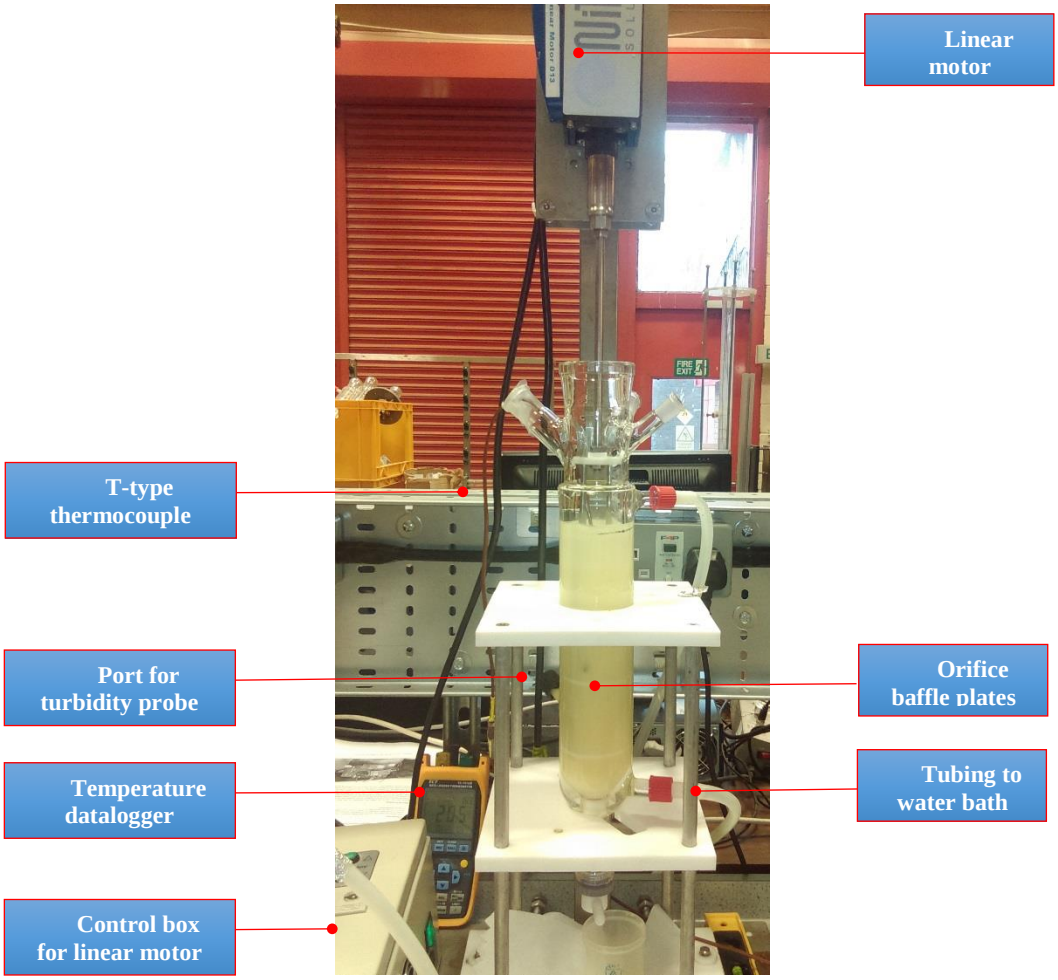

Fig 3.5: Picture of the OBC set-up used for MSZW measurements

To control the temperature of the content in the vessel (or column), the crystalliser was connected to a GP200-R2 water bath (Grant Inst. Cambridge Ltd) fitted with a heating circulator for pumping the heating or cooling water through the jacket of the crystalliser with silicone tubing; on the circulator are knobs that can be used to control and programme temperature profile. The temperature of the crystalliser content can be either controlled using the internal thermocouple within the bath that monitors the temperature of the water flowing through the jacket, or by connecting a TXPEP plastic external probe to the bath and using the probe to monitor the actual vessel content temperature; the former method would require an additional thermocouple to monitor and log the actual vessel temperature. The water bath was interfaced with an HP Compaq PC which operated under Windows-based Grant Labwise™ version 1.0 software for display, monitoring and logging of temperature data. Additional accessories used for temperature control were T-type thermocouples which were interfaced with the PC operating under Windows-based Temp Monitor_S2 version 1.0.16 software via a digital datalogger for data acquisition.

The two batch set-ups were used in comparison with each other based on their power dissipation rates.

Turbidity measurements: HEL's CrystalEyes system (HEL Group, UK) which consists of turbidity and temperature (PT100) probes, both encased in hard-wearing Hastelloy for protection and chemical compatibility was used for these measurements. The probes which are about 5 mm in diameter were inserted about two-third into the crystalliser vessel; the turbidity probe has an in-built near-infrared (NIR) light source that sends light from the solution into which it was inserted, back to the detector via an adjoined mirror; the turbidity value is then measured as a function of the intensity of light transmitted. The probe was assembled such that the gap between the light source and the adjoining mirror was between 4 – 5 mm, and it was positioned within the vessel in a way that the agitated particles perpendicularly cut through the light beam. The system was interfaced with an HP Compaq PC which operated under Windows-based HEL WinISO version 2.3.117.1 software for real-time display, logging and data analysis. Both probes (temperature and turbidity) were able to fit into the STC but only the turbidity probe could be fitted into the OBC due to access restrictions; hence a T-type thermocouple was used to monitor and log the temperature in place of the probe.

The mixing intensity for each of the crystallisers was estimated based on *power density* calculations which is a function of the vessel configuration. Therefore operating conditions were set such that the power density was the same in both set-ups as equal basis of comparison. The equations used to estimate the power density in both set-ups are given below; and the required parameters are shown in **Table 3.2.**

STC
$$P_d = \frac{N_p S_i^{\,3} D_i^{\,5} \rho}{V_L} \tag{3.1}$$

OBC
$$P_d = \frac{2\rho N_b}{3\pi C_D^{\,2}} \left(x_0 2\pi f\right)^3 \left(\frac{1}{S^2} - 1\right) \qquad S = \frac{d^2}{D^2} \tag{3.2}$$

Table 3.2: Parameters used to estimate power density (a representative function of mixing intensity)

STC		OBC	
Parameter (unit)	**Value**	**Parameter (unit)**	**Value**
Tank diameter – d (m)	0.1	Column diameter – D (m)	0.05
Impeller diameter – D_i (m)	0.076	Baffle orifice diameter – d (m)	0.024
Power number – N_p	1	Baffle spacing (m)	0.065
Fluid density – ρ (kg/m^3)	879	Baffles per unit length – N_b (m^{-1})	15.38
Fluid volume – V_L (m^3)	0.00035	Baffle free area ratio – S	

For the STC, the stirrer speed (S_i) was the variable while the *centre-to-peak* amplitude (x_0) and frequency (ω) were the variables for the OBC; *Goal Seek* function in MS Excel was used to match the power densities. The actual amplitude of the oscillator was set to $2x_0$ because it was calibrated as peak-to-peak while that required for power density calculations are centre-to-peak which are half the former,

For the cooling rate effects, linear rates were used and were determined by controlling the temperature of the process fluid inside the vessel and the temperature of the coolant (in this case, the water in the water bath). By the means of the Labwise software, with which the water bath was interfaced, three temperature programs were developed and sent to the bath controller, to provide three different cooling rates; however, the STC and OBC exhibit different degree of heat transfer (from the jacket to the inside wall of the tank (or column) and eventually into the bulk of the fluid content; this is mostly due to the different mixing and size configurations (particularly, the jacket sizes). Due to this, and coupled with the fact that there is a delayed response between the bath controller and the temperature sensor, the set temperature programs do not reach their end temperatures within the specified time; hence an external PT100 probe connected to the water bath was inserted into the vessel in order to monitor and log the actual content temperature within the vessel; this was conditioned in the bath by changing the isothermal sensor from *internal probe* to *external probe*.

The procedures

The required vessels were adequately cleaned and assembled as earlier described and shown in **Fig 3.2** and **Fig 3.4**. It should however be noted that the experiments for each set-up were run consecutively not simultaneously.

The palm oil feed which was in the semi-solid state (approximately 350 mL and 400 mL for the STC and OBC respectively) was added to the respective vessel with the use of a spatula and a glass beaker. Afterwards, the water bath was connected to the tank through the silicone tubing and the isothermal set-point temperature was set to 60°C in order to melt the oil in the tank; the oil was held at this temperature for about 30 mins, to ensure that it was completely melted.

With all necessary probes and accessories fitted, and all analytical tools prepared, agitation was then applied (through stirring or oscillation) to the crystalliser at the required mixing condition, to ensure that the system is close to homogenous as much as possible. For the mixing intensity experiments, having set the stirrer speed (or oscillation) to give the required intensity, the water bath controller was programmed to a nominal cooling rate of 0.5 ^{o}C/min and it was maintained at this rate for all the mixing conditions examined. Turbidity measurements were then recorded as the temperature program proceeded.

While for the cooling rate experiments, the bath controller was programmed consecutively to the different nominal cooling rates; all at a fixed mixing condition of 247 W/m^3, i.e. 203rpm and 12.5 mm/1.5 Hz for the STC and OBC respectively. The mixing condition was fixed at this point because from observations during the previous set of experiments (effect of mixing intensity), it was the point that guaranteed good-enough mixing while still minimising vortex formation and foaming effects in the STC and OBC respectively.

The temperature program with which the MSZW was analysed was a *cooling–holding–heating* cycle between the range of 20°C and 60^{o}C; a sample profile is shown below (**Fig 3.6**); the hold period was kept constant for all cooling rates at 1 hr; it should be noted that the heating segment of each profile was set to also run at the same rate specified in the cooling segment.

Each experiments was repeated at least twice to enhance result accuracy. The mixing intensities and cooling rates examined are shown below (**Table 3.3**).

Table 3.3: Operating conditions explored for MSZW analysis

Cooling rate (°C/min)	*OBC*		*STC*	*P_d (W/m^3)*
	x_0 (mm)	*ω(Hz)*	*S_i (rpm)*	
Constant (1.0)	10.0	1.0	108	38
	12.5		135	73
	15.0		163	127
	10.0	1.5	163	127
	12.5		203	247
	15.0		244	427
0.25	12.5	1.5	203	**Constant** (247)
0.5				
1.0				

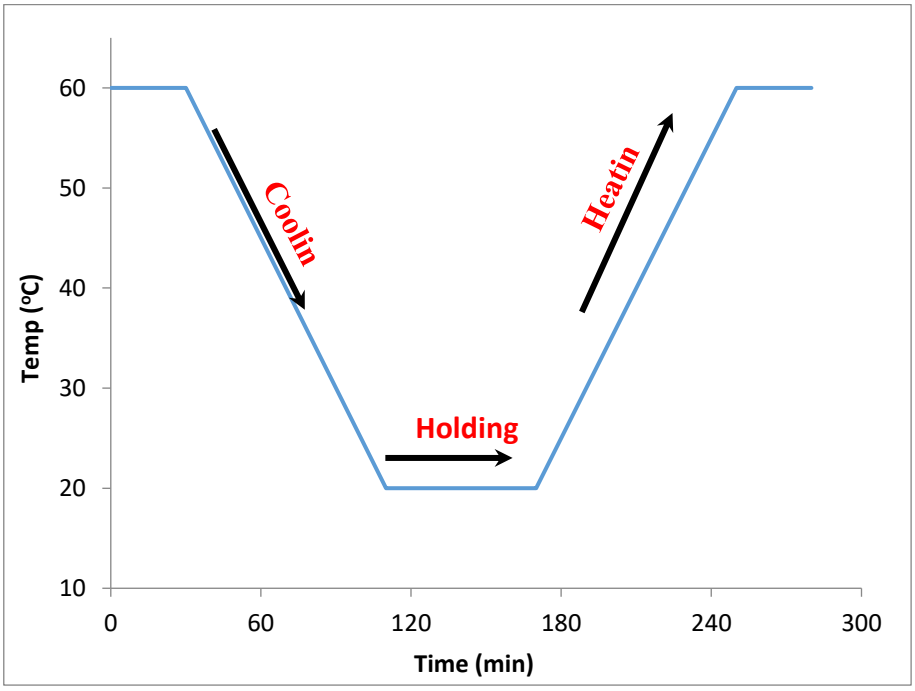

Fig 3.6: A sample of temperature profile used for MSZW analysis

3.2.2 Kinetics Parameter Extraction

In this part of the study, kinetics parameters that characterise the crystallisation of palm oil were estimated using existing empirical model equations. The aims of this are to evaluate and compare kinetics from a melt crystallisation extracted using models for both melts and organics; and to establish critical understanding of the various model approaches and their applications; and to assist the design and operation of continuous crystallisation. Three models were considered; the first two are from traditional melt crystallisation, while the last one is from solution crystallisation.

Experimental data such as induction times of crystallisation (τ) and melting point (T_m) were required for these analysis and calorimetry (DSC) was the technique employed in obtaining these data.

15–18 mg of palm oil sample was weighed into an aluminium pan and sealed with a pierced lid; an empty and sealed pan was used as a reference. The sample was heated to 353K at a rate of 10 K/min and held at this temperature for 10 mins. The sample was then cooled to the pre-set end temperature (293 – 301K) at 20 K/min and held at each of the end temperatures for crystallisation to occur. Since the crystallisation is an exothermic process, the onset of the exothermic peak during the isothermal period was taken as the induction time (τ) and all were evaluated using the DSC 214 software. At the end of the crystallisation process, the sample was then heated back to 353K at 10 K/min to obtain the melting curves.

Avrami Model: See section **2.2.2** for more information regarding this model. The value of ***x*** (in eq. 2.15) was estimated by integrating the isothermal crystallisation exothermic peak from the DSC measurement, as given by **Fig 3.7** and eq. (3.3) where ΔH_t is the heat of crystallisation (W/g) evaluated as the area under the crystallisation curve from the onset of the peak to time t using the DSC 214 software; ΔH_{tot} is the total area under the curve. More detailed description of the methodology can be found elsewhere[211]. The kinetic parameters, ***n*** and ***k,*** were obtained from the slope and the intercept of the plot of $[\ln(-\ln(1-x)]$ against $\ln(t)$ respectively. The unit of k here is the inverse of time to the power of n, depending on the index of crystallisation.

$$x = \Delta H_t \Big/ \Delta H_{tot} \tag{3.3}$$

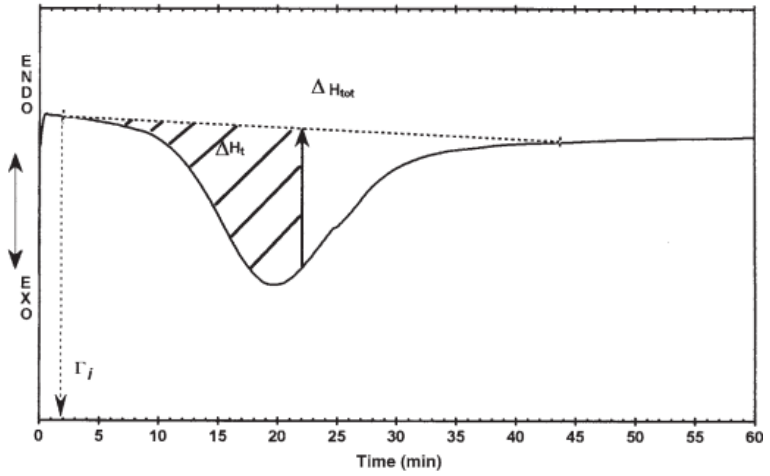

Fig 3.7: Determination of crystal solid fraction (*x*) from crystallisation exothermic peak obtained from DSC analysis[212]

The Fisher-Turnbull correlation: See section 0 for more information regarding this model. Using the DSC data obtained, a plot of ln(d*x*/d*t*) against ln(1-x) will give a slope equal to *n*, and the value of *A* can be obtained from the intercept and the ΔG_c evaluated from eq. (2.18) for the different end temperatures considered. Using these *A* values, the rate constant (k_n) can therefore be estimated according to eq. (2.19). The unit of k_n is the inverse of time (s^{-1}).

The MSZW (ΔT_{max}) results obtained from section **3.2.1** was used in this analysis. From a plot of $\boldsymbol{ln(\beta)}$ against $\boldsymbol{ln(\Delta T_{max})}$, the nucleation order (***n***) and the nucleation rate constant ($\boldsymbol{k_n}$) can be estimated from the slope and the intercept of the plot respectively and then compared with those from the two holistic models. For number basis, the unit of k_n is the inverse of time (s^{-1}).

3.3 Filtration Study

When the crystallisation process is complete, there is need for physical phase separation, extracting the solid product (stearin) from the liquid product (olein), through a filtration process. The eventual yield and purity of the products are largely dependent on the efficiency of the filtration process. Process conditions are also controlled such that the products possess characteristics that are favourable for effective filtration.

In this study, the effects of cooling rate and mixing intensity on filtration rate, purity and yield of the liquid product (olein) were examined in both stirred tank (STC) and oscillatory baffled crystalliser (OBC) – the set-up is shown in **Fig 3.8(a)** below and the conditions examined are shown in **Table 3.4**. For better temperature control, the filtration step was carried out in a hotbox (**Fig 3.8b**) where the temperature was maintained at 20^{o}C, the end temperature of the cooling process. Vacuum filtration was adopted using a *KNF N 810.3 FT.18* vacuum pump.

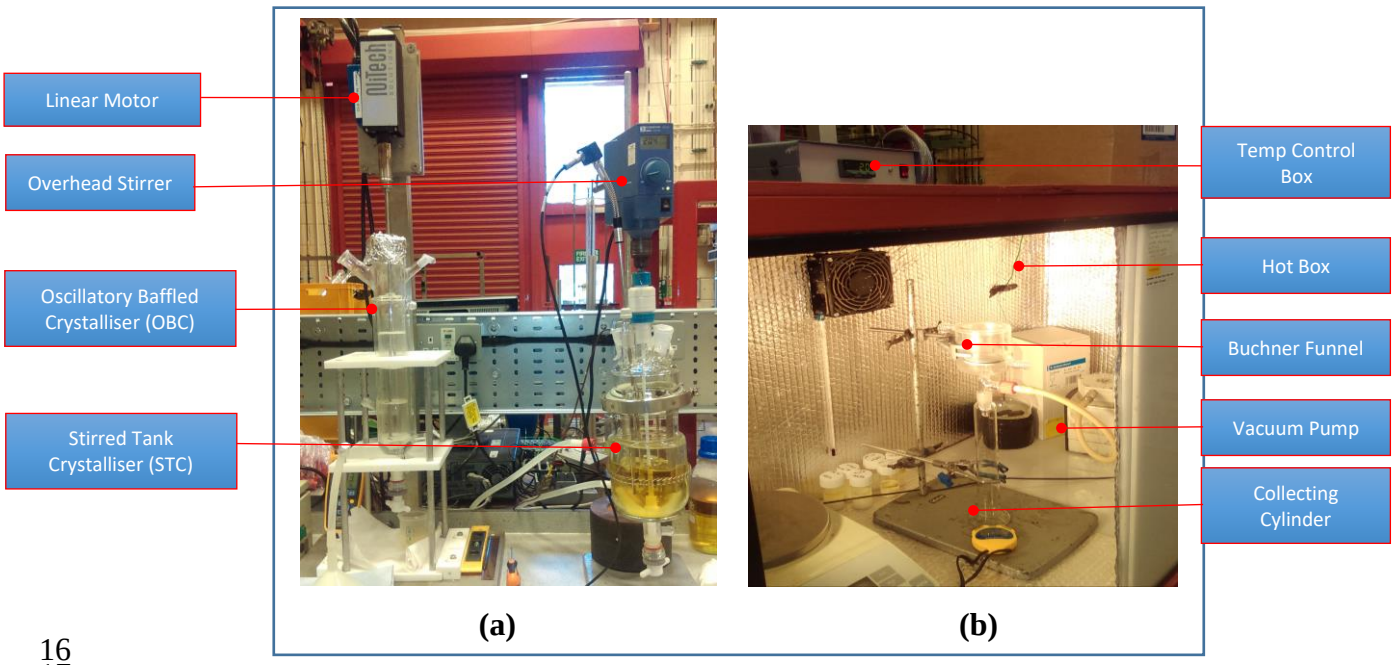

Fig 3.8: Set-up used for the filtration study in this research (showing the STC, OBC, and hot box used for temp-controlled filtration)

Table 3.4: Experimental conditions explored during the filtration study

Cooling rate (ºC/min)	0.25 – 1.0
Cooling profile	Linear
Temperature range (ºC)	50 - 20
Working volume (mL)	400 – 450
Mixing Intensity	STC: 200 – 240 rpm
	OBC: 1.2 – 1.5Hz and 30mm

At the end of the cooling process, weighed sample (~60 g) of the crystallised suspension was collected from the crystalliser vessel (through the outlet port) into a glass beaker, and immediately transferred to the Buchner funnel in the hotbox to begin the filtration step. Filtration was stopped when a *dryland* (i.e. no liquid on the top) of filtered cake was visible in the funnel. The olein (filtrate) and stearin (cake) were then weighed and analysed.

Solid Fat Content: This was required in determining the true olein yield of the filtrate product and done by partial integration of the area under the melting curve obtained from a DSC at different temperatures; a detailed description of this method is found in literature[193] and the actual thermal program adopted for the DSC analysis is based on a previous study by Nassu & Gonçalves[213].

3.4 Continuous Crystallisation

3.4.1 Set-up

After the completion of melt (palm oil) crystallisation in the batch set-ups (STC and OBC), the study then proceeded onto a continuous platform, Continuous Oscillatory Baffled Crystalliser (COBC), where a linear cooling profile was designed based on the tube configuration, and was used to formulate the temperature zones along the length of the column, this is a fundamentally different concept from conventional batch crystallisation. This was then adopted in the continuous crystallisation of palm oil.

The COBC crystalliser consist of 11 straight sections of jacketed baffled glass tubes (each tube is 700 mm long and has a diameter of 15 mm) connected together in series with glass U-bends which are also baffled. A glass piston drive assembly (Alconbury Weston Ltd, Stoke-on-Trent, UK) was connected to the first glass tube in the series via collars & gasket fittings, and this was used to supply the oscillatory fluid motion in the crystalliser. The feed palm oil was held in a 20 L jacketed stirred tank and connected to the crystalliser via a peristaltic pump. Circulating water baths were connected to the jacket of the feed oil tank and also to the tube jackets, at strategic positions along the tube length of the crystalliser to achieve the desired temperature zones. Sampling collars were also fitted at the required locations. **Fig 3.9** below shows the set-up of the COBC **while Fig 3.10** shows the division of the tubes into temperature zones.

The online monitoring of the evolution of concentration and crystal size distribution along the length of the crystalliser were achieved at the two strategic positions of a known distance apart, each (Jn7 & Jn10) with a turbidity (HEL Group, UK) and a particle imaging (Perdix, Netherland) probe respectively (see the positions of O in **Fig 3.10**). While the former provided data for MSZW and nucleation, the latter for crystal size distribution, thermocouples were inserted at four (4) different ports (O) to monitor and record the temperatures along the column length. The data obtained allowed the determinations of steady states (temporal and spatial), its stability between the two positions, together with the effects of operating parameters on these stabilities. The parameters examined are listed in **Table 3.5** below:

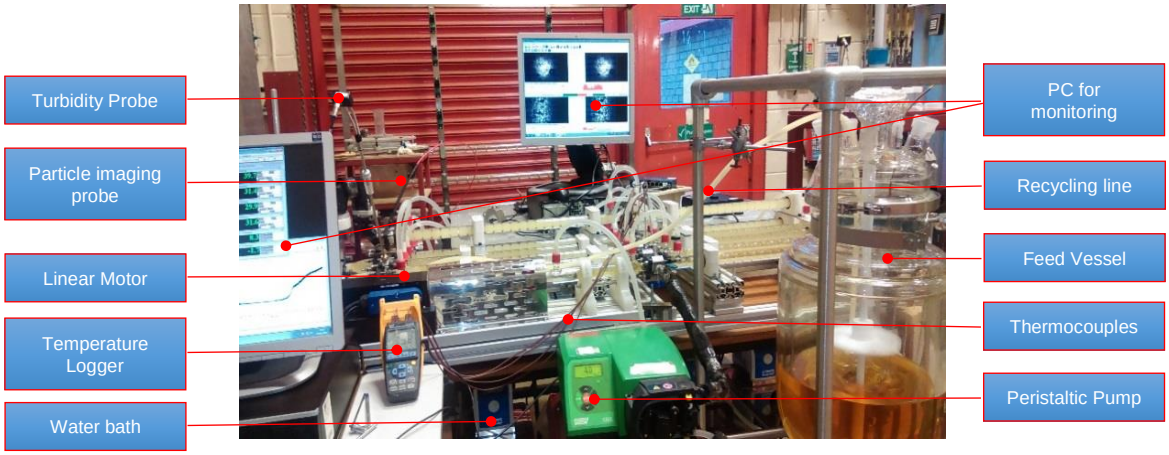

Fig 3.9: A picture of the set-up of the COBC used for looking into continuous crystallisation of palm oil in this research

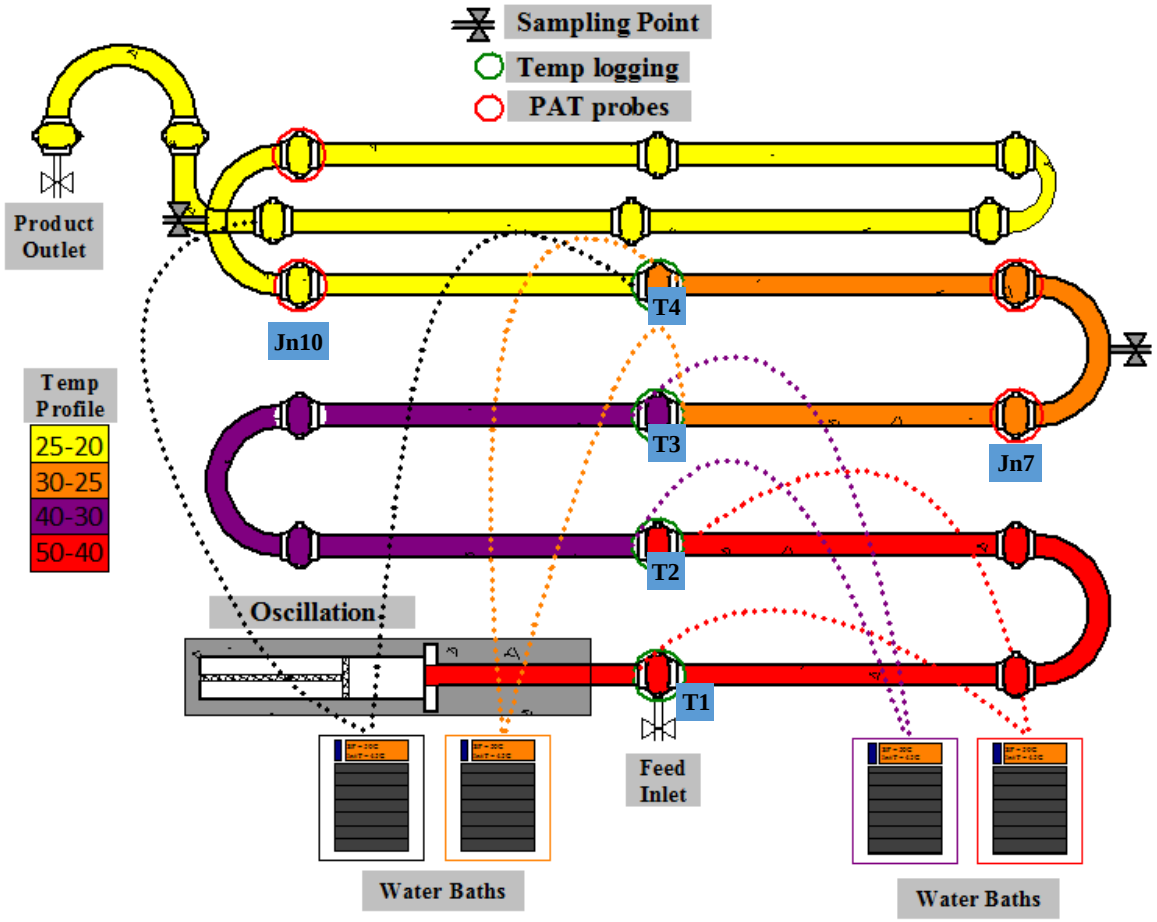

Fig 3.10: A schematic profile of the COBC set-up showing the temperature zones (colour-coded) and sampling/analysis ports

Table 3.5: The operating parameters examined during the study of continuous crystallisation of palm oil in the COBC

	Cooling (°C/min)	Flow (ml/min)	Mixing (Hz)*
High	1	76.68	2
Medium	0.5	53.86	1
Low	0.25	42.45	0.5
Constant	**Low** flow **High** mixing	**Low** cooling **High** mixing	**Low** cooling **Low** flow

*****The (peak-to-peak) amplitude was kept constant at 25 mm*

3.4.2 The Procedures

The feed oil in the feed vessel (a 20 L jacketed glass stirred tank) was completely melted at 65°C, after which it was pumped (at the selected flowrate) into and along the COBC column (made up of jacketed tubes) using a peristaltic pump; the pump had been initially calibrated to correlate the RPMs with flowrates (in ml/min) and the resultant equation was:

$$y(ml/\min) = 11.41 \times x(rpm) - 3.18 \qquad (3.4)$$

The linear motor was used to oscillate the oil net flow along the length of the crystalliser at the pre-set amplitude and frequency. During this period, the temperatures of the tube walls (Shell-side) for the entire length were maintained at 50°C using the connected water baths (Grant Inst. Cambridge Ltd); the oil was being recycled back into the feed vessel, to create a continuous flow loop, but the high temperature of the feed tank ensured that the inlet oil into the column is completely melted.

After about 45 – 60 min of pumping hot oil through the system – when most of the air bubbles in the bulk flow have been removed, the establishment of temperature zones of decreasing temperatures along the length of the COBC was then commenced, in this work, four temperature zones were used with zone 1 from 50°C to 40°C (red colour section in **Fig 3.10**); zone 2 from 40°C to 30°C (purple colour section); zone 3 from 30°C to 25°C (orange colour section) and zone 4 from 25°C to 20°C (yellow colour). The determination of how many zones to have depends on the solubility and the MSZW, generally the narrower the MSZW, the more

the zones. Each zone required a water bath, running its pre-set cooling program. In addition another water bath was used for the feed vessel. The temperature programs were designed such that they remained at the end temperatures until terminated.

As the temperature zones are forming, crystallisation of palm oil starts, a small volume (based on the volumetric flow rate) of the hot feed containing both olein and stearin together other minor fractions enters the crystalliser and goes through the pre-set temperature zones from the "tropic summer" to "summer" temperatures and from "summer" to "autumn" exit temperatures where two phases are visible and are directed to a product tank for filtration. Since our primary focus is on the quality of the product, plus there are physical constraints in the lab to store too much product, hence the exit stream was diverted back to the feed tank where the full dissolution takes place. This process continues, executing the continuous crystallisation until sufficient data have been obtained. Each run lasted for 3 – 4 hours (depending on the conditions being considered). The bulk flow temperature, turbidity and particle imaging of the formed crystals were being monitored with the inserted probes and the data logged for further processing. Afterwards about 1 – 2 hours, the cooling temperature programs were terminated and the baths were set to heat the oil back to 50°C to melt all sections, this brings us back to the start.

For the particle imaging, two Perdix light probes (ISPV-Mini, Netherland) were inserted into the COBC (which were positioned perpendicularly to the adjoining cameras) at the pre-determined locations (Jn7 and Jn10). In order to reduce curvature effects, square flanges were specially made for hosting these probes. The signals from the probes were interfaced with a Windows-based PC which operated the ISPV software for real-time capturing of the crystal images; the images being captured are simultaneously analysed by algorithms built into the software, such as size distribution (*equivalent diameter)* and number counts – a screenshot of the software window is shown in **Fig 3.11**. However, there were some limitations, e.g. bubbles being counted as crystals, difficulty in *zeroing* the computed data for pre-nucleation periods (i.e. before crystal formation). Hence care was taken to minimise as much as possible the presence of bubble in the bulk flow; also data generated during the pre-nucleation period were discarded.

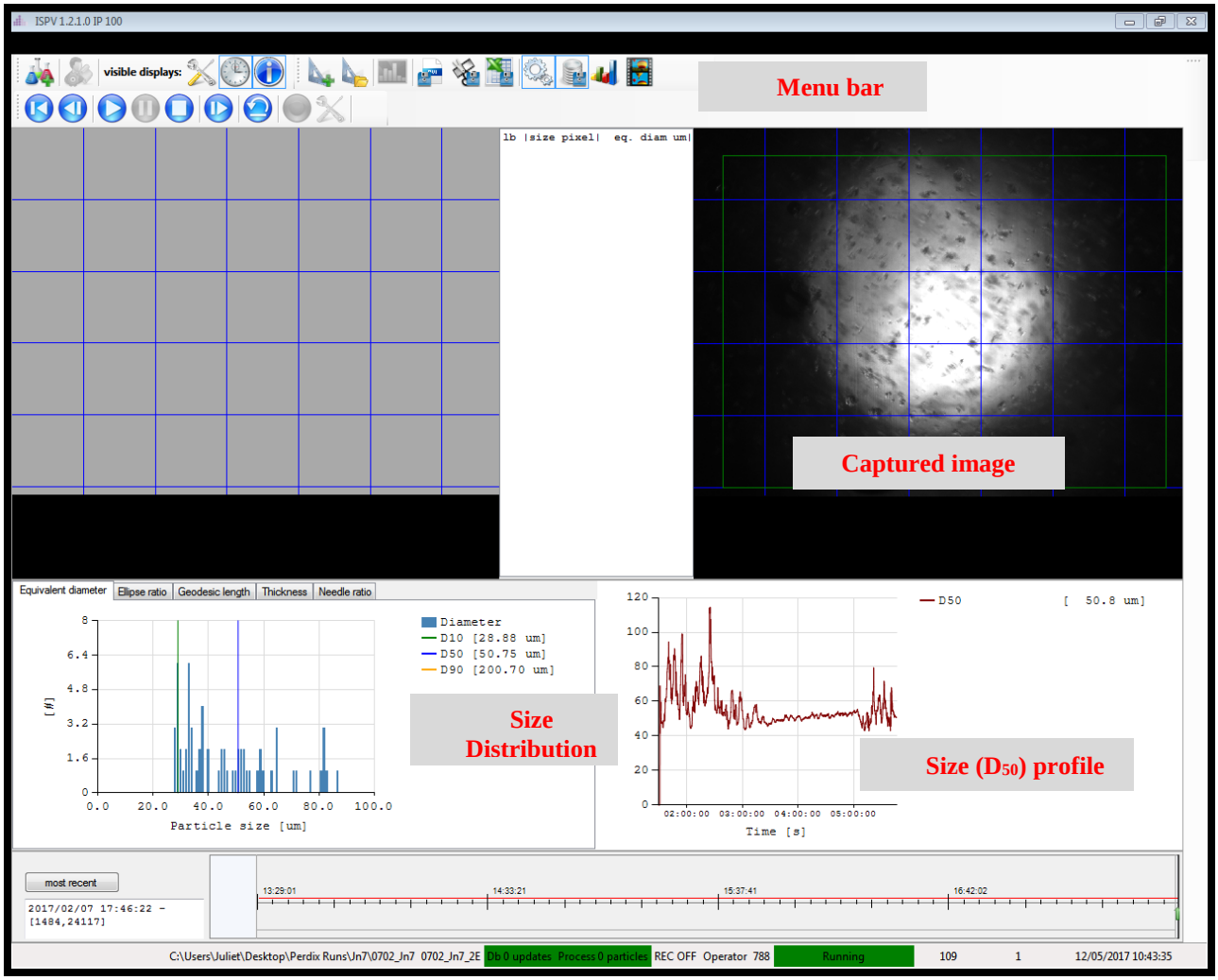

Fig 3.11: A screenshot of the ISPV software window used for image analysis by the Perdix Imaging system

3.5 Statistical Analysis

Analysis of Variance (ANOVA) with single factor was used to determine the significance of difference at $P < 0.05$. This provides the degree of confidence in data.

CHAPTER 4 – RESULTS: Initial Characterisation

In this chapter, the results obtained from the analysis of the raw materials (i.e. feed palm oil) were outlined and discussed using relevant theories and references. The analyses included compositional, thermal, iodine value, and development of solubility curve.

4.1 Composition Analysis

The precise compositions of the starting material have significant impact on fractionation process, it is essential to establish the full picture of this, which in turn aids the product analysis, comparison and discussions. In addition to the assay of fatty acid of the palm oil provided by the supplying company, a liquid chromatography analysis was also carried out in order to determine the triglyceride composition of the oil system. The resulting chromatogram for the palm oil is shown in **Fig 4.1,** and the graphical representation in **Fig 4.2** below; the % peak area is shown in **Table 4.1**; the TAG peaks were identified and assigned based on the presented chromatogram of TAG standards in a study carried out by Haryati *et al*[208] as shown in **Fig 4.3**. In this reference study, refractive index detector (RID) was used for their HPLC analysis, instead of the UV detector that was used in this research; it has however been reported in previous studies that RIDs require long separation times (especially for long chain TAGs), while UV offers relatively faster separation[210]; this is why the peaks in the chromatogram obtained below are at lower retention times compared to the reference chromatogram.

In view of this, the peaks were assigned based on the order of their appearance, using the PPO and OOP as the point of reference, since these two TAGs are the main content of palm oil as seen from their high relative % peak area (PPO, 14.2% and OOP, 15.7%); this is consistent with the FA composition provided, as shown earlier in **Table 3.1**, as it confirms the high content of palmitic acid (C16) and oleic acid (C18.1) in the assay. The extra peaks at the lower retention times (i.e. < 5.378 min) that could not be assigned were assumed to be partial glycerides components (e.g. diglycerides and free fatty acids). This compositional analysis gives an indication of the thermal properties of the oil system with respect to the melting and crystallisation characteristics (e.g. peak separation, temperature, transformation, etc.). For instance it is expected that solid fat product (stearin) should contain more saturated fats (e.g. PPP) and should have a higher melting point while the liquid product (olein) should contain

more unsaturated fats (e.g. OOO) and should have a lower melting point. The thermal analysis carried out on this fat system is discussed in detail in the next section.

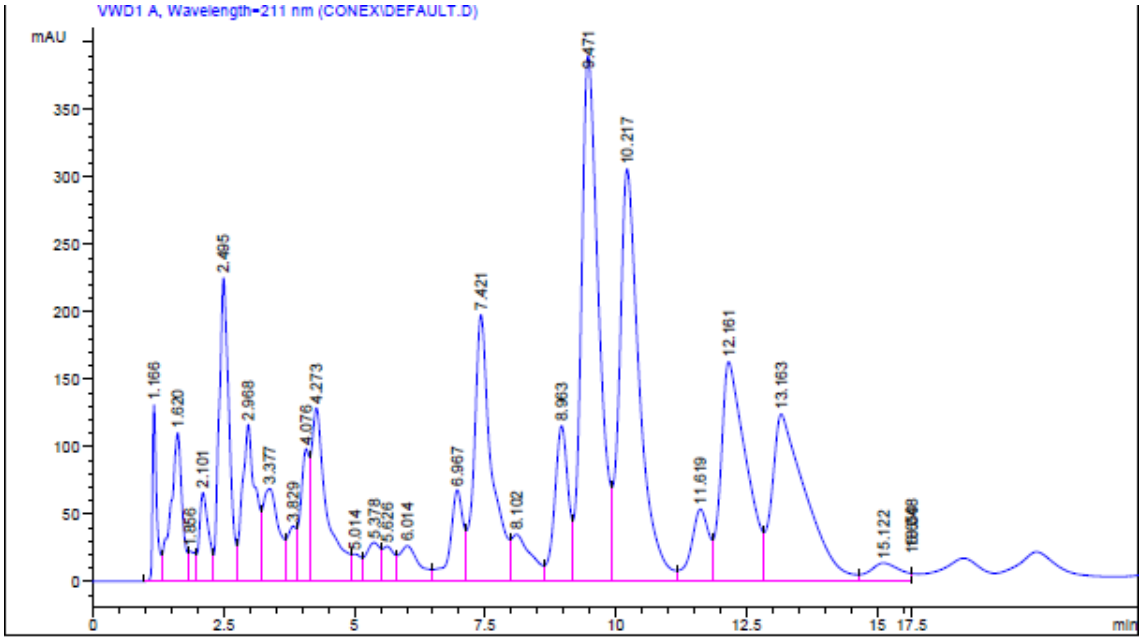

Fig 4.1: HPLC chromatogram obtained during the compositional analysis of RBD palm oil

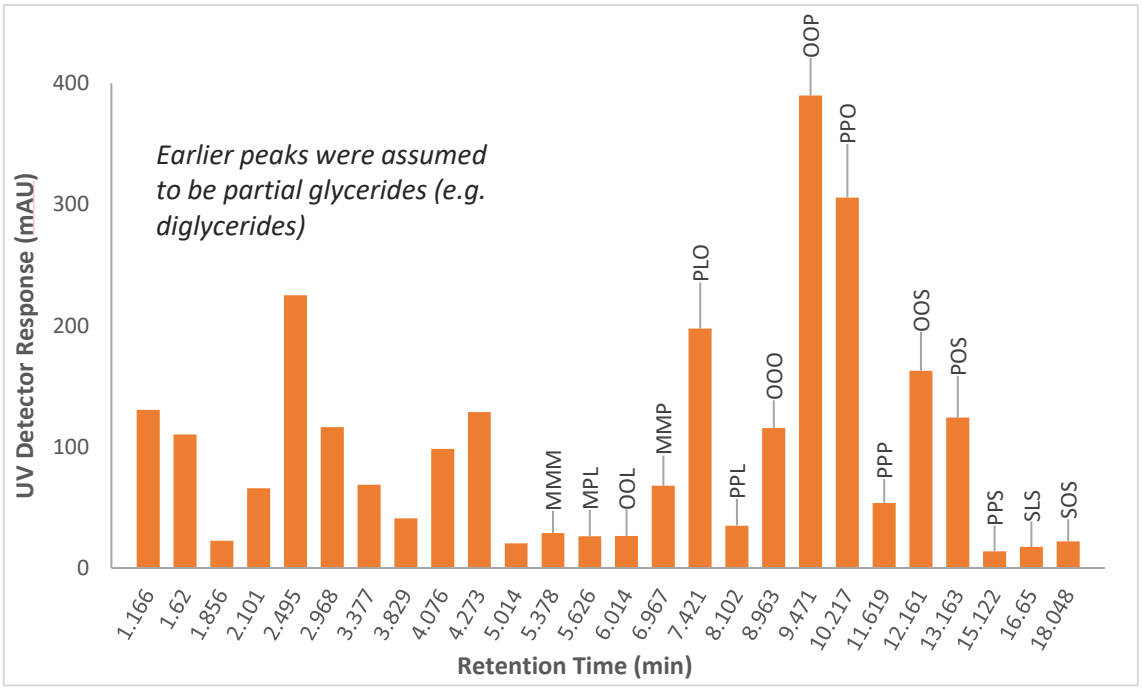

Fig 4.2: Graphical representation of HPLC chromatogram showing the assignment of the triglycerides present in the palm oil sample analysed

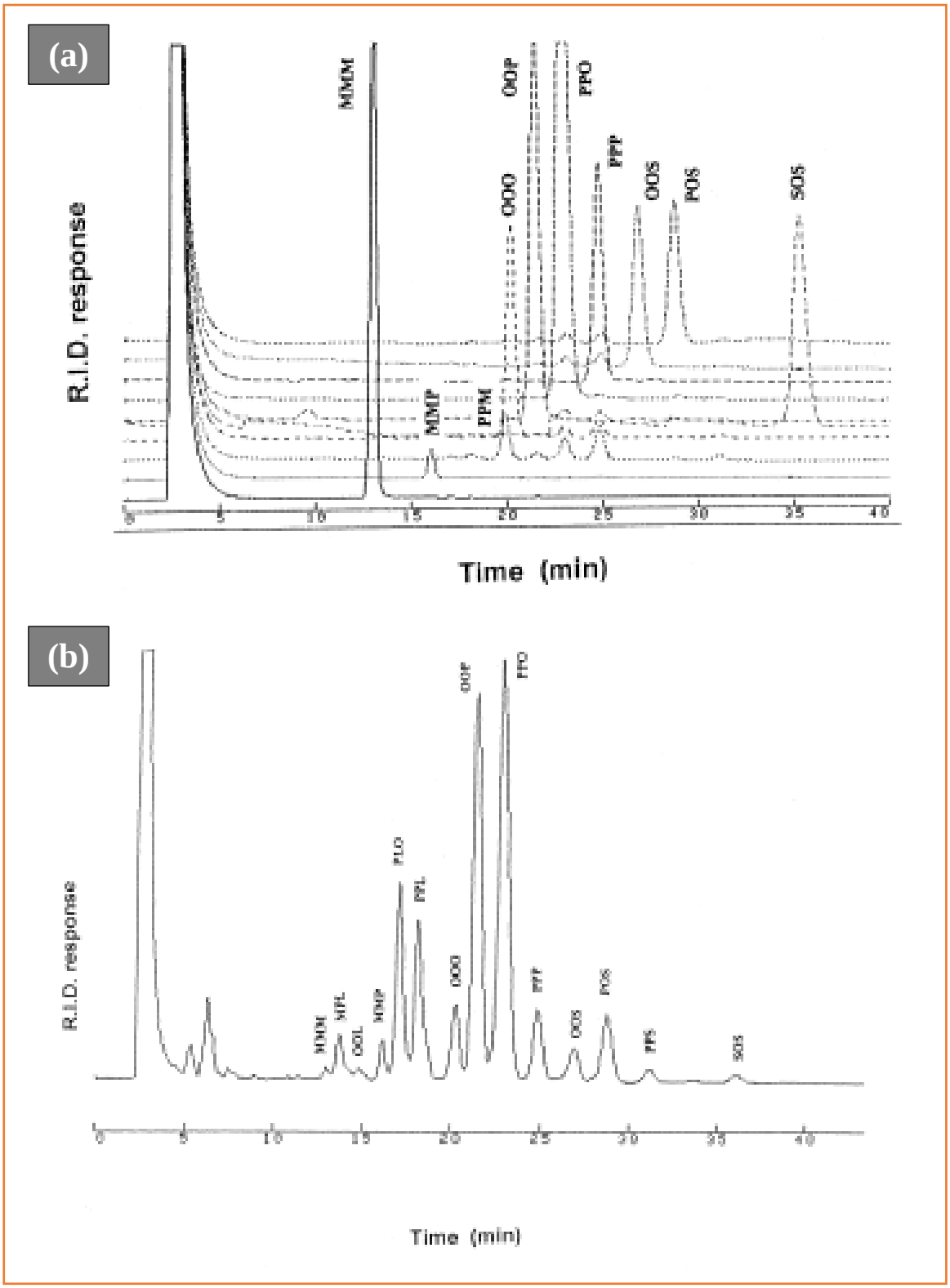

Fig 4.3: Reference chromatograms for standard TAGs (a) and palm oil (b) used for the peak assignment in the obtained chromatogram [208]

Table 4.1: Triglyceride composition of RBD Palm oil based on the % peak area of the peaks observed in the obtained chromatogram

Triglycerides	Ret. Time (min)	%Peak Area	Classification
OOO	8.963	3.656	Tri-unsaturated (4.87%)
OOL	6.014	1.220	
PLO	7.421	7.838	Monosaturated (33.15%)
OOP	9.471	15.784	
OOS	12.161	9.528	
MPL	5.626	0.704	Disaturated (30.35%)
PPL	8.102	1.627	
PPO	10.217	14.199	
POS	13.163	9.804	
SOS	18.048	2.412	
SLS	16.650	1.608	
MMM	5.378	0.963	Trisaturated (6.33%)
MMP	6.967	2.109	
PPP	11.619	2.176	
PPS	15.122	1.081	
	Total	**74.707**	
Others		25.293	

4.2 Thermal Profile

The palm oil feed was analysed by DSC, using heating/cooling steps. The presence of multiple peaks is expected in a single thermogram (i.e. within one temperature step) for palm oil due to its multi-component property; these peaks are often classified into 'high-melting peaks' and 'low melting peaks'. The endotherms and exotherms obtained from thermal analysis of fats by DSC provide useful information on the range of TAG distributions and polymorphic transformations occurring due to temperature effects.

The cooling thermogram (**Fig 4.4**) obtained for the palm oil used in this research shows two distinct exothermic peaks which correspond to crystallisation events; the onset and end of the peak profile was likened to fat formation due to molecular diffusion, and the end of crystallisation due to crystal solidification respectively. The peak at the lower temperature (-4.4°C) corresponds to crystallisation of the low melting fractions (LMFs); while the second one at 14.9°C is associated with the crystallisation of the high melting fractions (HMFs); the relatively broadness of the peaks is a reflection of the wide range TAG components present in each fractions A small shoulder was also observed at –29.4°C, which possibly corresponds to some of the unsaturated TAG components (e.g. OOP – cooling thermogram of its standard shows an exotherm between –22°C and –29°C[107]). It can be inferred that the LMFs represents the olein product, while the HMFs, the stearin products, according to a previous study carried out on palm stearin, where thermal analyses of the products from multiple cycles of re-crystallisations showed increased intensity in the peaks corresponding to the high melting fractions, and reduced intensity in the peaks for the low melting peaks fractions (which eventually disappeared over time)[214].

Linking this with the triglyceride compositions of palm oil discussed earlier in section 4.1, it was stated that the palm stearin product is expected to contain more saturated fats (such as tri-palmitic acid), which have higher melting temperatures, hence why the high temperature exothermic peak was related to the stearin product of palm oil. Conversely, palm olein is expected to contain more unsaturated fats (such as oleic acid), which have lower melting point hence why the low temperature exothermic peak was assigned to the olein product – to buttress this, a reported DSC thermogram of palm olein indicated that the high temperature peak was absent. It can therefore be concluded that thermal analyses, coupled with compositional analysis are useful techniques in providing information with regards to the TAG distribution of fat systems.

The melting thermogram of the palm oil feed (**Fig 4.5**) also shows two broad endothermic peaks; the endothermic peak between 20°C and 45°C corresponds to the melting of the high melting fractions, while the low temperature endothermic peak (between -10°C and 10°C) corresponds to the low melting fractions. However, analysing melting thermograms is more complicated and less straightforward due to peak broadening and overlaps; it has therefore proven more useful in identifying polymorphic transformations, as opposed to using it to characterise the thermal profile[215], although melting thermograms of fats have also been instrumental in quantifying the amount of crystallisable fats (also known as *solid fat content* – see section 2.5.5) present in the sample, based on the obtained endothermic peaks[216] for instance, an exothermic peak was observed at *ca*. 15 °C, and this was attributed to polymorphic transformation during the melting process i.e. recrystallization of a more stable form (see section **2.3.5** for more information regarding this). Hence according to Che Man & Swe, the peak at the low temperature region (between -10°C and 10°C)were attributed to the β_2' and α polymorphs, while the peak at the high temperature region was attributed to the β_1' and β_1 polymorphs [217] – also see section **2.3.5** for more information regarding polymorphs of palm oil; x-ray diffraction analyses will however be required to ascertain these polymorph assignments. Though polymorphism of palm oil is outside the scope of this research study, and was not investigated further, the information provided by these thermal studies would still prove essential in understanding some of the crystallization properties of palm oil as discovered in further studies.

Again, linking this to the broad products classification of palm oil (i.e. stearin and olein), it can then be inferred that the solid product (taken as stearin) will crystallise as the α-polymorph while at the low temperature region (<10°C), but a conversion to the β-polymorph would expected when operating at higher crystallisation temperature (>20°C) with the transition occurring around 15°C – 20°C, based on the melting profile obtained.

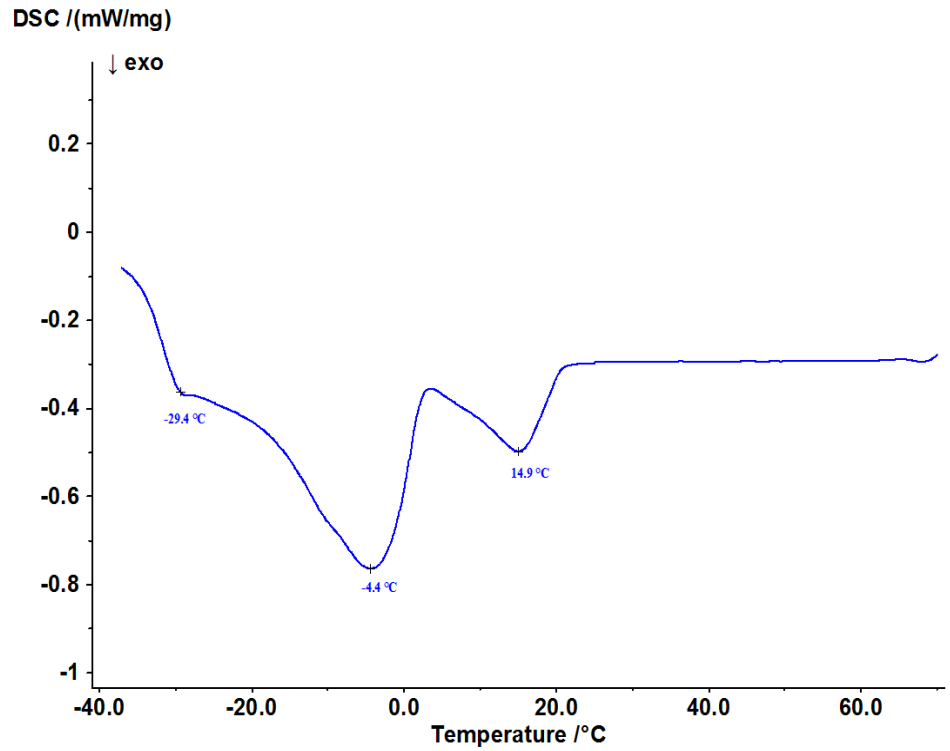

Fig 4.4: Cooling DSC thermogram obtained for the RBD palm oil used in this research

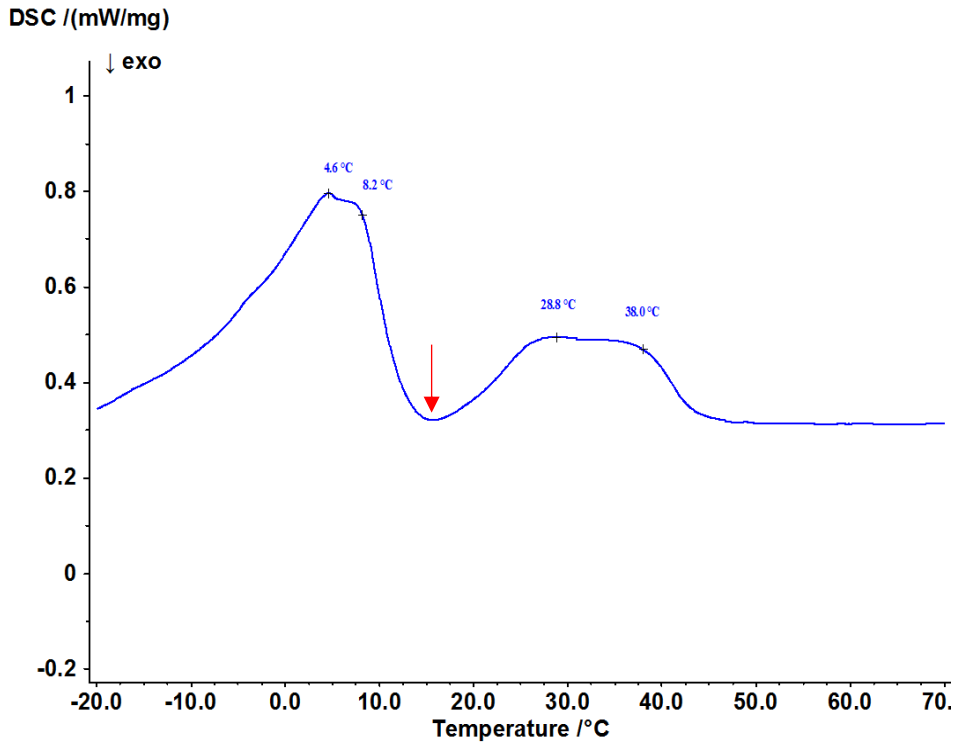

Fig 4.5: Melting DSC thermogram obtained for the RBD palm oil used in this research

4.2.1 Extended Thermal Studies

In addition to using the DSC technique to characterise the thermal profile of the palm oil system, it is also useful to expand this study by examining the effects of some of the parameters adopted during the analysis. Such parameters include cooling/heating rates and repeated heat/cool cycles.

DSC thermal analyses were carried out on the palm oil feed at different cooling rates between 1 °C/min and 10 °C/min, and the resulting thermograms are shown in **Fig 4.6**; it can be observed that though the profile remains relatively similar, the exothermic peak temperatures (which represents the crystallisation events) reduced (from 18.8 °C to 14.5 °C for the HMFs and from 2°C to -3.9°C for the LMFs) when the cooling rate was increased from 1 to 10 K/min, which indicates that cooling rate has an effect on the crystallisation events, which is as would be expected in any crystallisation process, since it has been established in previous crystallisation studies that increasing the cooling rate increases the rate of crystallisation rate (see more information on this in later section in 5.1.1). Also it was noticed that the peaks became broader with increasing cooling rate; this is an indication of a wide range of TAGs crashing out into the solid phase when the crystallisation process is rapid (i.e. fast cooling rate) which then require a longer relaxation period for the solid phase to stabilise in order to form a stable crystal product; conversely, when the crystallisation process is slow (i.e. lower cooling rate), the fractions have enough time to collate and crystallise into TAG groups of similar chain length and bond types thereby producing relatively sharper exothermic peaks [158]. However, a 4°C reduction in peak (crystallisation) temperature when the cooling rate is increased by 10-fold may not be considered overly significant in the grand scheme of things with regards to crystallisation of palm oil; hence the more important conclusion to be drawn here is that the cooling rate programmed into the DSC profile for thermal analysis does have an effect on the resultant thermograms hence care should be taken that the appropriate analysis parameters are considered.

Furthermore, DSC analysis involving repeated cycles of cooling and heating (melting) steps with cooling/heating rate kept constant, were also examined, and the resulting thermograms are shown in **Fig 4.7**; it can be observed that there were negligible differences between the first and second cycles, with respect to the corresponding peak temperatures and the required enthalpy changes in both the cooling and melting steps. This could imply that the thermal

history which the palm oil has been exposed to has limited impact on its crystallisation and subsequent melting behaviour. Therefore, thermal degradation of palm oil due to repeated exposure to high temperature might be less of a concern depending on the range of temperature considered, as it should be noted that only two cycles were considered in this analysis.

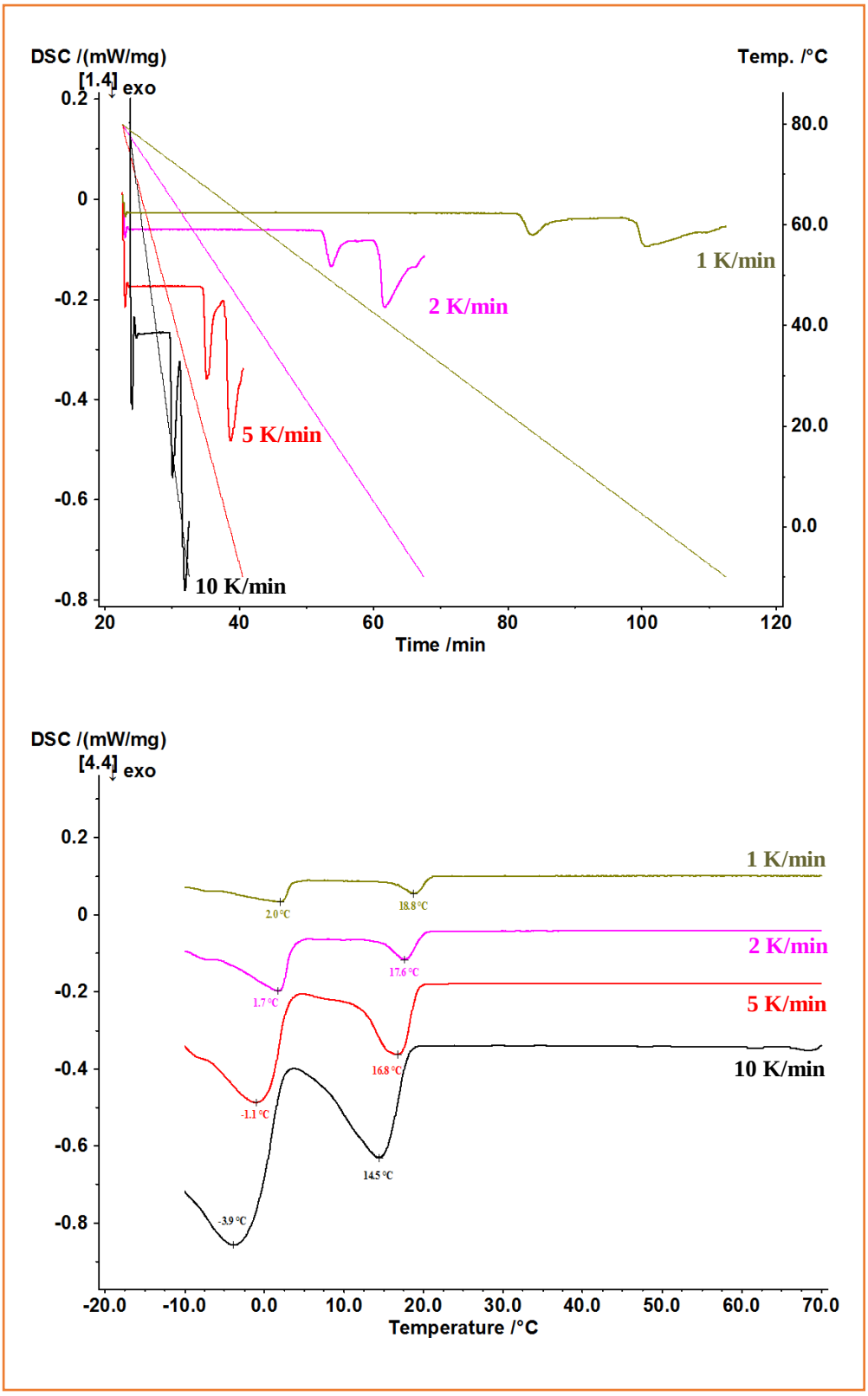

Fig 4.6: DSC Cooling thermograms showing the effect of cooling rate on thermal events (time-based (up) and temperature (down))

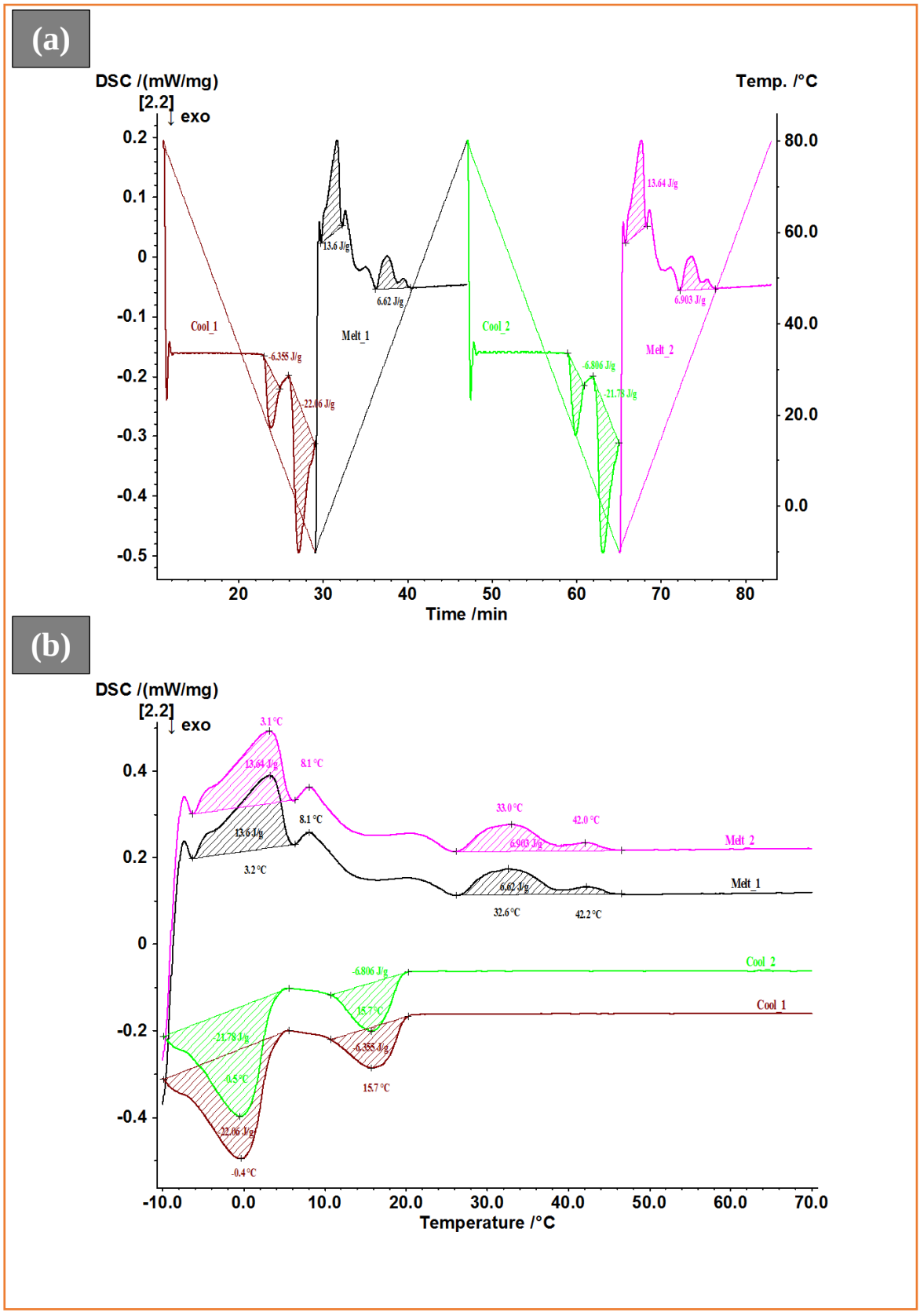

Fig 4.7: DSC thermograms showing the effect of repeated temperature cycles on thermal events, time-based (a) and temperature-based (b)

4.3 Iodine Value

Raw data of the result obtained from the titration experiments were sent to the PC through the operating software package; tables containing these data are located in the appendices. In order to verify the IV results obtained directly from the titrator, a manual calculation, based on the IV of the pure samples (olein and stearin) and the weight percent of their contributions in a particular blend, was carried out in accordance to a previous study[169] where ***x*** represents the weight fraction and subscripts ***o*** and ***s*** are olein and stearin. For instance, if the IV of pure olein and stearin are 54.04 and 35.96 respectively, for a blend, *i* that contains 40% olein and 60% stearin, the IV is calculated as thus:

$$\begin{aligned} IV_i &= [IV_o \times x_o] + [IV_s \times x_s] \\ &= [54.04 \times 0.4] + [35.96 \times 0.6] \\ &= 43.19 g / 100 g I_2 \end{aligned} \qquad (4.1)$$

The graph below (**Fig 4.8**) shows the experimental IV determined by titration for the different blends considered and as expected, the IV increases with increasing olein concentrations due to higher degree of unsaturation (presence of C=C bonds); a good correlation with a coefficient of $R^2 = 0.9964$ was observed. These experimental values showed good correlation with the calculated values.

Using the same method, the IV of the palm oil feed was determined as **52** gI_2/100g oil; hence using the fitting equation of the below graph, it can be estimated that the feed contains **0.837** olein *wt*. fraction and **0.163** stearin *wt*. fraction.

Given that it has been established that iodine value determination is based on the adopted halogen's reaction with the carbon double bonds, taking a closer look at the molecular structure of a typical unsaturated triglyceride molecule (see **Fig 4.9**), it could be argued that the halogen could also break the C = O (in the carboxyl group), as opposed to be intended C = C bond. Firstly, the bond energy of C = O is stronger than the C = C (799 > 614 kJ/mol[218]) hence the C = C will be the easier bond to break. Also, beside the fact that the iodine value is a well-established technique in the determination of the degree of unsaturation, the C = O is a common

entity for all triglyceride molecules irrespective of whether they are saturated or not, hence there will be no trend to follow if it was the target bond by the halogen.

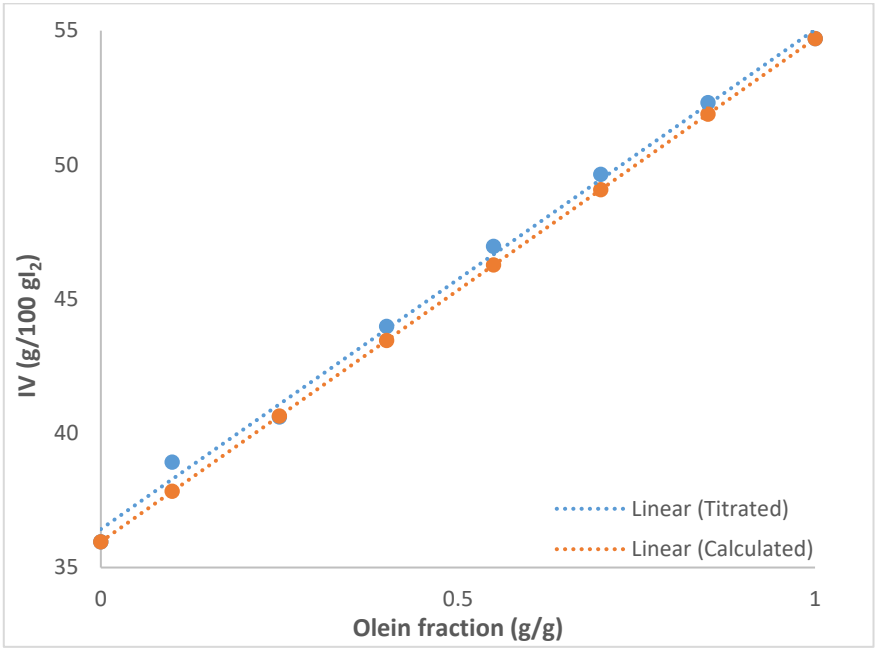

Fig 4.8: Graphical representation of iodine values (g/100 gI_2) obtained for blends with different Olein content (g/g)

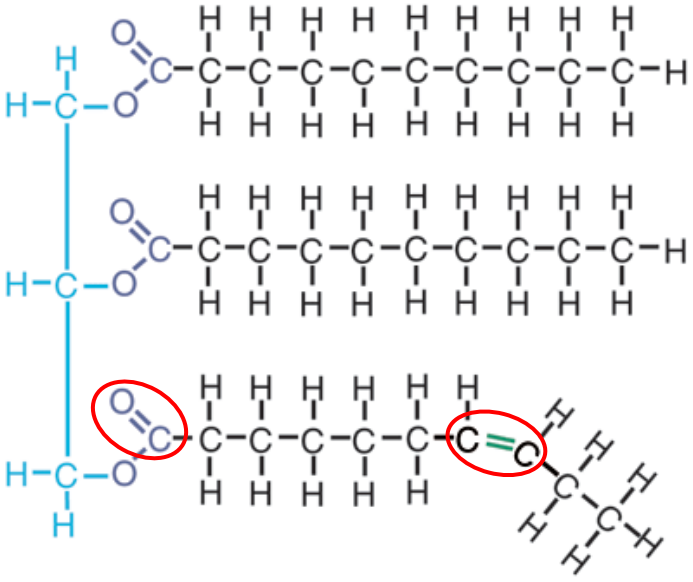

Fig 4.9: Simplistic structure of unsaturated TAG molecule, showing the C=C bond

4.4 Solubility

Two following techniques were considered for the development of the solubility of stearin in olein for the palm oil sample used in this research study.

4.4.1 Calorimetry

According to Zhou & Hartel[175], the Hildebrand equation was used to determine the heat of fusion (ΔH_{fus}) and melting temperature (T_m) from solubility (x) data at chosen temperatures (T), which were then compared with those obtained from DSC analyses; the x values were determined by gravimetric method and subsequent chromatography (for compositional analysis of the filtrate. However, for this study, the equation was used reversely, in that the ΔH_{fus} and T_m data was obtained from the DSC analysis for the palm oil feed, and then plugged into the equation to determine the solubility values (x) at a range of chosen temperature (T) values.

The melt profile of palm oil is shown in **Fig 4.5**, and the Hildebrand equation is shown in eq. (2.31). The parameters obtained from the interface software are shown below in **Fig 4.10.** The 'peak-end' temperature (when the profile returned to the base line) indicates the completion of the melting process, hence it was chosen as the melting temperature (T_m) of palm oil – previous studies have used similar approach in establishing the melting temperature of palm oil from DSC analyses due to the broadness of the endothermic peaks.[104, 175].

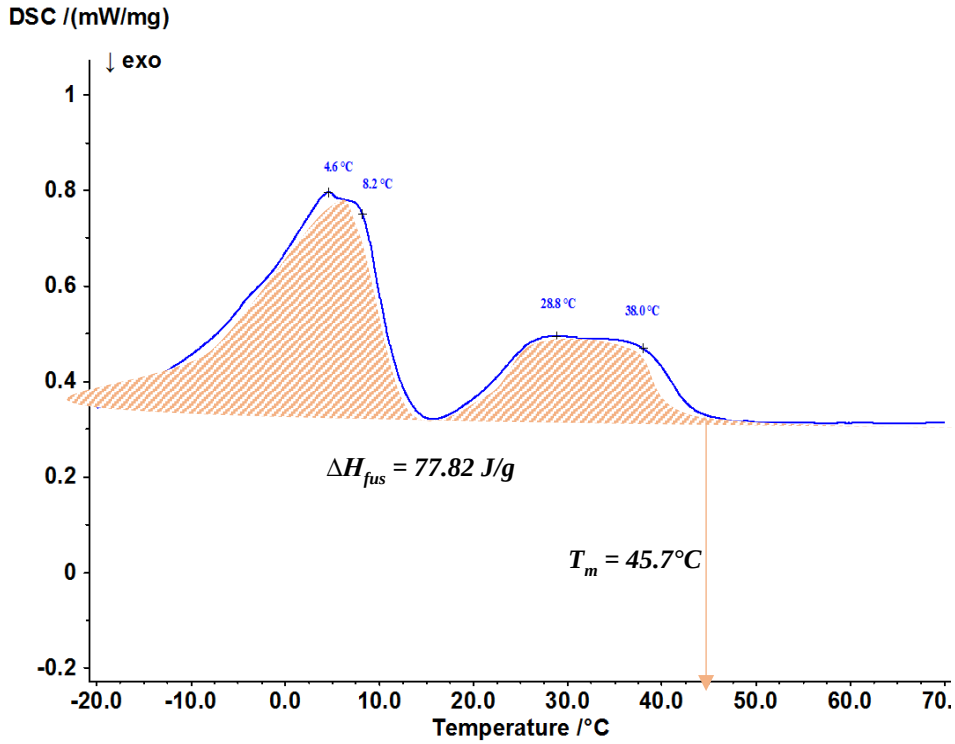

Fig 4.10: Parameters obtained from the DSC thermogram required for solubility curve determination using Hildebrand equation

To convert T_m from °*C* to *K*, 273.15K is added

T_m = 45.7 + 273.15 = **318.8 K**

$1/T_m$ **= 0.00314 K^{-1}**

To convert ΔH_{fus} from *J/g* to *J/mol*, it is multiplied by the molar mass of stearin which was taken as 830 g/mol (*assuming C16:0 forms the bulk of the FA content*)

ΔH_{fus} = 77.82 x 830 = **64590.6 J/mol**

R **= 8.314 J/mol-K**

$$\frac{\Delta H_{fus}}{R} = \frac{64590.6}{8.314} = \mathbf{7768.9\,K}$$

Hence, *ln(x)* can be calculated at chosen temperatures, T from 10°C to 45ºC. The table of results can be found in the appendices. The resultant solubility curve is given below.

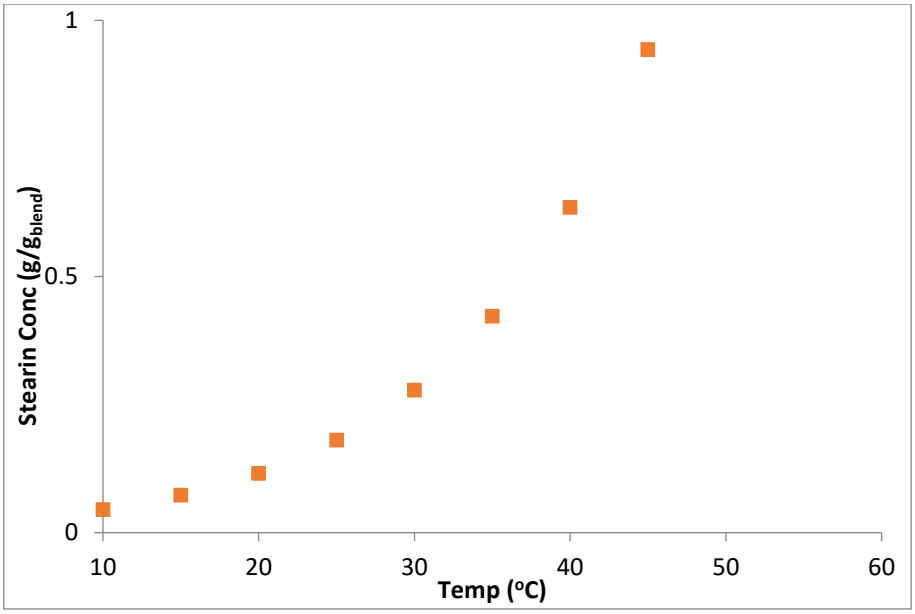

Fig 4.11: Modelled solubility curve of palm stearin (g/g$_{blend}$) using Hildebrand equation

4.4.2 Turbidity

The clear point (T_{cp}) obtained for each blend after the cooling/heating process was determined as the temperature at which the % light transmittance from the turbidity probe reaches 100% during the subsequent heating process (more detailed explanation is provided in section 5.1.1). A sample profile is shown in **Fig 4.12** and the resultant solubility curve is shown in **Fig 4.13** with an exponential fit of 0.9855 confidence level.

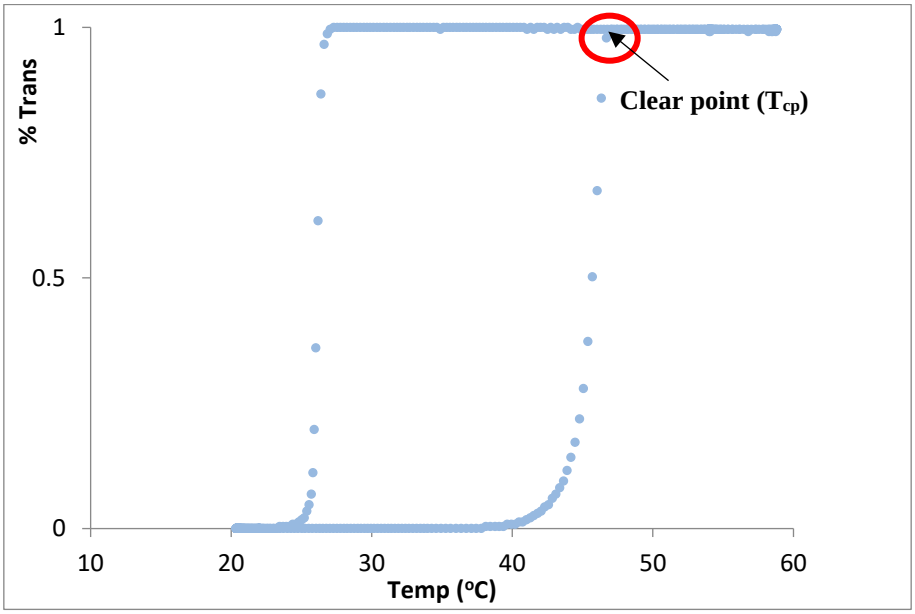

Fig 4.12: A sample turbidity/temperature profile of cooling → heating steps indicating clear point (T_{cp}) using in calculation for solubility curve determination

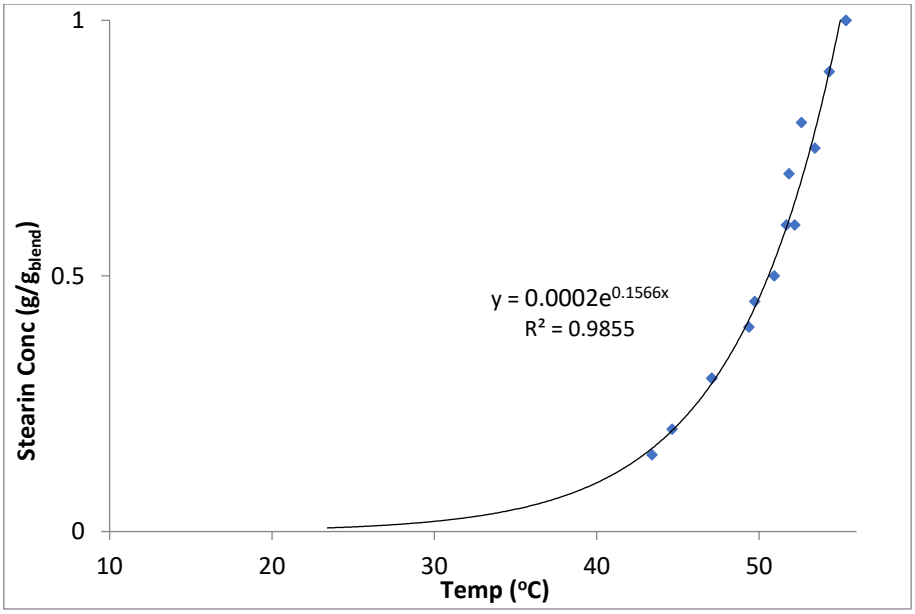

Fig 4.13: Solubility curve fitting using the clear points (T_{cp}) obtained from the turbidity measurements

These two curves were then compared with a solubility curve of palm stearin in palm olein, generated from a previous study carried out on model lipid systems; it should however be noted that compositional method using chromatography technique was used in this *referenced* study but it was chosen as a reference due to the similarity of the palm oil composition used to this present research[175]. From the comparison made (see **Fig 4.14**), the wide difference between the curve from the Hildebrand equation and the reference curve would be due to the fact that the equation was designed with the supposition that the two systems (olein and stearin in this case) form an ideal solution but due to the wide range of the TAGs present in palm-based fats & oils, (*see HPLC chromatograms*), there are bound to be aberrations from this ideal property. The stearin's fatty acid content on purely palmitic acid ($C_{16.0}$) could also have contributed to the variation. However, it could be seen that the curve from the turbidity analysis was closer to the reference, hence was chosen for further usage in this research; the slight difference would be attributed to the differing TAG compositions of the stearin and olein used in each studies.

In view of this, the clear point (T_{cp}) of the palm oil feed was determined using the turbidity measurement and estimated as 45°C; hence using the fitting equation (**Conc = 0.0002e$^{0.1566T}$**), the stearin concentration of the feed was estimated as **0.230 g/g**; comparing this with the iodine value estimation of 0.163 g/g, a consistency can be inferred within reasonable margin of experimental error.

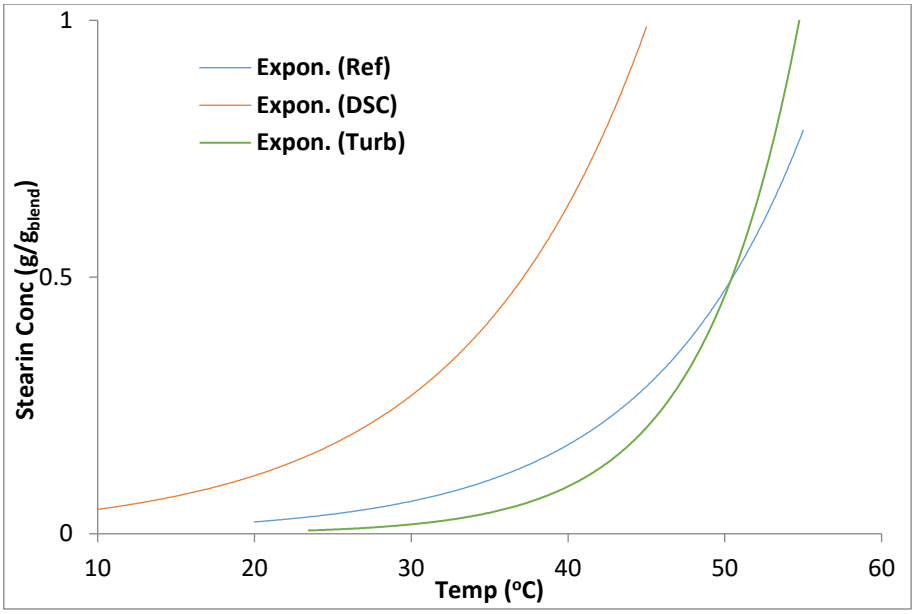

Fig 4.14: Comparison of solubility curves obtained from the various analysis methods considered in this study, as well as a curve from a previous study used as a reference

CHAPTER 5 – RESULTS: Analyses in the Batch Mode

In this chapter, the results obtained from the experiments carried out in the batch operation were outlined and discussed using relevant theories and references. The experiments included kinetics study, with respect to metastable zone width (MSZW) measurements and parameter estimation, and filtration study.

5.1 Kinetics Study

This was in two parts: Firstly, the effects of cooling rate and mixing intensity on metastable zone width of palm oil crystallisation was examined. Secondly, these MSZW data coupled with existing model equations were used to extract kinetics parameters to characterise the crystallisation process.

5.1.1 Metastable Zone Width

The turbidity system used for this analysis was designed to measure the intensity of light sent through the solution and back to the detector via a mirror; as the particles concentration increases, the light intensity drops, and turbidity increases. Hence the output signal of the turbidity decreases as the crystallisation process proceeded[219]; a sample output signal is shown in **Fig 4.12**. From this profile, the point where the turbidity signal picked up denotes the onset of nucleation; the maximum turbidity signal is an indication of complete crystallisation but it is subject to the maximum solid concentration the probe is designed to detect; the point where the signal returned to its set minimum during the heating segment denotes complete dissolution (i.e. melting) of the solid particles (i.e. stearin) and the oil is completely clear.

For the MSZW analysis, *% transmittance* data was used, which is basically the inverse of the turbidity data. A *pre-nucleation* baseline temperature range was selected from the raw data, and the turbidity signal within this range was averaged and taken as the set minimum. The temperature at which the signal *increased by 10%* of this minimum value during the cooling step was taken as the nucleation temperature (T_{nu}), while the temperature at which it dropped back to 10% above the minimum during the heating step was taken as the dissolution temperature (T_{ds}); MSZW was then calculated as the difference between T_{nu} and T_{ds}. This

calculation method was based on a previous study[43, 220]. To convert the turbidity values to percentage transmittance, the below expression was used:

$$\left[1-\left(\frac{I_{act}-I_{\min}}{I_{\max}-I_{\min}}\right)\right]\times 100 \qquad (5.1)$$

Where I_{act} = Actual turbidity value

I_{min} = Minimum turbidity value in the data set

I_{max} = Maximum turbidity value in the data set

Effect of mixing intensity on MSZW

At a constant cooling rate of 1.0 °C/min, a graphical representation of the MSZW results obtained at different mixing conditions in the STC and OBC are shown in **Fig 5.1**. A glance at these graphs and also at Table 5.1 show an average MSZW of 19 °C for the STC, and 20 °C for OBC for all the mixing intensities considered, which is within similar range reported in previous studies on palm oil crystallisation; the negligible change in the MSZW with mixing intensity indicates that the nucleation behaviour of palm oil is practically independent of the mixing conditions (with respect to power density, P_d) considered in both set-ups, because the nucleation temperature, hence the MSZW was generally similar for the range of mixing intensities considered. It could therefore be inferred that crystallisation of palm oil is more kinetically-controlled than mass transfer controlled; this is consistent with the fact presented earlier in this thesis (section 2.2) that crystallisation from melt (CfM) is dominated by heat transfer effects, and this is what differentiates it from the regular solution crystallisation which is dominated mass transfer effects[45]. For instance, a decreasing trend in MSZW with increasing mixing intensity was reported in a related previous study based on L-glutamic acid (a typical API) which was attributed to increased mass transfer and reduced interfacial boundary layer[221], this goes further to reiterate the differences between API (solution) and palm oil (melt) crystallisation in this aspect.

However, an inflection in the turbidity profile was observed during the heating step between 30 °C and 40 °C (see orange circle in **Fig 5.1**), and this was consistently observed in subsequent turbidity data obtained through out this study; this could be attributed to the suspected

polymorphic transformation to a more stable crystal form that occurs during the melting process which is often characterised by a consecutive crystallization and melt event during thermal analysis (i.e. an exothermic peak indicating the crystallisation event, followed immediately by an endothermic peak indicating the melting event), as explained in sections **2.3.5** and **4.2** with respect to the exothermic event observed in the DSC melting profile of palm oil. A zoomed-in view into this region showed that the inflection became relatively less defined with increasing mixing intensity (see **Fig 5.2**), which might indicate that crystallization of the more stable polymorph was already favoured at the higher mixing condition dismissing the need for polymorphic transformation into the stable crystal form during melting.To support this hypothesis, in a previous crystallisation studies carried out on L-glutamic acid, it was reported that the α-form (the less stable polymorph) was favourably crystallised in the stagnant zones (i.e. poorly mixed regions) within the crystallisation vessel (a stirred tank crystalliser was used in this referred study), which relates to low mixing condition, while the β-form (the more stable polymorph) was favourably crystallised at higher mixing intensity conditions[43]. Linking this to the thermal analysis discussed earlier, considering the temperature region where this inflection was observed in the turbidity heating profile (between 30°C – 40 °C), it can be inferred that the β-polymorph of palm oil solid product can be selectively targeted and obtained if the crystallisation process was carried out within this temperature region – recall it was highlighted in section 4.2 that the high temperature endothermic events observed between 20°C and 40 °C were attributed to the β_1' and β_1 polymorphs.

Alternatively, the inflection could also be said to be a function of the thermal history that the palm oil batch had been subjected to, as it should be noted that the same batch of palm oil was repeatedly used for all the experiments carried out in this section of the study; however from the profile obtained from repeated cool/heat cycles during DSC thermal analysis shown in **Fig 4.7**, it was established that repeated heating/cooling events had little effect on the crystallization properties of palm oil in relation to nucleation temperature and corresponding energy change; though a more significant effect might have been observed if more cycles were examined and/or if the temperature range considered was wider such that deleterious effects to the chemical structure of the triglycerides chains/bonds becomes a concern. Therefore, it can be concluded that the hypothesis relating to the polymorphism was more likely responsible for the inflection observed in the heating step of the turbidity profile. This then suggests that mixing intensity plays an essential role in crystal polymorphs. This would however require further

investigation, but was not covered within the scope of this research study. Furthermore, it has been reported that CfM generally exhibit faster growth rates – between 10^{-4} and 10^{-6} m/s compared to 10^{-7} and 10^{-9} m/s for solution crystallisation[49]; this suggests rapid diffusion and integration (i.e. mass transfer) of the crystalline particles to the crystal surface, to which the similar structural property of both solute (stearin) and solvent (olein) could be attributed. Also, due to the fact that the viscosity of the resulting slurry becomes relatively high at low temperatures, the rate of heat transfer across the system could begin to diminish thereby becoming the rate-determining (i.e. controlling) factor[92]. **Table 5.1** shows that the mean MSZW was 19.3±0.1°C in the STC and 20.2±0.2°C in OBC; this minimal difference observed between these two set-ups (1.0±0.2°C) attests to the previous observation explained above regarding the independence of the crystallisation behaviour of the palm oil on mixing conditions; the close nucleation temperatures (mean = 25.3±0.1°C) also confirms this inference. It can therefore be concluded that the mixing properties (intensity and mechanism), within the range considered, has little to no effect on the inherent properties of palm oil (a typical ***melt***) crystallisation.

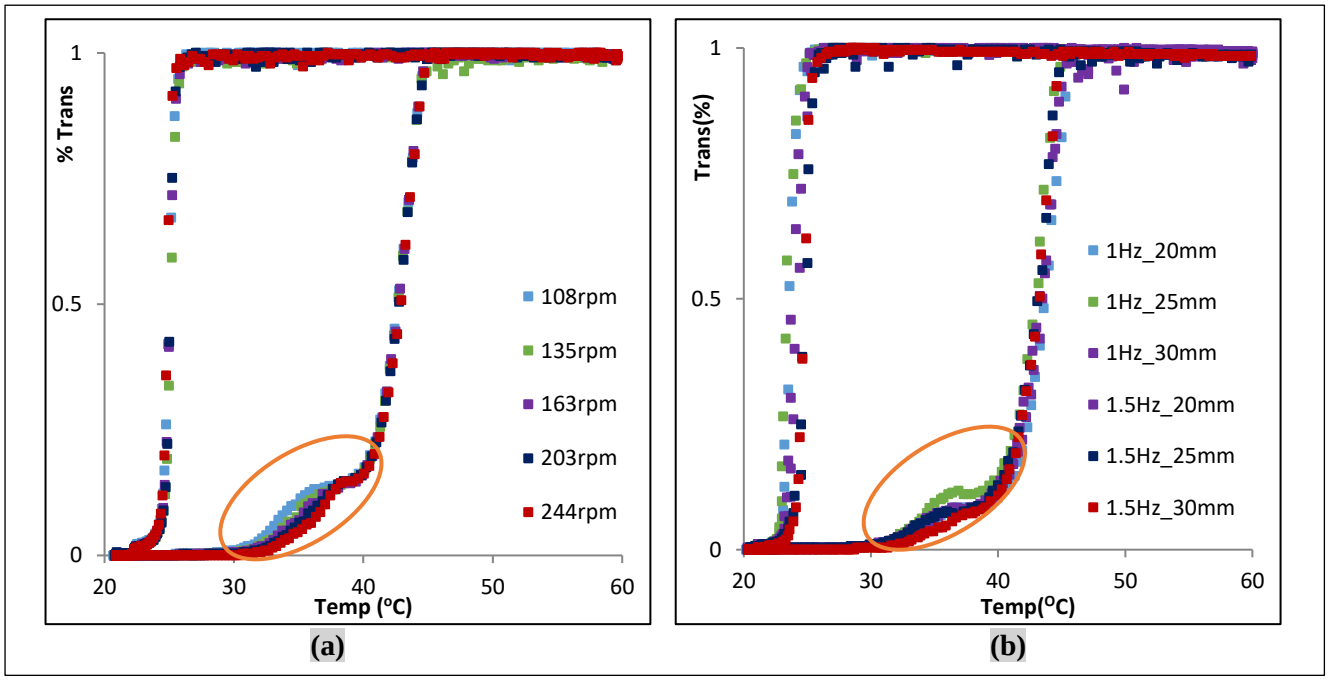

Fig 5.1: MSZW profiles obtained for variable mixing intensities at constant cooling rate of 1.0 °C/min for STC (a) and OBC (b)

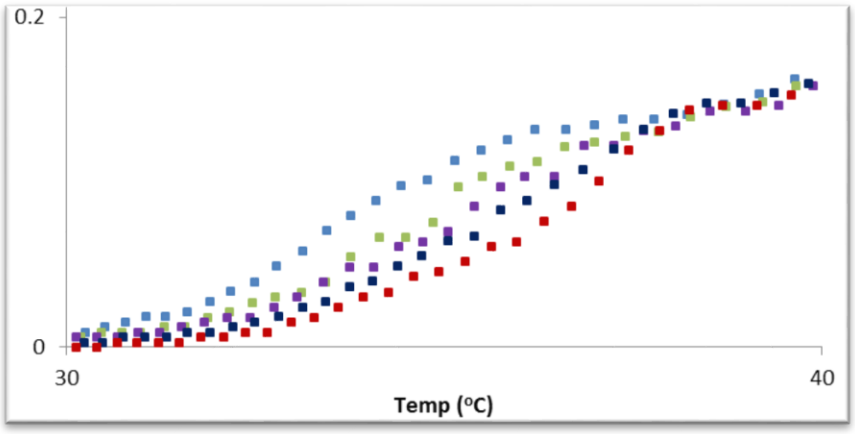

Fig 5.2: Zoomed-in view of MSZW profile for variable mixing intensity showing the inflection between 30°C and 40°C

Table 5.1: Results obtained for MSZW at variable mixing intensities at constant cooling rate

P_d (W/m^3)	STC			OBC		
	T_{nu}	T_{ds}	MSZW	T_{nu}	T_{ds}	MSZW
37.5	25.7	44.9	**19.2**	25.0	45.3	**20.3**
73.3	25.8	44.9	**19.1**	24.5	44.9	**20.4**
126.6	25.5	44.6	**19.1**	25.3	45.4	**20.1**
126.6				25.0	45.7	**20.7**
247.3	25.5	44.9	**19.4**	25.4	45.2	**19.8**
427.4	25.2	44.7	**19.5**	25.4	45.1	**19.7**

Effect of cooling rate on MSZW

The MSZW showed some dependence on cooling rates as shown in **Fig 5.3** and **Table 5.2**; it was observed to increase from 17°C – 20°C for STC, and 17°C – 22°C for OBC with increasing cooling rate. This is consistent with related previous studies on crystallisation [40, 109], and has been attributed to a higher rate of supersaturation within a specified time scale, and longer relaxation period required for stable nuclei to be formed at fast cooling rates[222]. However, the relatively low sensitivity of the MSZW to change in cooling rate (that is the small magnitude of the difference of only 3 – 5°C when cooling rate was quadrupled) should be noted, and this is consistent with a previous study where the MSZW reportedly varied from 13°C – 19°C (difference of 6°C) for cooling rates increasing from 0.2°C/min to 3°C/min (increased by over 10x) [109] – compare with a MSZW increase of 25°C when the cooling rate was increased from 0.5 °C/min to 3 °C/min in the crystallisation study of L-glutamic acid,

which is a typical API[220]. This low sensitivity of the MSZW to change in cooling rate in the crystallisation of palm oil was attributed to the fact that the oil/fat system is already highly supersaturated by the time the *cloud point* (as detected by the turbidity probe) is reached such that majority of the crystallisable materials crystallises (crashes out) at the onset of nucleation indicating *instantaneous* nucleation mode (see the sharp drop in %transmittance from $T < T_{nu}$ in **Fig 5.3**) which then implies that the equilibrium concentration (C^*) at the cloud point is so low that the supersaturation ($\Delta C = C - C^*$) at this point is approximately equal to the starting concentration (C). It is therefore probable that the range of cooling rates considered in this study (0.25 °C/min – 1.0 °C/min) is not wide enough to detect a significant variation in the metastable zone width of the palm oil crystallisation. This conclusion is consistent with the relatively small change in exothermic peak temperature when the cooling rate was increased, during the thermal analysis discussed in section 4.2.1. It should however be noted that the starting concentration of crystallisable material (that is TAG fractions that consist of saturated fats) present in the system also plays an important role on how cooling rate affects its nucleation behaviour; in other words, the solid fat content of the system to be crystallised is an essential factor in characterising the nucleation kinetics with respect to cooling rate; see section 2.5.5 for more information on solid fat content. This was however not investigated further in this study, and will be recommended as a future work for this research.

Regarding the inflection in the turbidity profile, which had been attributed to the polymorphic transformation of palm oil crystal forms, it was observed to be within similar temperature region as discussed earlier (30 – 40°C), but it was observed to have shifted to a higher % transmittance region for the 0.25 °C/min in the STC results; this can simply be attributed to the sensitivity of the turbidity probe at the time bearing in mind that the probe system is designed in such a way that it is unable to distinguish between real crystals and bubbles formed due to the high agitation in the vessel. It was stated earlier that the effect of cooling rate on the polymorphism is largely a function of the starting concentration – a previous study reported that the β crystal form was obtained for a higher starting concentration (40 – 45 mg/mL) irrespective of the cooling rate adopted, while the α form was obtained at a lower concentration (15 – 30 mg/mL); but this study was based on the OBC system hence the results were attributed to the more uniform mixing achieved in the oscillatory baffled system, because a different result was said to be obtained in the stirred tank system where the α form was obtained but transformation to the β form was only obtained when a higher mixing condition

was applied [220]. This again strengthens the significant impact that mixing have on crystal polymorphism, and also buttress the role of starting concentrations.

For results comparison between STC and OBC, the nucleation temperatures (T_{nu}) do not show any particular trend between these two set-ups, again echoing the inference drawn earlier regarding the negligible effect of varied mixing conditions on palm oil crystallisation with respect to nucleation temperature. However, the MSZW was observed to be generally higher in the OBC, which was actually more to do with variation in the dissolution temperature (T_{ds}) as opposed to the nucleation. It is expected that the dissolution temperature should be unaffected by the operating conditions (i.e. cooling rate and mixing intensity), since the composition of the starting material remained unchanged; the dissolution temperature is meant to represent the saturated temperature, while the heating profile in the turbidity profile should represent the solubility curve of the system being analysed[223]; hence this discrepancy, which was more evident when the cooling rate was varied, suggests that the heating rate does have some impact on the solubility of the palm oil fractions; in the previous study referred to earlier, the heating rate adopted in the MSZW experiments was kept constant irrespective of what cooling rates were considered, but in this research, the heating rate was varied along with the cooling rates which may explain the observed discrepancies in T_{ds}. Having said that, it should however be noted that this theory of constant T_{ds} is mostly applicable to systems consisting of pure solutes (i.e. single component systems), but palm oil is a multi-component system, each having different thermal properties (e.g. solubility) that would behave differently under different cooling rate conditions. For instance, in the referred study which involved a mixed system of POP and PPP, it was reported that high melting fractions (HMFs) separate from the solution at low cooling rates causing a higher T_{ds}; whereas at higher cooling rate, both HMFs and mid-fractions co-crystallise and dissolve at lower temperature causing a lower T_{ds}. In summary, it can be concluded that temperature has more effect than mixing on the crystallisation of palm oil, and its multicomponent property plays a major factor in distinguishing this process from the generic solution crystallisation.

Given the apparent effect of heating rate on the dissolution temperature of palm oil, the true dissolution temperature (*true*-T_{ds}, which would represent the kinetic solubility) can be taken as the dissolution temperature at 0 °C/min. This is determined as the *y*-intercept of the plot of obtained dissolution temperatures (T_{ds}) versus the heating rates (which was the same as the

cooling rate used). See graphs in **Fig 5.4**. Using the *equation of line* for these graphs, the true dissolution temperatures (i.e. the kinetic solubility) of the palm oil used in this study can be extrapolated as 45.9°C and 48.3°C in the STC and OBC respectively. The higher value observed in the OBC could be attributed to the effect of mixing mechanism (stirring vs. oscillation) on the heat transfer across the crystallisation vessel; this was however not investigated further in this study.

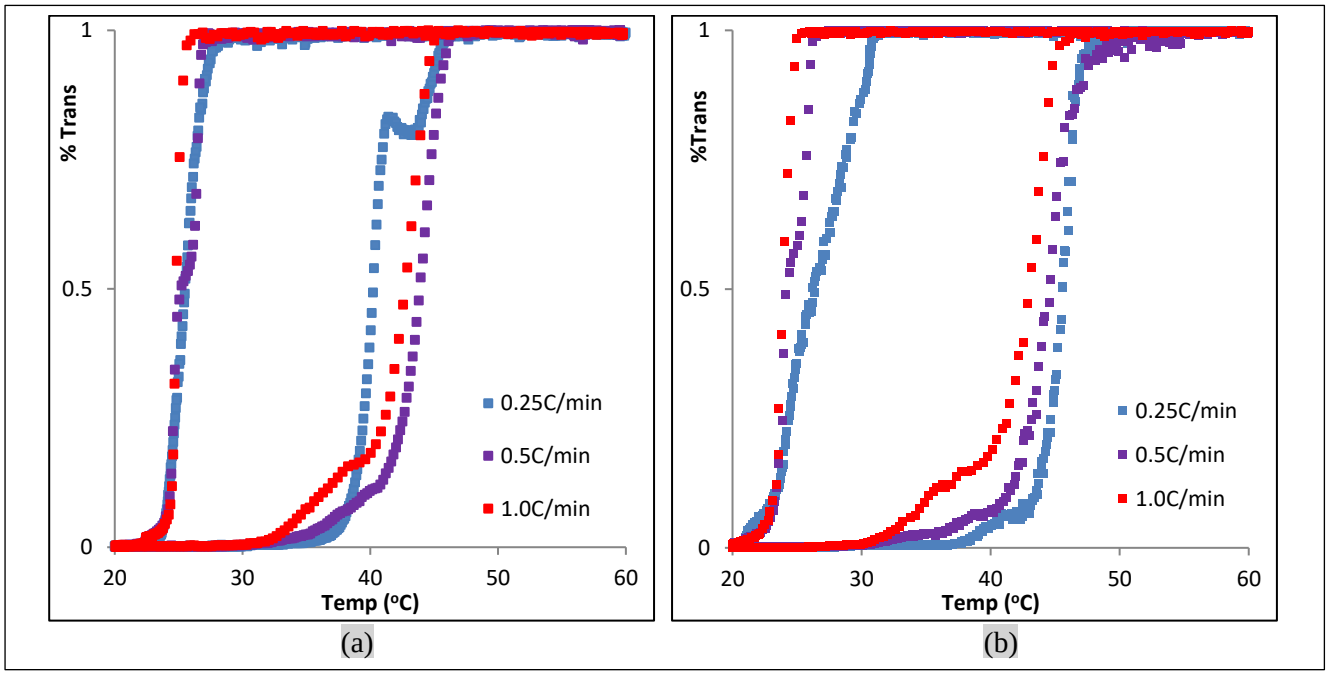

Fig 5.3: MSZW profiles at variable cooling rates at constant mixing intensity for STC (a) and OBC (b)

Table 5.2: Results obtained for MSZW at variable cooling rates at constant mixing intensity

ΔT/t (°C/min)	STC (°C)			OBC (°C)		
	T_{nu}	T_{ds}	MSZW	T_{nu}	T_{ds}	MSZW
0.25	27.9	45.6	**17.7**	30.4	47.4	**17.0**
0.5	26.2	45.6	**19.4**	25.2	47.2	**22.0**
1.0	25.4	45.0	**19.6**	24.6	45.5	**21.0**

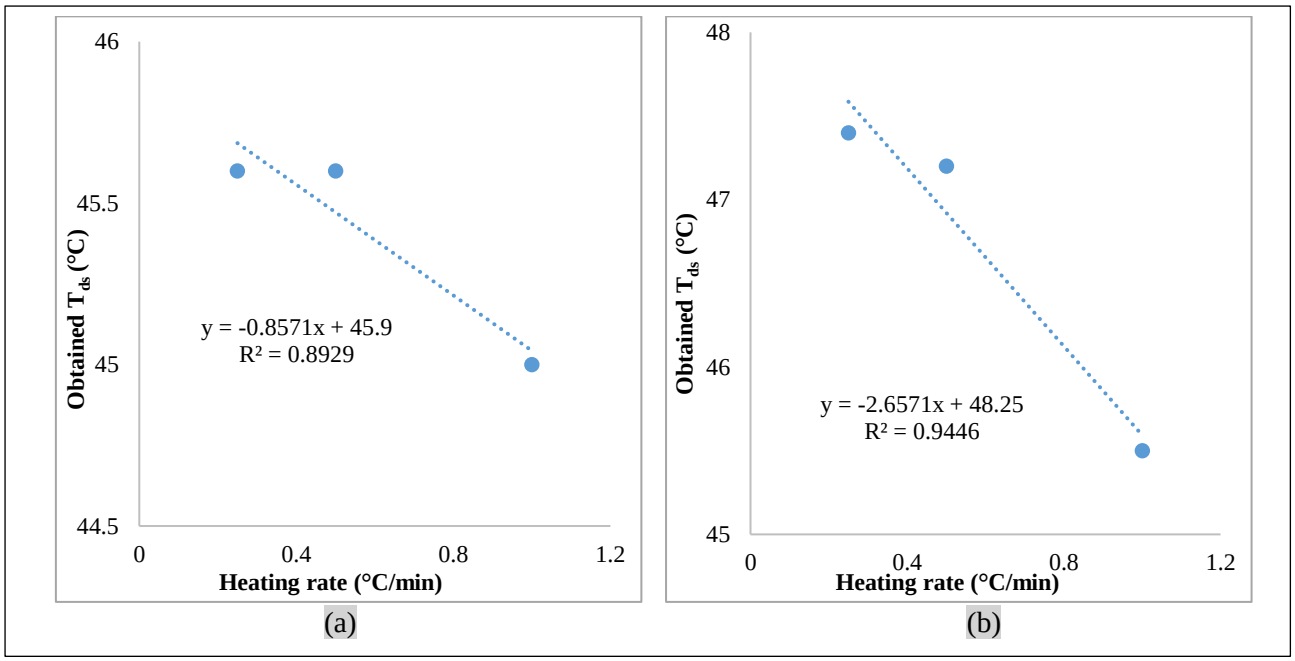

Fig 5.4: Plot of obtained dissolution temperature vs. heating rate used to determine the true dissolution temperature, for STC (a) and OBC (b)

Data Reproducibility

In order to establish the reliability of the turbidity data obtained in this study, the experiments were repeated, maintaining the same batch of feed palm oil and operating conditions (i.e. same mixing intensity and cooling rate); this was also in order to examine if there was any (deleterious) effects of repeated thermal history on the crystallisation behaviour of the palm oil feed. From **Fig 5.5** and **Table 5.3**, it can be observed that the nucleation and dissolution temperatures for each set of experiments are comparable to one another; though for the 0.25 °C/min dataset in **Fig 5.5a**, the %transmittance at which the inflections in the heating step of the turbidity profile (earlier attributed to polymorphic transformation into a more stable crystal form, β, of palm oil) were observed to have varied between repeats, and this could be simply related to the sensitivity of the turbidity probe at the time of the experiments, since these inflections were still within the same temperature region for each set of experiments. From the data shown in **Table 5.3** below, the standard error is <5% hence a confidence level of 98% can be assumed. All in all, it could be concluded that the turbidity data is quite reliable and that re-using the same batch of palm oil through repeated cooling/heating cycles has no significant effect on the crystallisation kinetics results obtained with respect to nucleation temperature and consequent metastable zone width; this is consistent with the conclusion drawn in section 4.2.1 above during the extended thermal analyses where repeated cool/heat cycles showed exothermic and endothermic events at similar peak temperatures and enthalpy changes for each cycles.

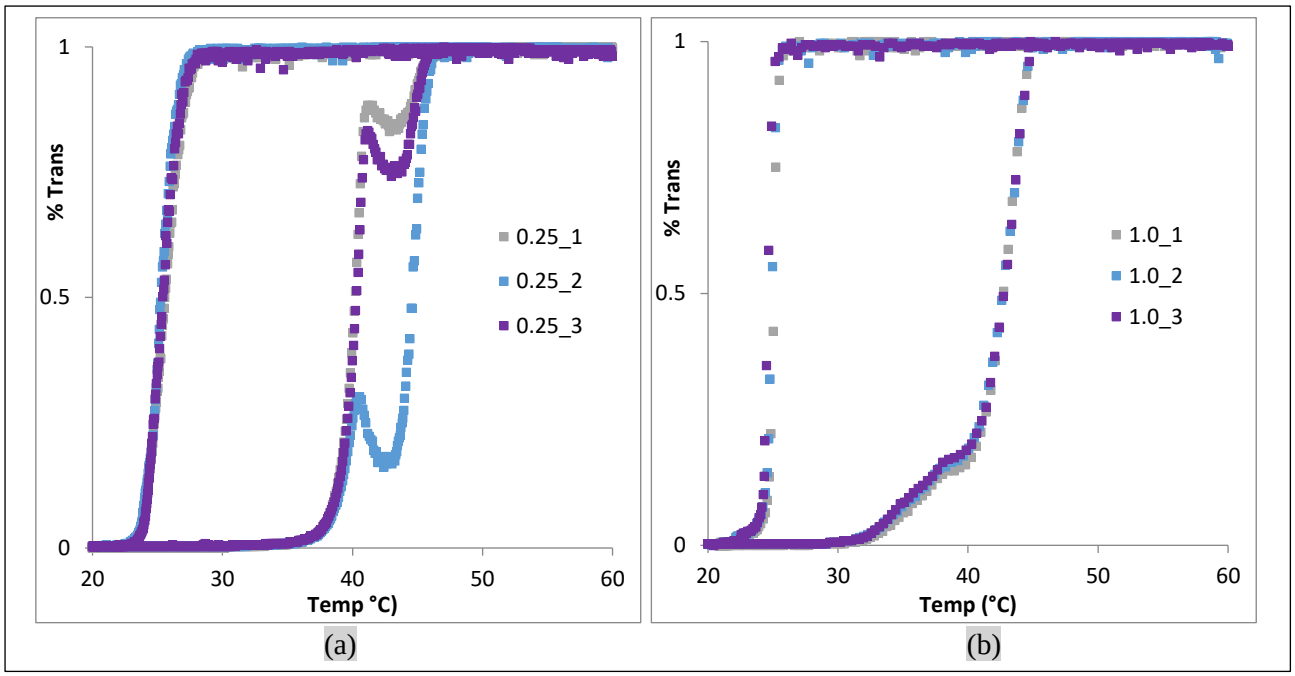

Fig 5.5: Turbidity profile for repeat experiments (cooling rates of 0.25 °C/min and 1.0 °C/min) demonstrating data reproducibility (*mixing intensity = 203 rpm,*)

Table 5.3: Extracted turbidity data from repeated experiments as shown in Fig 5.5

	0.25 °C/min			1.0 °C/min		
	T_{nu}	T_{ds}	MSZW	T_{nu}	T_{ds}	MSZW
1	27.9	45.6	17.7	25.5	44.9	19.4
2	27.3	46.2	18.9	25.5	45.0	19.5
3	27.9	45.6	17.7	25.2	45.1	19.9
Average			**18.1 ± 0.4**			**19.6 ± 0.2**

5.1.2 Kinetics Parameter Extraction

This section of work has been published in the International Journal of Engineering Research & Science (IJOER) – Vol.2, Issue 10.

In this section, the aims of the study are to evaluate and compare the kinetics from a typical melt (i.e. palm oil) crystallisation and those obtained from the crystallisation of organics, using data extracted using empirical models; the study also aims to establish critical understanding on the various model approaches and their applications.

Data Obtained for Model Analysis

For the palm oil feed, it has been assumed that the solid phase is the *stearin* while the liquid phase is *olein,* and these are represented in the cooling and melting thermograms obtained from the thermal analyses carried out, as discussed earlier in section 4.2. The analyses referred to was carried out based on variable temperatures (i.e. changing with time), hence it is referred to as 'Dynamic Thermal Analysis' where the effect of cooling rate on the crystallisation behaviour of palm oil was established. Also, it is from this analysis that the melting point (T_m) of the palm oil feed was obtained (to be discussed later).

Some of the other data required for the model analysis were also obtained from DSC analysis but in the isothermal mode, where thermal profiles obtained at specified end temperatures were explored. The isothermal crystallisation thermograms at different end temperatures between 293 K and 301 K are shown in **Fig 5.6** where the crystallisation enthalpy changes (that is exothermic events) are plotted as a function of time. The induction time (τ) is determined as the period from the beginning of the isothermal process to the time when the thermal trace deviated from the baseline due to crystallisation event i.e. exothermic peak onset (see annotation on **Fig 5.6**). It can be seen that the time taken for crystallisation to begin (i.e. induction time, τ) increased with increasing end temperatures, from *ca*. 20 min – 70 min when end temperature was increased from 20°C (293 K) to 28°C (301 K). This can be attributed to reducing degree of supercooling with increasing end temperature, in that the higher the end temperature, the closer to the equilibrium temperature the system becomes, thereby reducing the crystallisation driving force. In order to assess further the effect of end temperatures on the crystal properties, a batch of melted palm oil was cooled to the respective end temperatures, and the slurry was sub-sampled and analysed by light microscopy. Images obtained from the

polarised light microscope is shown in **Fig 5.7**, where show different crystal morphologies from samples collected after about 1 hr for the different crystallisation temperatures is observed; for instance, fully-formed spherulitic crystals were observed at 293 K, dendritic spherulites at 303 K and a developing spherulites at 298 K, which supports only one morphology at a given crystallisation temperature studied. the apparent 'loosened' crystal morphology observed at the higher temperature can be taken as a function of temperature on the crystal network of fat systems.

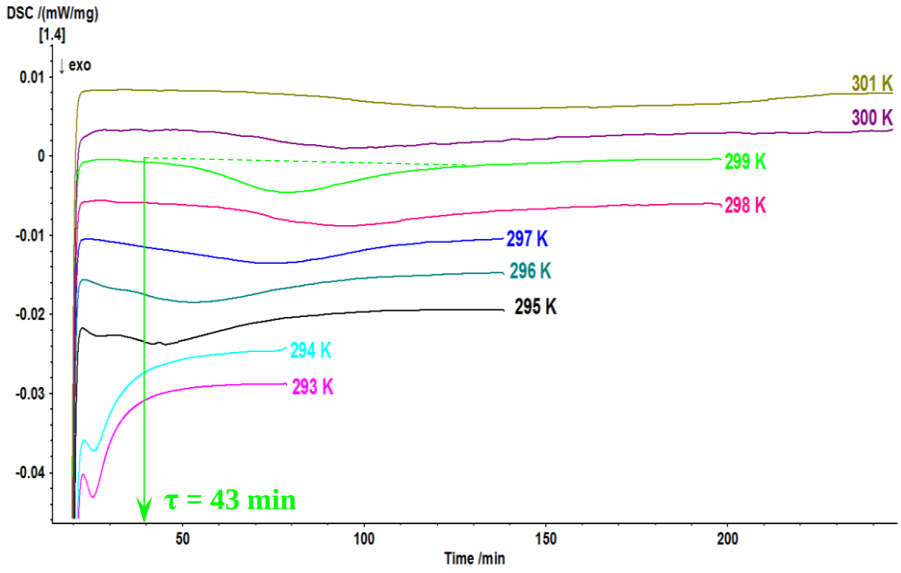

Fig 5.6: Isothermal DSC thermograms showing induction times (τ) at different end temperatures

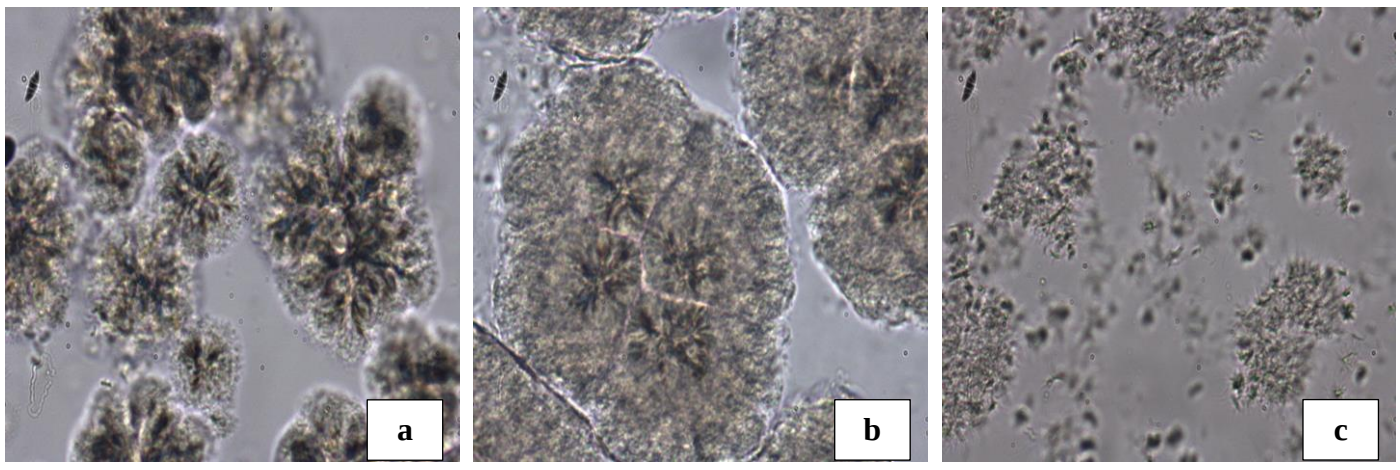

Fig 5.7: Microscopic non-polarised images of palm stearin crystals obtained from crystallising at 293 K (a), 298 (c), and 303 K

Avrami Model

Using the DSC isothermal crystallisation thermograms and the induction time analysis, a plot of the solid fraction (***x***) against time (***t***) is shown in **Fig 5.8** which is the well-known sigmoid curve for isothermal fat crystallisation (***x*** can also be referred to as the percentage of crystallinity). The changing gradient within each of the curve has been attributed to the stages involved in a crystallisation from the initial formation of nuclei, followed by a rapid growth of these nuclei to form crystals, then the slowing down by impingement due to colliding crystal faces[62, 224], as indicated on the right of the graph. The particular shape of this curve for each end temperature is a pointer to the crystallisation properties of each condition. The highlighted stages were relatively more defined at the higher temperatures (≥296 K) showing obvious "S" shaped curves, but the stages were not as obvious at the lower temperatures (≤296 K). this is due to the fact that nuclei formation and subsequent crystal growth occur at a faster rate at low temperatures such that the whole crystallisation process is completed within a short period of time; the short induction time observed earlier in the isothermal thermograms of the low end temperatures attests to this[7].

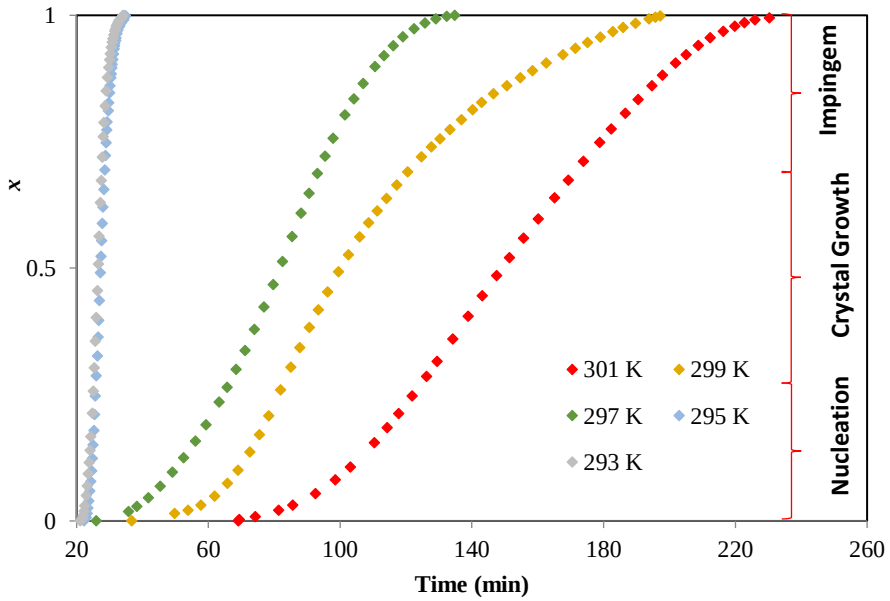

Fig 5.8: Percentage of solid fat fraction (*x*) per induction time (min) at different end temperatures

It is therefore evident that crystallising at different end temperatures will show different mechanisms with respect to the crystallisation rate and also the crystal product properties, hence the Avrami theory has been used to assess this further.

By plotting ln[-ln(1–*x*)] against ln(*t*), ***x*** values between 25% and 75%[64] are shown as a function of the crystallisation time in **Fig 5.9**, a good linear relationship (R^2 > 0.99) was obtained, indicating the applicability of the model to the fat system used in this study. The resultant ***n*** and ***k*** values from the gradient and intercept of this plot are shown in **Table 5.4** for the different end temperatures considered. It can be seen from this table that the Avrami exponent (***n***) for the palm oil used in this study was relatively unaffected by the end crystallisation temperatures within the range considered, as it was relatively constant (2.5±0.2, P > 0.05 using ANOVA with single factor analysis). This implies that the crystallisation mechanism within the end temperatures considered, were relatively similar. The ***n*** value is an indication of the growth mechanism of the crystals formed according to Kawamura[225] and Wright *et al*[226], which ranges from *rod-like* growth (from instantaneous nucleation) for n = 1 to *polyhedral (spherulitic)* growth (three-dimensional) for n = 4, which then suggests that smaller n-values correspond to faster nuclei formation and eventual growth, while a larger n-value is an indication on slower (and more complex) crystal formation . In this study however, the average n-value obtained is ≈ 3 hence the crystal growth mechanism can be taken as *plate-like* (i.e. two-dimensional growth), bearing in mind that only a range of 8 °C (20 – 28 °C) was covered in this study. A related previous study where the considered temperature ranged from -10°C to 20°C, an increase in n-value with increasing temperature was observed, and the trend was reported as changing from rapid nucleation due to high supercooling (or supersaturation) at low temperature to periodic nucleation due to low degree of supercooling (or supersaturation) at high temperature[7]. It should also be noted that the small range of temperature considered in this study might be responsible for the similar morphology of crystals observed at the different temperatures by light microscopy, which were just differing in level of formation from fully formed spherulites to loosened dendritic ones (see Fig 5.7).

Previous studies have however reported ***n*** values around or greater than 4 for palm oil crystallisation which was attributed to sporadic and heterogeneous nucleation. The difference between the n-values obtained in this study and the reported range for palm crystallisation could be due to differing triglyceride compositions of the palm oil sample used in the respective studies; also, the cooling rates used for the DSC analyses has also be highlighted as a possible determining factor (unpublished work by Toro-Vazquez *et al*[212]).For the overall rate constant (*k*) also shown in **Table 5.4**, it generally decreases with increasing end temperatures, indicating a slower crystallisation process at higher temperatures as expected[43]; this is a

function of the driving force of crystallisation which reduces with increasing end temperature, thereby slowing down the crystallisation rate. The sharp increase in the rate constant (k) from 296 K to lower temperatures can be linked to possible polymorphic transition occurring at those temperature regions; this would however require further assessments such as x-ray diffraction technique, to ascertain the polymorphic forms of crystals at those temperature regions (this was not explored further in this study) . In summary, the rate constants (k) obtained from this work fall within the similar range as the previous work, suggesting similar crystallisation kinetics [227].

It should be noted that the *n*-dependency of the unit of these ***k*** values (s^{-n}) makes it impossible to compare with related values from other models; hence the trend of the ***k*** with respect to the end temperatures, as opposed to the actual values, is the key element from this model.

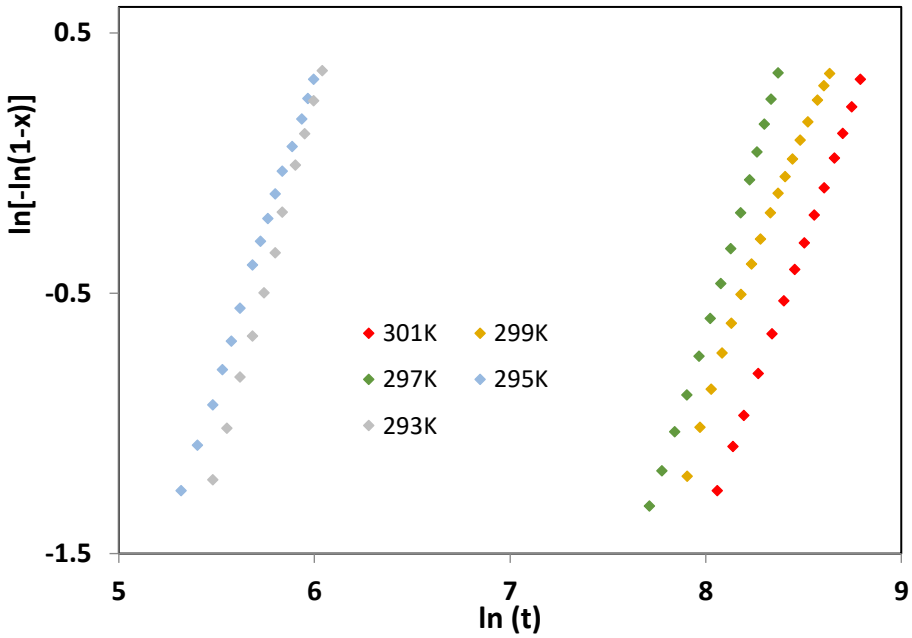

Fig 5.9: Plot of ln[-ln(1–*x*)] vs. In(*t*) used to determine kinetics parameters in Avrami model analysis

The Fisher-Turnbull model

The results discussed above give an indication of the *overall* crystallisation kinetics. In order to examine just the nucleation occurrence, the Fisher-Turnbull equation was used to estimate the activation free energy barrier (ΔG_c) needed for the formation of stable nuclei. The related plot of ($\ln(T\tau)$ against $1/T(\Delta T)^2$) and the calculated values of ΔG_c together with the estimated nucleation rate constants (k_n) using eq. (2.19 – 2.21) are shown in **Fig 5.10** and **Table 5.4** respectively. Note that the melting temperature (T_m) used to calculate ΔT was taken as the peak end temperature of the melting curve shown in **Fig 4.5** which was estimated as 45.7°C, using the thermal analysis software. The 'peak-end' temperature (when the profile returned to the base line) indicates the completion of the melting process, hence it was chosen as the melting temperature (T_m) of palm oil – previous studies have used similar approach in establishing the melting temperature of palm oil from DSC analyses due to the broadness of the endothermic peaks.[104, 175]. The plot shown in **Fig 5.10** effectively displays the relationship between the energy barrier for nucleation (the vertical axis) and the inverse of supersaturation (the horizontal axis); the data indicates that the higher the crystallisation temperature, the higher the energy barrier (higher ΔG_c) to be overcome, again due to the lower degree of supercooling at higher end temperatures, which is as expected[228].

Fig 5.10 showed a good linear relationship, but a discontinued linearity was observed from about **298 K**. This discontinuity can be attributed to the formation of crystals of different polymorphic states; according to Ostwald's rule of stages[229], in that nucleation of the less stable polymorph (α) was favoured especially at low end temperatures (higher supersaturation) where nucleation rate is higher with less energy barrier[112] while the reverse is the case at higher temperature; hence it can therefore be inferred that the crystals formed at $T \geq 298$ K is the β polymorph[230]; this trend is similar to results shown in previous studies by Chen *et al*[104] and Ng[215]. The features of the discontinuity and the different nucleation mechanisms leading to different polymorphs are also clearly shown in **Table 5.4** where higher nucleation rate constants (k_n) were extracted at lower end temperatures and vice versa; the corresponding *n* values (see equation 2.21) obtained here was *~1* hence the nucleation process can be taken to be *first* order.

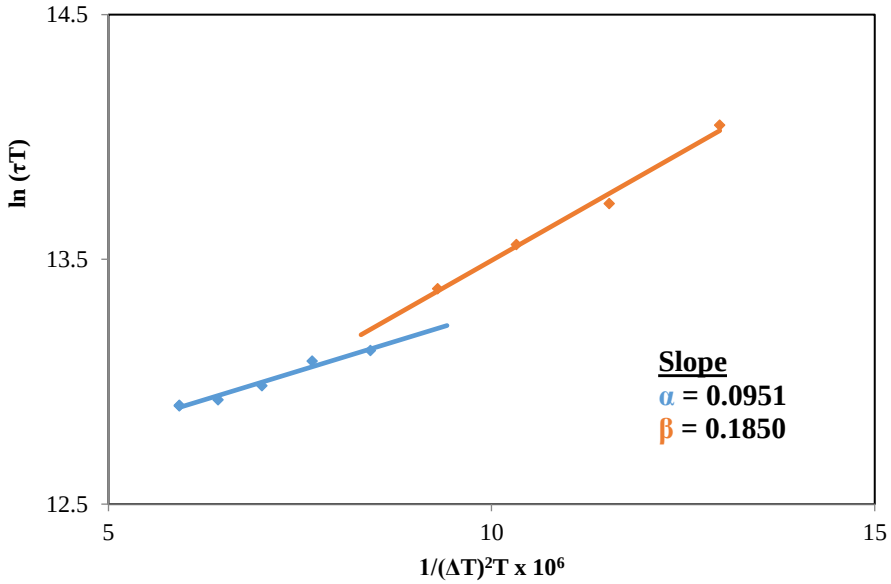

Fig 5.10: Plot of ln($T\tau$) against 1/T$(\Delta T)^2$ using to determine kinetics parameter from Fisher-Turnbull equation

The property, ΔG_d, being the activation energy for molecular diffusion, takes into account the impeded molecular movement due to increased viscosity at low temperatures; hence it is expected that the nucleation rate becomes more influenced by ΔG_d as the end temperature is reduced[52]. This was however not explored further in this study.

The Nyvlt model

To extract non-isothermal kinetics from the Nyvlt model, the measurements of metastable zone width (ΔT_{max}) as a function of cooing rates (β) are required. The metastable zone width (MSZW) can be determined as the difference between the 'dissolution' and the crystallisation temperatures at each of the cooling rates. The results for stirred tank (STC) shown in **Table 5.2** were used for this analysis. By plotting $ln(\beta)$ against $ln(\Delta T_{max})$, the nucleation order (n) and the nucleation rate constant (k_n) was evaluated according to eq. (3.8) and are also shown in **Table 5.4**. Values of *n* between 6.0 and 16 were reported for fat systems of different POP and PPP concentrations in a previous study[109]; the value obtained from this study (~9) is within the quoted range. The kn value obtained here (3.99 x 10-4 s-1) is a lot lower than those reported for solution crystallisation of some organics (e.g. adipic acid in a previous study[231]), and this may be attributed to the relatively slower rate of molecular growth to a stable nuclei for

triglyceride systems due to the high viscosity; a higher nucleation order (~9) also supports the influence of mass transfer on melt crystallisation[232].

Table 5.4: Kinetics parameters obtained from all the models considered in this study (T_m = 318.85K)

	Avrami model		*Fisher-Turnbull model*		*Nyvlt model*	
T_c *(K)*	***n***	***k x 10^{10} (s^{-n})***	***ΔG$_c$(kJ/mol)***	***k$_n$ x 10^6 (s^{-1})***	***n***	***k$_n$ x 10^6(s^{-1})***
293	2.7 ± 0.2	2866	1.37	4188	8.97	399
295	2.3 ± 0.1	1646	1.63	4158		
296	2.2 ± 0.0	282	1.79	669		
297	2.5 ± 0.1	12	1.98	465		
299	2.3 ± 0.4	12	4.75	476		
301	2.7 ± 0.4	4	6.01	202		

Comparison of models

Comparing the nucleation rate constants (k_n) evaluated between the Fisher-Turnbull and the Nyvlt models, the Nyvlt (non-isothermal) nucleation rate constant is of similar order of magnitude to the Fisher-Turnbull (isothermal) values at the higher end temperatures (298 – 300 K), while of an order of magnitude lower for the lower end temperatures. The values themselves match reasonably well for the cooling rates investigated, giving the fact that the model assumptions are widely different; where the Nyvlt model took a polythermal approach to estimate the kinetic parameters with the assumption that supersaturation rate corresponds to nucleation rate from the onset of nuclei formation and there is no growth in nuclei[34], while the Fisher-Turnbull model was based on isothermal conditions with homogenous nucleation being assumed in the crystallisation process. These two models can be used for estimating nucleation parameters for both melts and organics.

The dependency of the *k* values on the growth mechanism (*n*) evaluated from the Avrami model together with the fact that it describes the *overall* crystallisation rate makes any comparison irrelevant. Furthermore the growth mechanism (*n*) from the Avrami model has a completely different definition from the apparent nucleation order predicted from the Nyvlt model which is dependent on the formation process of stable nuclei[87], once again no comparison is possible.

5.2 Filtration Study

As stated earlier, the effects of cooling rate and mixing intensity on filtration rate, purity and yield on the olein product of palm oil crystallisation were examined.

5.2.1 Filtration Rate

This was determined as the average volume of filtrate (mL) collected in the measuring cylinder per unit time (min) of filtration; the calibrations on the cylinder with a stopwatch were performed for this measurement. Within the conditions examined, it was observed that the filtration rate increased slightly with increasing cooling rate (**see Table 5.5**). This was deemed opposite to the expected trend since it is an established fact that slower cooling produces larger crystals which should filter quicker than smaller crystals. Even though *pre-filtration* microscope images of the stearin crystals confirm larger size from slow cooling (**see Fig 5.11**), the peculiarity of fat crystals in comparison to typical *brittle* crystals should be brought to consideration here. The malleable property of the fat crystals makes it easily compacted into a clump of solid mass during the filtration process (**see Fig 5.12b**); at this point, crystal size becomes less influential in the filtration process. Hence the trend in the filtration rate with respect to cooling rate can be attributed to compaction/clustering of the fat crystals although these were not quantitatively examined. Moreover, it could also be argued that the range of cooling rate examined within the time scope is not wide enough to ascertain with confidence the effect of cooling rate on filtration. With respect to the effect of mixing, the higher mixing condition showed slower filtration and this was attributed to the wide crystal size distribution which encouraged oil entrapment. Break up of solid lumps at high agitation was reported as a contributing factor[233].

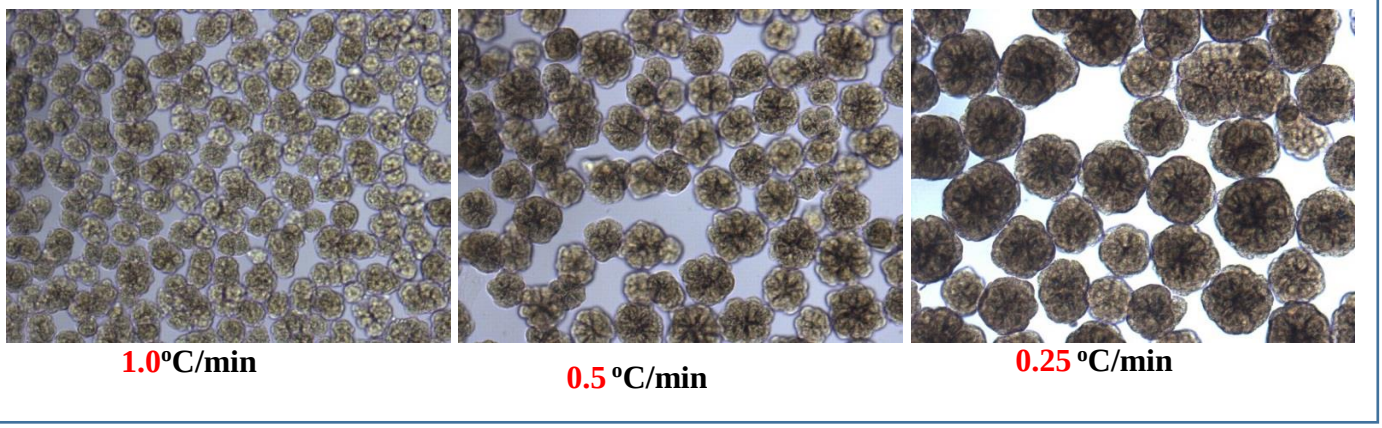

Fig 5.11: Microscopic non-polarised images of stearin crystals crystallised at different cooling rates

Fig 5.12: Sample pictures of isolated palm olein (a) and stearin (b) products after filtration

5.2.2 Yield

The yield of the filtrate product (olein) was determined based on a mass balance and the solid fat content (SFC) of the palm oil feed; from the DSC analysis, the resultant %solid curve is shown in **Fig 5.13,** hence at T_c = 20°C (being the end crystallisation of this study) the SFC of palm oil feed was estimated as 30%

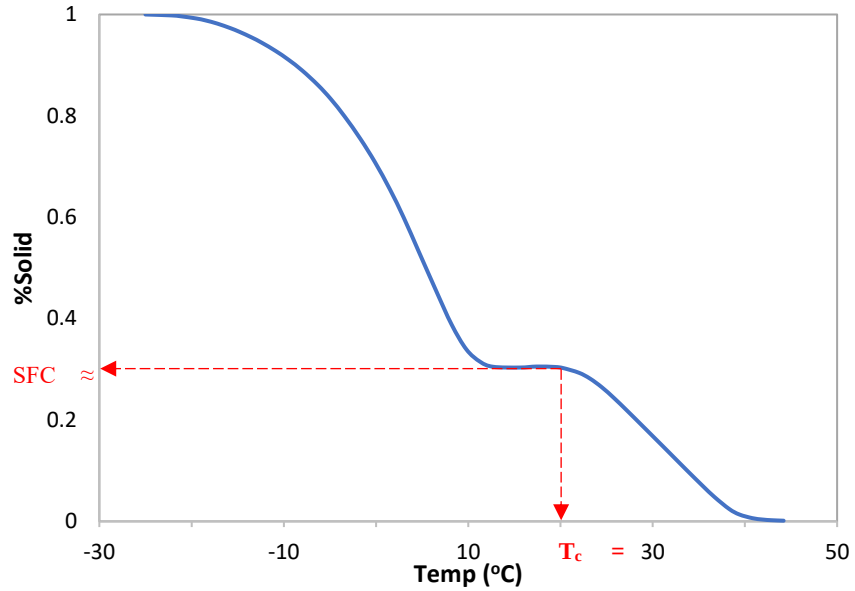

Fig 5.13: Curve showing %Solid fat content (SFC) in the palm oil using in this research, using data obtained from DSC analysis (T_c = 20°C, SFC = 30%)

A sample calculation on how the olein yield was calculated is shown below:

$$\text{Mass of sample filtered} = 66.5\ g$$

$$\text{Mass of filtrate collected} = 37.2\ g$$

$$\therefore \%\ \text{filtrate (olein)} = \frac{37.2}{66.5} = 55.9\%$$

$$\%\ \text{cake (stearin)} = 100 - 55.9 = 44.1\%$$

Since

$$SFC_{20C} = 30\%$$

$$\therefore \text{Liquid fraction (olein) in feed} = 70\%$$

Hence

$$\text{True olein yield} = \frac{55.9}{70} = 79.9\%$$

$$\%\ \text{Oil trapped in cake} = \frac{44.1 - 30}{44.1} = 32\%$$

Whilst the olein yield did not vary significantly with cooling rate and vessel type, it could be observed that the yield was generally higher at the lower mixing condition, and this was attributed to the less oil entrapment at this condition (explained earlier).

5.2.3 Purity

The product purity was determined by analysing the iodine value of the filtrate (olein) as this gave a measure of unsaturation of the oil sample – the purer the oil, the higher its iodine value. Detailed description of iodine value analysis can be found in **section 3.1.3**. From the results presented in **Table 5.5**, it can be inferred that none of the examined parameters had any significant effect on the olein purity ($P > 0.05$); this can be linked to the fact that the driving force of the crystallisation process which is the degree of supercooling (50 → 20°C) was kept constant throughout the study hence the measurement of unsaturated TAGs concentrated in the liquid product (olein) should remain unaffected. This inference agrees with reported results in previous studies by Ab Latip et al[149] and deMan[234] who reported insignificant difference in iodine value of the olein product within the range of cooling rate and mixing speed considered. The apparent low iodine values (IV of typical olein is 56 – 57; see **Table 2.3**) reported here would most likely be due to the quality of the reagents used for the analyses; to ascertain this, repeat analyses with a different batch of reagents would be recommended for future work.

Table 5.5: Summary of results obtained from the filtration study carried out

	High Mixing						Low Mixing					
Cooling rate (°C/min)	**1**		**0.5**		**0.25**		**1**		**0.5**		**0.25**	
Vessel	**STC**	**OBC**	**STC**	**OBC**	**STC**	**OBC**	**STC**	**OBC**	**STC**	**OBC**	**STC**	**OBC**
Av. filt. rate (ml/min)	0.93	1.39	0.85	1.22	0.65	1.03	1.45	1.53	1.15	1.40	0.92	1.81
True olein yield (%)	68.23	75.70	76.01	75.69	59.94	76.90	79.83	78.41	78.09	77.60	72.56	74.73
Oil entrapped in cake	0.43	0.36	0.36	0.36	0.48	0.35	0.32	0.33	0.34	0.34	0.39	0.37
Olein purity (IV)	48.74	48.41	48.71	48.94	48.56	48.91	48.81	48.42	48.45	48.43	48.5	48.46

In summary, the filtration of oil-based systems (in the case, palm oil) is a lot slower than that of the average organic solution crystallisation due to the viscosity of the oil system and the easy clustering of the fat crystals. Whilst cooling rate influenced the filtration properties, it had little effect on the purity of the filtered product (olein). Mixing however showed some influence on the overall filtration process and product yield.

CHAPTER 6 - RESULTS: Analyses in the Continuous Mode

In this chapter, the results obtained from the experiments carried out in the continuous operation were outlined and discussed using relevant theories and references. In order to effectively carry out a continuous crystallisation process, one of the prevailing huddles to overcome is the ability to monitor and control the process, particularly in a plug flow system such as the COBC where its tubular configuration limits the surface area available for the implementation of in-line process analytical tools (PAT). Hence, the experiments carried out in this section explored the effects of operation parameters – temperature ramps, flowrates and mixing intensity – on temporal and spatial steady state properties.

In continuous crystallisation, the unsaturated solution is flowing through the COBC with pre-setup temperature zones of decreasing temperatures, supersaturation is built up gradually along the path, leading to nucleation and crystal growth all in flow. The operational principles and protocols are thus entirely different from these of traditional batch systems, leading to new concepts and parameters to be investigated, e.g. supersaturation profile, steady states of operation, crystal growth profile and so on. In the final part of this PhD study, the characteristics of steady states in the continuous crystallisation of palm oil in a COBC were investigated with respect to the effects of operating parameters – temperature ramping, net flowrate and mixing intensity. These effects were examined in relation to the solute concentration (supersaturation), mean crystal size (crystal growth rates) and nucleation temperature (nucleation kinetics). In the COBC, we have placed two turbidity probes (inferring solute concentration), two process image cameras (crystal size and number count) at two strategic locations, and four thermocouples (temperature) (Jn7 & Jn10 and T1 – T4 in **Fig 3.10**) along the length of the COBC, this would allow us to examine two types of steady states: the spatial (data from two locations at a known distance) and the temporal (data from either location at two different times). This information is essential not only for the purposes of stability, repeatability and reliability of the operation, but also for modelling, control and prediction. This work reported in this thesis is the first of its kind. Before presenting the results, there are a number of notices that must be given here.

Firstly, according to **Table 3.5**, three different temperature ramping of 0.25, 0.5 and 1 ^{o}C/min were achieved by setting the appropriate cooling programmes on the water baths in each zone. This means that the time taken for the cooling process to get to the end temperatures of the zones was varied, while the feed rate was kept unchanged (e.g. at 1.0 ^{o}C/min, it will take 20 min to cool from 50°C to 30°C at Jn7, and 25 min from 50°C to 25°C at Jn10, etc.)

Secondly, due to the practicality of the physical setup, T3 and T4 in **Fig 3.10** are not the actual temperatures for Jn7 and Jn10 respectively; these are estimated using the adopted flowrate and temperature difference along the tube length, with the assumption that the temperature changes linearly along the tube length; see below sample calculation.

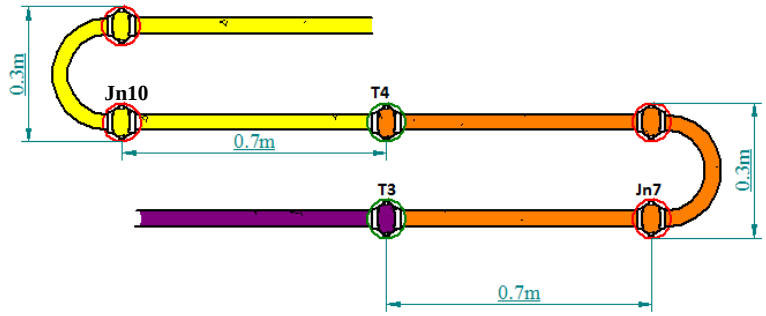

Inside cross-sectional area (A) of COBC tube $= 1.77 \times 10^{-4} m^2$ (Tube inside diameter $= 15\text{mm}$)

If the temperatures are:

$\text{T3} = 30^{o}C$

$\text{T4} = 26^{o}C$

Distance (L) from $\text{T3} \rightarrow \text{T4} = 0.7 + 0.3 + 0.7 = 1.7\text{m}$

For a flowrate (Q) of 42 ml/min $(4.2 \times 10^{-5} m^3/\text{min})$,

$$\text{Fluid velocity } (u) = \frac{Q}{A} = \frac{4.2 \times 10^{-5}}{1.77 \times 10^{-4}} = 0.237\text{m/min}$$

$$\text{Time taken } (t) \text{ for flow to move from T3} \rightarrow \text{T4} = \frac{L}{u} = \frac{1.7}{0.237} = 7.16\, min$$

Therefore;

$$\text{Rate of temp change } (\dot{T}) \text{ along the tube length} = \frac{(\text{T3-T4})}{t} = \frac{30 - 26}{7.16} = 0.56^{o}\text{C/min}$$

$$\text{Temp. at Jn7} = \text{T3-}\left[\left(\frac{L_{\text{T3}\rightarrow\text{Jn7}}}{u}\right) \times \dot{T}\right] = 30 - \left[\frac{0.7}{0.237} \times 0.56\right] = 28.35^{o}C$$

$$\text{Temp. at Jn10} = \text{T4-}\left[\left(\frac{L_{\text{T4}\rightarrow\text{Jn10}}}{u}\right)\times\dot{T}\right] = 26 - \left[\frac{0.7}{0.237}\times 0.56\right] = 24.35^{o}C$$

Thirdly, when the concentration of solids formed is too high in the COBC, there are too many particles in the view field for the cameras to differentiate crystal images from the background; hence this was addressed in deciding which temperature range to operate at (50 °C – 25 °C, as opposed to 20 °C used in the batch studies), such that clear images of solids are viewed at all experimental conditions.

Fourthly, since the turbidity probes measure the percentage transmittances of light and do not give quantitative information on solute concentration, but qualitative data can still be extracted from the information provided by the turbidity analysis of the system. Hence, the % transmittance data was considered relatively to each other, in an attempt to extract the concentration *trends* with respect to steady state; this was however done with limited certainty bearing in mind the various contributing factors that could influence the light transmittance in a crystallisation vessel, some of which include bubble formation, minimum detectable particle size, measurement window, etc. It should also be noted here that turbidity probes are designed to detect a range of crystal size/density outside of which the signals become unreliable i.e. the % transmittance will still read 100% (which corresponds to clear solution) even if nucleation has already commenced but the crystal size/density is below the detectable range; in the same vein, the % transmittance will read 0% when the maximum detectable crystal size/density has been reached even if the actual size/density increases further.

6.1 General Trends

6.1.1 Repeatability

This section highlights the general effects of the examined parameters on the overall crystallisation properties and operation. Each experimental run was repeated at least twice; given the susceptibility of the measurement tools (turbidity and imaging light probes) to disturbances by bubbles and fouled windows; reasonable repeatability was observed in the obtained profiles for repeat experiments – see **Fig 6.1** for sample repeat runs (experiments were run at the same temperature ramping, same flowrate, same mixing conditions but at different times). The earlier-stated effects of bubble formation within the crystallisation vessel/column on the measurement tools were evident in the profiles shown. For instance, taking a look at the profiles on the right in **Fig 6.1**, a sudden drop in transmittance (top graph) was observed between 40 – 50 min, which corresponded to a sharp drop/increase in the particle count at Jn10/Jn7 (bottom graph). This could be associated with bubble formation causing misrepresentation of events, in that the turbidity probe was analysing the bubbles as particles, while blocking the window for the imaging probe.

6.1.2 Effect of temperature ramping

Fig 6.2 below shows the profiles of the turbidity at Jn7 (blue dots) and Jn10 (green dots) – the top three graphs; the temperature ramping at T3 (yellow) and T4 (grey) – the top three graphs; the D_{50} taken as *relative* (not actual) mean sizes at Jn7 (blue curve) and Jn10 (green curve) – the middle three graphs; the crystal number counts at Jn7 (blue) and Jn10 (yellow) – the bottom three graphs. The profiles for three temperature ramps are given in the three graphs vertically from left to right. The flow rates were fixed at 42 ml/min for all ramping.

The temperatures measured at T3 in **Fig 6.2** decreased from 40 to 30 °C (the vertical axis on the right of the top three graphs), while from 40 to 25 °C at T4 that is located further away from T3. All the temperature ramps are smooth and repeatable, indicating the achievement and the reliability of the temperature zones. At the slowest ramping (0.25 °C/min), the decreasing slope in the temperatures were much longer than that at faster rates due to corresponding programme inputted into the water baths. At the ramping of 0.25 °C/min (the top left graph in **Fig 6.2**), the turbidity (% transmittance) remained unchanged for a while before dropping due to crystal formation (i.e. nucleation). At the fastest ramping (1.0 °C/min) however, the decrease

in the % transmittance was almost instant. This is expected for the set up applied since it could be associated with the established that crystallisation rate increases with increasing cooling rate due to the high supersaturation generated at this condition. This was also responsible for the temperature at which the turbidity system detected the occurrence of crystallisation (i.e. drop in % transmittance) which was taken as the nucleation temperature; it was observed that at the fast ramping, the nucleation temperature (*ca*. 28 °C) was lower than that observed at the slow ramping (*ca*. 34 °C) . However, the trends was observed to level off for the two rates of 0.25 and 0.5 ^{o}C/min between 30 – 50 min (i.e. after the initial decrease), the reason for this is unsure, perhaps due to the tips of the turbidity being blocked or the presence of air bubbles in the flow, see section **6.1.1** and **Fig 6.1** for the discussion on the effects of bubbles on the measurement signals.

The moment when the turbidity signals drop refers to the occurrence of nucleation and this was corresponded by the sharp increase detected in the crystal number counts (the bottom three graphs). Generally the number counts were initially higher at Jn10 (the later position in the column) than that at Jn7 (the earlier position), this makes sense since more crystals are formed and/or more relatively larger crystals are expected as the oil feed flows through the tubes. The crystal count profiles for Jn7 were generally on the increase, before reaching close to steady points, while for Jn10, a decreasing trend was observed after the initial sharp increase. This might be an indication that crystal sizes are growing, while the numbers are going down; it could also be the crystals aggregating together, which is not an uncommon occurrence in fat systems. Furthermore, given that the initial increase observed in crystal count corresponds to spontaneous nucleation, observing this at both Jn7 and Jn10 locations suggests that the nucleation event occurred throughout both locations initially, but crystal growth (and possibly aggregation/agglomeration) took over at Jn10, again explaining the subsequent decline in crystal count observed at Jn10. **Table 6.1** lists the nucleation temperatures (point at which the %transmittance reduces significantly at Jn7 i.e. < *ca*. 95%) for the different temperature rampings. The nucleation temperature reduces (i.e. wider MSZW) with increased ramping; this is expected as higher supersaturation rates are attained at faster cooling which implies that the onset supersaturation (due to supercooling) required for nucleation to commence increases with decreasing ramping, this is again expected as seen from previous studies[220].

The crystal size profile are the middle graphs; the mean crystal sizes at Jn7 and Jn10 locations are more or less steady at the same magnitude for all the ramping considered; but the mean sizes at Jn10 were higher than that at Jn7, this is expected and will be discussed in more detail in section **6.2** . The '*irregularities'* observed in the size trends before the nucleation commenced have been attributed to *noise* signals in the imaging tool due to system instability and should be discarded.

6.1.3 Effect of flowrate

Here, the temperature ramping was kept constant at 0.25 °C/min while the oil flowrate through the COBC was varied between 42 – 77 ml/min by adjusting the rpm of the feed pump; this then varied the net flow Reynolds number (Re_n). Since the length of the crystalliser remains the same, varying (e.g. increasing) the oil flowrate would vary (e.g. reduce) the residence time of the oil inside the COBC. However, the duration of the run shown in the corresponding graphs was kept the same, hence the same time scales for the horizontal axes in the corresponding graphs shown.

The turbidity and size profile are shown in **Fig 6.3** below. At a high flowrate condition, the feed oil (and eventual crystal molecules) will take longer time to travel through the required temperature zones (compare 4.61 min from Jn7 to Jn10 at 77 ml/min with 8.33 min at 42 ml/min); it is therefore expected that nucleation commenced further away from Jn7, at a location closer to Jn10 at the high flowrate of 77 ml/min, hence the nucleation and subsequent growth of crystals to stable sizes will occur to a lesser degree, and may have been outside the measurement window between Jn7 and Jn10. This is evident in the very gradual slope of the turbidity profile (decline in % transmittance) obtained for the high flowrate experiment (top-right graph), compare with the relatively steeper gradient observed at the lower flowrate. Also, for a given ramp and mixing condition, the temperature at which the significant decline of the % transmittance commenced generally reduced with increasing flowrate (*ca*. 29 °C at 42 ml/min and 34 °C at 77 ml/min – see

Table 6.2); this is again following the presumption that extent of the crystallisation process (i.e. degree of de-supersaturation) is lower at high flowrate conditions. In addition, high feed flowrate through the column implied that the feed is spending shorter time within the

measurement windows (which were fixed for all the experiments carried out in this section), and it should be noted that certain length of *induction time* is required for nuclei to grow to the detectable sizes, and this time might not be readily provided at the high flowrate conditions. The eventual decline in the turbidity profile with time to ~0% at 77 ml/min could be attributed to some unplanned events such as fouling either on the tube walls (posing as seeds to induce further nucleation) or on the mirror of the turbidity probe (blocking the light transmittance). This was however not explored further in this research.

With regards to the particle count profile particularly at Jn7 (blue trace in bottom graphs in Fig 6.3), a significantly lower count was observed at the high flowrate condition, which buttress the notion of lower degree of de-supersaturation due to inadequate time available for nuclei growth to stable sizes. The count profile at Jn10 could be taken to be within similar range for all the flowrates considered, and this would support the statement made earlier, suggesting that a bulk of the nucleation events might have occurred at a location further way from Jn7, and closer to Jn10. Again, the eventual drop in the particle count at Jn10, below that of Jn7 (after an initial sharp increase) was observed, and this was earlier attributed to the occurrence of possible crystal agglomeration/aggregation, as explain in section 6.1.2.

The smaller mean size of crystals obtained at high flowrate are also indications of the reduced degree of de-supersaturation at this condition, as explained earlier. Regarding the relationship between the mean sizes at Jn7 and Jn10 for the high flowrate, a reverse trend was observed, when compared with the other flowrate conditions examined; the mean size at Jn10 appeared smaller than that of Jn7, which is opposite to what was observed to the other flowrate conditions; again, this can be attributed to the suggestion that nucleation commenced at a location closer to Jn10, while secondary effects (such as unintentional seeding by previously formed crystals) was responsible for the eventual crystal formation observed at Jn7, given the simulated *forward↔backward* fluid motion adopted in the mixing mechanism of the oscillatory baffled system.

6.1.4 Effect of mixing intensity

Here, the effects of the oscillation intensity on the concentration and mean size profiles with respect to the steady state characteristics were examined at constant temperature ramping (0.25°C/min) and flowrate (42 ml/min). The oscillation intensity was varied by varying the oscillation frequency (ω) between 0.5 – 2 Hz, while amplitude (x_o) was kept constant at 25 mm (peak-to-peak), thereby varying the oscillatory Reynolds number (Re_o).

It can be observed from the profiles in **Fig 6.4** that the nucleation temperature was slightly lower at low mixing condition (top graphs), even though the supercooling, which is the driving force for crystallisation, was unchanged. Though negligible influence of mixing conditions on MSZW (for batch process) with respect to nucleation temperature was highlighted in **section 5.1.1**, the above observation, coupled with the more gradual decline in % transmittance observed in the turbidity profile, and also the considerably low crystal count at 0.5 Hz (compared to 2 Hz) are all indications of a reduced nucleation rate at low mixing conditions. This trend of results were reported in previous studies, where it was established that high mixing conditions led to reduced MSZW (i.e. higher nucleation temperature) due to higher shear that drives molecules from the bulk solution to the crystal surfaces [43]. Consequently, a reduction in the average mean size was observed at high mixing and this would be due to higher shear rates favouring attrition and nucleation at high mixing conditions[43, 235]. Crystal size increase was observed along the tube length for all mixing conditions as the mean size at Jn10 was consistently higher than Jn7.

These inferences demonstrates the versatility of continuous crystallisation studies, and therefore the limitation of batch studies, as some *time-based* information that could not have been obtained in batch studies were readily obtained in this study.

Table 6.1: Nucleation temperature at varied temperature ramping

Ramp (°C/min)	T_{nu} (°C)
1.0	27.9
0.5	30.5
0.25	34.4

Table 6.2: Nucleation temperature at varied flowrate

Flowrate (ml/min)	T_{nu} (°C)
42	34.4
54	35.9
77	29.6

Table 6.3: Nucleation temperature at varied mixing

Mixing intensity (Hz)	T_{nu} (°C)
2	34.4
1	31.6
0.5	31.7

6.2 Steady State Evaluation

Some of the previous steady state studies that have been carried out on the continuous oscillatory baffled crystalliser (or reactor) i.e. COBC(R), or on similar set-up include fluid mechanics and mixing performances using fibre optics probes for in-line monitoring[236], continuous crystallisation of a model API where rapid turnaround in the production of the desired product was reported in comparison to batch processes[1], steady state characterisation of anti-solvent crystallisation of salicylic acid, where evolution of solution concentration and crystal size with time were investigated[237], to mention but a few. It is clear that a number of studies have been conducted on the COBC in an attempt to understand its operations, and how its unique configurations impacts processes and products.

Apart from the last sited example of previous studies which is quite similar to the studies carried out in this section of the research, the novelty of this research is the fact that it attempted to characterise the steady state of the crystallisation of palm oil, an edible fat and oil product, using in-line analytical techniques to obtain essential real-time data. This is an area that had not been explored before now in regards to the combination of the adopted technology and the model system it was considered for. More studies have been done in the batch system but limited studies have been carried out in the continuous system which was also posed a challenge during this research as limited information are available for referencing and comparison.

For the COBC set-up used in this study, extracting data at different times at Jn7 and Jn10 individually allows the establishment of ***temporal*** analysis, while analysing the data at the two locations, Jn7 and Jn10, which are 2 metres apart enables the establishment of ***spatial*** characterisation. Crystal size data for a crystallisation period of 60 min are shown in corresponding tables (times correspond to *x*-axis of the graphical profiles shown earlier). The relation between size and % transmittance data are highlighted in *spatial analysis* where their evolutions along the tube length of the crystalliser (i.e. from Jn7 → Jn10) are discussed.

6.2.1 Temporal Analysis

The analysis of temporal steady states of crystal sizes involves looking at the size data at either Jn7 or Jn10 for different times.

For different **temperature ramps,** it can be seen from **Table 6.4** that the mean size at Jn7 steadied at an average of 50.64 ± 0.19 μm at about t > 75 min for all the ramps considered, while that of Jn10 steadied at 62.10 ± 0.94 μm. Since the driving forces at Jn7 are smaller than that at Jn10, the increase of crystal sizes at Jn10 is expected. The temporal size steady states can be examined either every 15 min or over 60 min using the data in **Table 6.4**; the relative changes in crystal size were small, within 6% at Jn7 and 10% at Jn10 for the period of t_{90} to t_{120} hence steady state was evidently achieved at both locations. Also the overall stability was reasonably good for the cooling times examined, with interval changes of ≤ 6% for both 0.25 and 1.0 ^{o}C/min, between t_{90} and t_{120}.

Likewise, the temporal steady states of concentration are estimated by analysing the corresponding transmittance data shown in **Table 6.5**, and this can unveil some interest facts. Though it was observed that the turbidity profiles showed continuous decline in % transmittance with time, the relative change however reduced with time especially at 1.0 °C/min where the change reduced from an average of 17% to >1.0% at both Jn7 and Jn10. This could suggest that though temporal steady state with respect to concentration might not have been reached within the process duration, it was approaching it. In addition, unplanned events such as secondary nucleation or even fouling of the probe mirror may also be contributing factors to the continuous decline if the turbidity profile. At 0.25 °C/min however, the changes in the %transmittance with time were relatively more erratic which would imply that temporal steady state was not achieved at this low ramping condition within the process duration.

Table 6.6 links the change in % transmittance with the change of crystal size. With respect to Jn10, a 2.6% size increase required a 63% decline in % transmittance at 1.0 °C/min, while a 3.1% size increase at 0.25°C/min required 54% decline between t_{90} to $t_{120.}$ This does not show any particular trend hence it can be concluded that temperature ramping has little effect on the size and concentration changes with time. Since the same operational duration was applied to

all, the consumption rate of solute concentration would in theory deliver the same growth rate for crystals.

Table 6.4: Summary of size data at varied temperature ramping

Ramp (°C/min)	Location	Mean size (µm)				
		t_{60}	t_{75}	t_{90}	t_{105}	t_{120}
1.0	**Jn7**	50.64	50.45	51.34	50.29	50.39
	Jn10	54.53	59.28	62.38	62.86	64.01
0.5	**Jn7**	53.14	51.94	50.76	50.57	50.06
	Jn10	58.82	58.38	59.25	62.40	68.00
0.25	**Jn7**	58.63	54.86	51.82	50.39	50.18
	Jn10	61.95	60.64	59.62	58.94	61.44

Table 6.5: Summary of transmittance data at varied temperature ramping

Ramp (°C/min)	Location	% Transmittance				
		t_{60}	t_{75}	t_{90}	t_{105}	t_{120}
1.0	**Jn7**	0.30	0.15	0.06	0.03	0.02
	Jn10	0.41	0.22	0.13	0.05	0.05
0.5	**Jn7**	0.71	0.51	0.31	0.17	0.04
	Jn10	0.74	0.60	0.44	0.26	0.15
0.25	**Jn7**	0.59	0.59	0.48	0.31	0.21
	Jn10	0.55	0.57	0.51	0.33	0.24

Table 6.6: The relationship between % transmittance and size for different temperature ramping

Ramp (°C/min)	Location	t_{90-120}	
		% Size Change	**% Transmittance**
1.0	**Jn7**	1.9	0.67
	Jn10	2.6	0.63
0.25	**Jn7**	3.2	0.57
	Jn10	3.1	0.54

The mean size data for different **flowrates** is shown in **Table 6.7**. As the residence time was reduced at high flowrate, smaller mean size was observed, which is expected since less time was available for the crystals to growth. The changes observed in the size data was reducing with time (e.g. within 3% for Jn7 and 5% for Jn10 between t_{105} and t_{120}), and this might suggests that temporal size steady state was indeed achieved within the time period considered for all the flowrate conditions. A close look at the size profile in **Fig 6.3** (middle graphs) indicated that the period where steady state was achieved was between *ca*. 100 – 130min time stamps, beyond which instability in the crystal sizes were observed, which then suggests that the steady state with respect to crystal size was lost outside the stated time window; the instability was also observed in the particle count profile beyond the stated time window (see bottom graphs). This occurrence is a real possibility in that the fat crystal density at this point may have been too high due to supercooling such that analysis window had been blocked and no *real* data could be obtained. This occurrence was also been reported in the previous study earlier mentioned where steady state was said to be lost due to high solid concentration that led to the blockage of the crystallizer[237].

The corresponding % transmittance data in **Table 6.8;** a continuous decline with time was observed, as the crystallisation process proceeded, which is again an indication that temporal steady state with respect to concentration was not achieved. Comparing the overall change in % transmittance (which to an extent is an indication of solute consumption), it can be observed that the decline was faster at the low flowrate than that at the high flowrate (average of 56% at 42 ml/min vs 22% at 77 ml/min). This is as expected since the smaller mean size obtained at the high flowrate would correspond to lower solute consumption, indicating lower degree of crystallisation. For instance, between $t_{90\rightarrow120}$ at Jn10, the crystal size at 42 ml/min changed by 3.1% and caused a 54% decline in %transmittance, while at 77 ml/min, a size change of 1.6% caused 22% loss of transmittance. Since all other operational parameters were kept unchanged, the highest flow rate of 77 ml/min is about 1.8 times faster than the lowest rate of 42 ml/min, so the change in % transmittance was accordingly reduced by ~2.4 times, matching up with about 1.9 times less growth (see **Table 6.9**). These numbers generally agree well with each other as the driving force (i.e. degree of supercooling) was the same for all flow rates conditions examined. It is clear that the temporal analysis can also be used to check and verify operational consistency.

Table 6.7: Summary of size data at varied flowrate

Flowrate (ml/min)	Location	Mean size (µm)				
		t_{60}	t_{75}	t_{90}	t_{105}	t_{120}
42	**Jn7**	58.63	54.86	51.82	50.39	50.18
	Jn10	61.95	60.64	59.62	58.94	61.44
53	**Jn7**	49.26	47.14	47.49	48.17	48.06
	Jn10	55.97	52.81	53.30	54.29	53.99
77	**Jn7**	43.65	45.54	50.64	49.64	48.07
	Jn10	57.95	45.50	44.19	44.24	43.48

Table 6.8: Summary of transmittance data at varied flowrate

Flowrate (ml/min)	Location	% Transmittance				
		t_{60}	t_{75}	t_{90}	t_{105}	t_{120}
42	**Jn7**	0.59	0.59	0.48	0.31	0.21
	Jn10	0.55	0.57	0.51	0.33	0.24
53	**Jn7**	0.74	0.74	0.71	0.61	0.50
	Jn10	0.67	0.63	0.57	0.54	0.48
77	**Jn7**	0.95	0.94	0.86	0.75	0.67
	Jn10	0.89	0.92	0.87	0.81	0.68

Table 6.9: The relationship between % transmittance and size for different flowrate

Flowrate (ml/min)	Location	t_{90-120}	
		% Size Change	**% Transmittance**
42	**Jn7**	3.2	0.57
	Jn10	3.1	0.54
77	**Jn7**	5.1	0.22
	Jn10	1.6	0.22

The mean size and the corresponding % transmittance data for different **mixing** conditions are given in **Table 6.10** and **Table 6.11** respectively. While other operational conditions remained unchanged, it is expected that an increase in mixing intensity would lead to smaller sizes due to attrition (breakage) effect brought about by the induced collision between crystals and also with the other solid entities such as baffles, tube walls, impellers, etc.[238]. The temporal analysis would provide some insights to breakage of particles; the change in crystal size with time was less than 7% for Jn7 (mean size = 51.44±0.96 μm), and 5% for Jn10 (mean size = 59.87±0.62 μm) between t_{90} and t_{120}. This suggests that temporal steady state might been reached within this time period. However, looking at the size profile in **Fig 6.4**, the occurrence of temporal steady state was more evidently sustained at mixing condition of 1.0 Hz (between 100 – 160 min compared with between 100 – 130 min for 2.0 Hz mixing condition); occurrence of steady state was more difficult to pinpoint for the 0.5 Hz mixing condition as the size profile continually changed with time. The crystal size at 2 Hz was consistently lower than that of 0.5 Hz by a percentage ranging from 3 – 8% between t_{90} and t_{105}. Overall, a ~6% reduction in the average mean size when the oscillation frequency was quadrupled (x4) indicates a rather lower attrition rate than expected. This might suggest that the deleterious effect of high mixing on physical crystal properties (e.g. size) is minimal in the oscillatory baffled crystalliser, compared to the conventional stirred tank crystallisers[220]. This could then be acknowledged as an attractive feature of this novel technology, with respect to fat crystallisation.

Conversely, the transmittance data in **Table 6.11** shows a higher rate of transmittance decline (which corresponds to solute consumption) at high mixing intensity – 56% for 2 Hz vs 19% for 0.5 Hz between t_{90} and t_{120}; also the actual % transmittance per time was consistently lower at the high mixing condition, indicating higher solute consumption since the more solutes are consumed, the higher the crystal density hence the more turbid the slurry is leading to a lower % transmittance. This suggests a higher degree of nucleation at the high mixing condition – also see considerably low crystal counts at the low mixing condition of 0.5 Hz (bottom left graph in **Fig 6.4**) to buttress this. The formation of more nuclei at high mixing may also be responsible for the 6% mean size reduction, as opposed to the attrition effects discussed earlier. **Table 6.12** zooms into the data at the high and low mixing conditions; an ~8% mean size reduction (64 → 59 μm) vs ~61% decrease in % transmittance (84% → 33%) at t_{105}, when oscillation frequency is increased from 0.5 → 2 Hz denotes that the effect of high mixing on

nucleation rate outweighs its effect on attrition rate with respect to palm oil crystallisation. This is an interesting discovery which again proves the novelty of this research.

Table 6.10: Summary of size data at varied mixing intensity

Frequency (Hz)	Location	Mean size (µm)				
		t_{60}	t_{75}	t_{90}	t_{105}	t_{120}
2.0	**Jn7**	58.63	54.86	51.82	50.39	50.18
	Jn10	61.95	60.64	59.62	58.94	61.44
1.0	**Jn7**	57.84	54.06	52.75	50.85	50.26
	Jn10	65.68	60.44	56.93	57.05	57.53
0.5	**Jn7**	65.25	57.69	55.23	51.82	49.70
	Jn10	88.97	69.01	62.54	63.96	60.79

Table 6.11: Summary of transmittance data at varied mixing intensity

Frequency (Hz)	Location	% Transmittance				
		t_{60}	t_{75}	t_{90}	t_{105}	t_{120}
2.0	**Jn7**	0.59	0.59	0.48	0.31	0.21
	Jn10	0.55	0.57	0.51	0.33	0.24
1.0	**Jn7**	0.85	0.86	0.81	0.71	0.59
	Jn10	0.78	0.78	0.71	0.69	0.59
0.5	**Jn7**	0.93	0.96	0.92	0.84	0.73
	Jn10	0.90	0.90	0.88	0.84	0.73

Table 6.12: The relationship between % transmittance and size for different mixing intensity

Frequency (Hz)	Location	t_{90-120}	
		% Size Change	**% Transmittance**
2	**Jn7**	3.2	0.57
	Jn10	3.1	0.54
0.5	**Jn7**	10.0	0.20
	Jn10	2.8	0.17

6.2.2 Spatial Analysis

Here, the size and transmittance data at the two locations, Jn7 and Jn10 at the same time are considered for each of the conditions examined.

It is expected that crystal size increases along the length of the COBC from Jn7 to Jn10, and these were observed for all the **temperature ramping** considered – see **Table 6.4**, and the mean size data can then be used to evaluate rate of local crystal growth. Equally spatial data of % transmittance in **Table 6.5** can be employed to estimate the rate of solute consumption. In theory, the crystal growth is fed by the concentration depletion, so analysing these two rates concurrently, should provide some insight on the events occurring along the tube length. Looking closely at **Table 6.4**, for t_{120}, a 14 µm increase in crystal size along the tube length was fuelled by about 3% difference in % transmittance at 1 °C/min, while 11 µm increase in size was also met by about 3% difference in % transmittance.

It is expected that the faster the ramping, the faster the rate of supersaturation; so the consumption rate along the tube length at 0.25 °C/min should in theory be proportional to that at 1 °C/min i.e. if the difference in spatial % transmittance is 3% at 0.25 °C/min, it should be ~12% at 1.0 °C/min). However, the disproportional data obtained here (e.g. the similar range of size increase and change in % transmittance from Jn7 → Jn10, at both rampings) suggest some other events other than crystal growth, such as agglomeration is responsible for the size increase along the tube length of the crystalliser, which is not a function of solute depletion but interactions between already-formed crystals. This agglomeration phenomenon (depicted in **Fig 6.5**) is reportedly common with fat crystals, and it is sometimes referred to as *spherulitic growth* which is where multiple crystals grow radially by aggregating together with a central nucleus to form what is called a *spherulite* [80]. It is clear that temporal analysis has not only led to the evaluations of local supersaturation and crystal growth rates, but also enable estimation and characterisation of local agglomeration, hence control and prediction.

It is understandable that the method adopted in relating the % transmittance data to concentration trends is very crude, taking into account that bubbles formation could also affect the normal function of the turbidity probe. Nevertheless, there was a temperature difference of about 5 °C between Jn7 and Jn10, this would then suggest that agglomeration event had

occurred at one or both ramping conditions, more so at the faster rate (see slightly higher crystal size at $t_{90\rightarrow120}$ at Jn10 for 1.0 °C/min); sample images shown in **Fig 6.6** obtained at the two respective rates, which supports this suggestion. The decreasing crystal count at Jn10 (bottom graphs in **Fig 6.2**) attests to the agglomeration theory. The difference in %transmittance between Jn7 and Jn10 was ≤10%, which might suggest that spatial steady state was reached with respect to solute consumption but the rate of size increase (agglomeration events) along this tube length was continually on the increase which led to some puzzling questions: what was feeding the agglomeration events? Should the consumption rate for individual crystal be different from agglomerates? There are no answers for these questions within the scope of this PhD work.

Table 6.13: Spatial link between % transmittance and size for different temperature ramping

Ramp (°C/min)	Location	t_{120}			
		Mean Size (μm)	Δ (μm)	% Transmittance	Δ (%)
1.0	**Jn7**	50	14	0.02	0.03
	Jn10	64		0.05	
0.25	**Jn7**	50	11	0.21	0.03
	Jn10	61		0.24	

The data pairs between Jn7 and Jn10 at a specific time in **Table 6.13** can be used to evaluate the local growth (or *agglomeration*) rate, knowing that the time difference between the two ports is 8.33 min at a flowrate of 42.45 ml/min; a sample calculation is shown below. At 28 °C (301K), the overall crystallisation rate constants estimated by the Fisher-Turnbull and the Nyvlt models in **Table 5.4** are 202×10^{-6} and 399×10^{-6} /s respectively for the same compound at an isothermal condition, but the actual growth rates of crystals cannot be determined. Using the spatial measurements, the local growth rate of crystals can for the first time be evaluated, the value of 0.027 μm/s over a temperature difference of 5 °C is within the range reported in a previous study for triglycerides which is considered relatively lower than most organic compounds[80].

$$\text{Mean size at Jn7} = 50.39\ \mu\text{m}$$

$$\text{Mean size at Jn10} = 64.01\ \mu\text{m}$$

$$\dot{G} = \frac{\Delta s}{t} = \frac{64.01 - 50.39}{8.33 \times 60} = 0.027\ \mu\text{m/s}$$

For the **flowrate** experiments, at the lowest flowrate condition of 42 ml/min, the data in **Table 6.7** showed a significant size increase (15 - 22% increase which translates to an average size increase of 10 µm between t_{90} and t_{120}) from Jn7 to Jn10, but with a minimal change in % transmittance (3%). Meanwhile, at the fastest flowrate condition (77 ml/min), the crystal size could be considered more or less similar at both locations; from another point of view, it could be said that the crystal size decrease from Jn7 to Jn10 (average of ~11% decrease which translates to an average size decrease of 5 µm), while the % transmittance also remained fairly similar (1 - 6%). The absence of crystal size increase along the tube length (expectantly due to growth or agglomeration) at the high flowrate could be linked to the low residence time, such that relatively lesser time is available for crystals to grow while the driving force remained the same for all flow rates.

This is consistent with inference drawn earlier for the high flowrate condition, in that the relatively high rate at which the feed oil was passing through the column of the crystalliser could have led to the possibility of a large portion of the nucleation/crystallisation event occurring at a location closer to the latter sampling point (i.e. Jn10). However, the crystallisation occurrence eventually detected at Jn7 could be a function of secondary events such as solid crystals formed initially at the latter location posing as seeds that facilitated the nucleation events at Jn7; the *upstroke↔downstroke* oscillatory motion of the net fluid flow would be contributory factor to this. The considerably higher crystal counts at Jn10 compared to Jn7 at high flowrate (bottom-right graph in **Fig 6.3**) attest to this conjecture that bulk of the crystallisation occurred at a location closer to Jn10.

It is therefore obvious that high flowrate is not a desirable condition to promote appreciable crystal growth along the length of the crystalliser. Even though the velocity ratio (ψ) for the all the flowrates considered (3.5 – 6.2) were within the range recommended for close-to-plug flow mixing regime (see **section 2.4.1** for more detailed explanation), lower flowrates are preferable for the formation of crystals of consistent mean size, and to allow adequate time for the promotion of crystal growth, but not too low to impede adequate heat and mass transfer ($Re_n >$ 50 is advised[239]). Otherwise, a longer tube length (and perhaps very slow cooling conditions) will be required to counter the effect of the short residence time at high flowrate but this will lead to increased footprint and longer operation times, thereby increasing the production cost.

Mixing effects on spatial size evolution as shown in **Table 6.10** indicate evident size increase along the tube length from Jn7 to Jn10 for all mixing conditions; increase of 15 – 22% at 2Hz and 13 – 23% at 0.5Hz. Again the % transmittance evolution data in **Table 6.11** showed negligible change (3% at 2 Hz and 4% at 0.5Hz). It is expected that increased frequency will discourage crystal growth (agglomeration) and promote attrition (breakage) instead, due to higher shear rate[235]. Though this was not evident in the individual Jn7 → Jn10 size differences (spatial size increase was observed even at high mixing), it was true in some instance e.g. the % size increase at t_{105} was higher at 0.5Hz – 23% vs 17% at 2 Hz. Also, reference should be made to the ~6% size reduction observed from t_{90} to t_{105} for both Jn7 and Jn10 when frequency was increased from 0.5 to 2 Hz. Overall though, the rate of size increase from Jn7 → Jn10 (agglomeration) was within similar order for the mixing conditions.

The mixing effects was more evident when considering the % transmittance in relation to solute consumption (low transmittance = high solute consumption) where a ~59% decrease in transmittance was observed when frequency was increased by a factor of 4. Though this does not quite meet the proportional expectation (4x increase in frequency vs ~2.5x decrease in % transmittance), its relative significance demonstrate the pronounced effect of mixing on nucleation - see the low crystal count at low mixing in **Fig 6.4** (bottom-left graph) to buttress this.

For this study, the effect of mixing intensities was explored by changing the oscillation frequency between 0.5 – 2.0 Hz, while keeping the amplitude constant at 25 mm (peak-to-peak). Even though the effect of oscillation amplitude was not examined in this study, it had been reported that too low amplitude could result in the blockage of the COBC column due to poor mixing of the crystal suspension; an optimum amplitude of 20 mm was reported as this led to uninterrupted process run for a duration of 180 min[237]. Comparing this to the amplitude of 25 mm used in this study, it can carefully be stated that it was within the optimum, range for the process since no blockage was experience throughout the experiment runs which lasted for >120 min in all instances.

In general, the velocity ratio (ψ), which is the ratio of oscillatory Reynolds number (Re_o) to net flow Reynolds number (Re_n), ranged from 1.6 – 6.2, and could be said to still be within the recommended range for plug flow (see section 2.4.1); however the optimum mixing condition

with respect to crystal properties (i.e. size) would at $\omega = 1.0$ Hz as the profile at this condition showed steady state of mean size being achieved and maintained for a reasonable length of time during the continuous crystallisation process; at a value of $\psi = 3.1$ which is not too far from the recommended optimal value of 2.5[133].

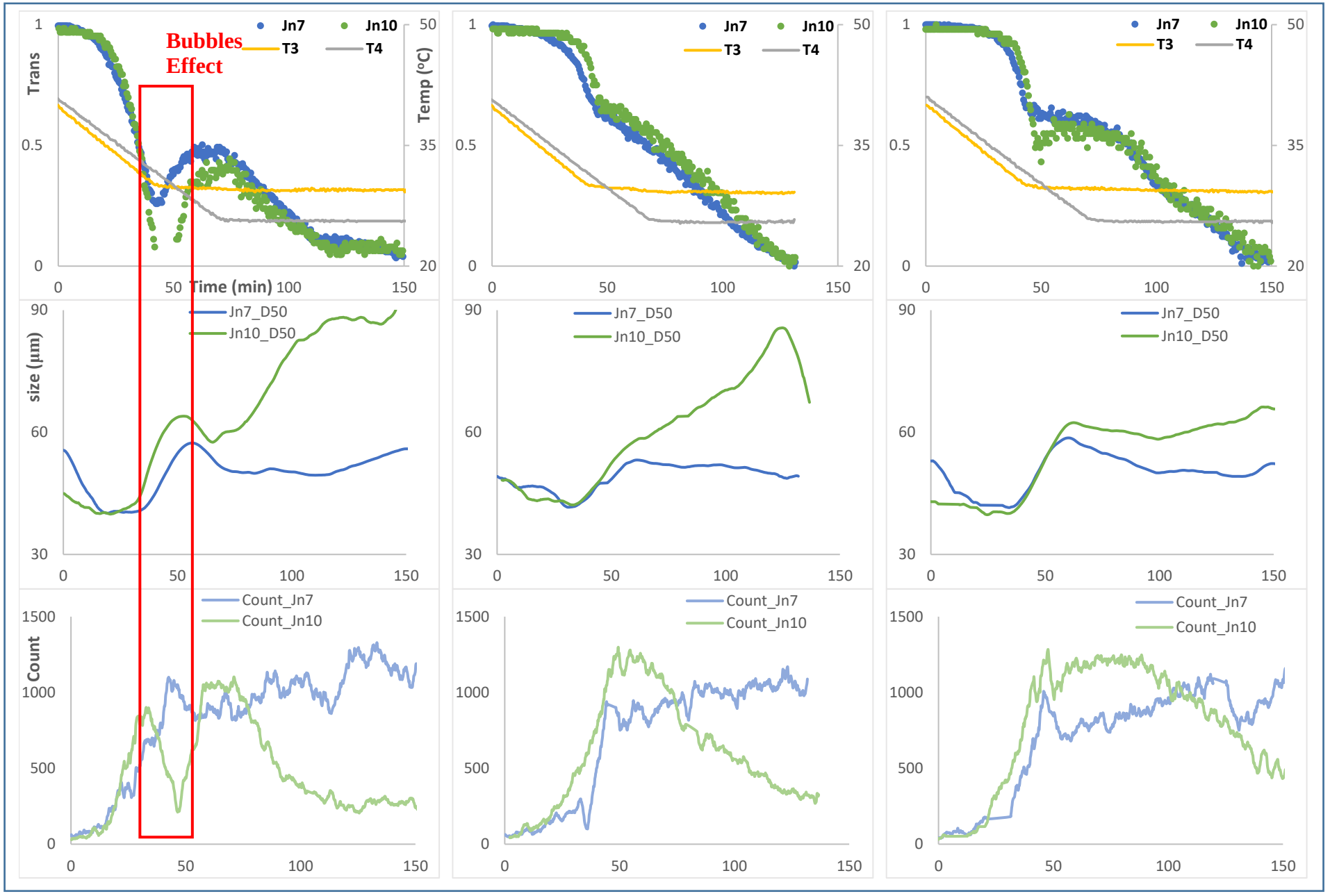

Fig 6.1: Turbidity and size profiles obtained from the study on continuous crystallisation showing repeatability

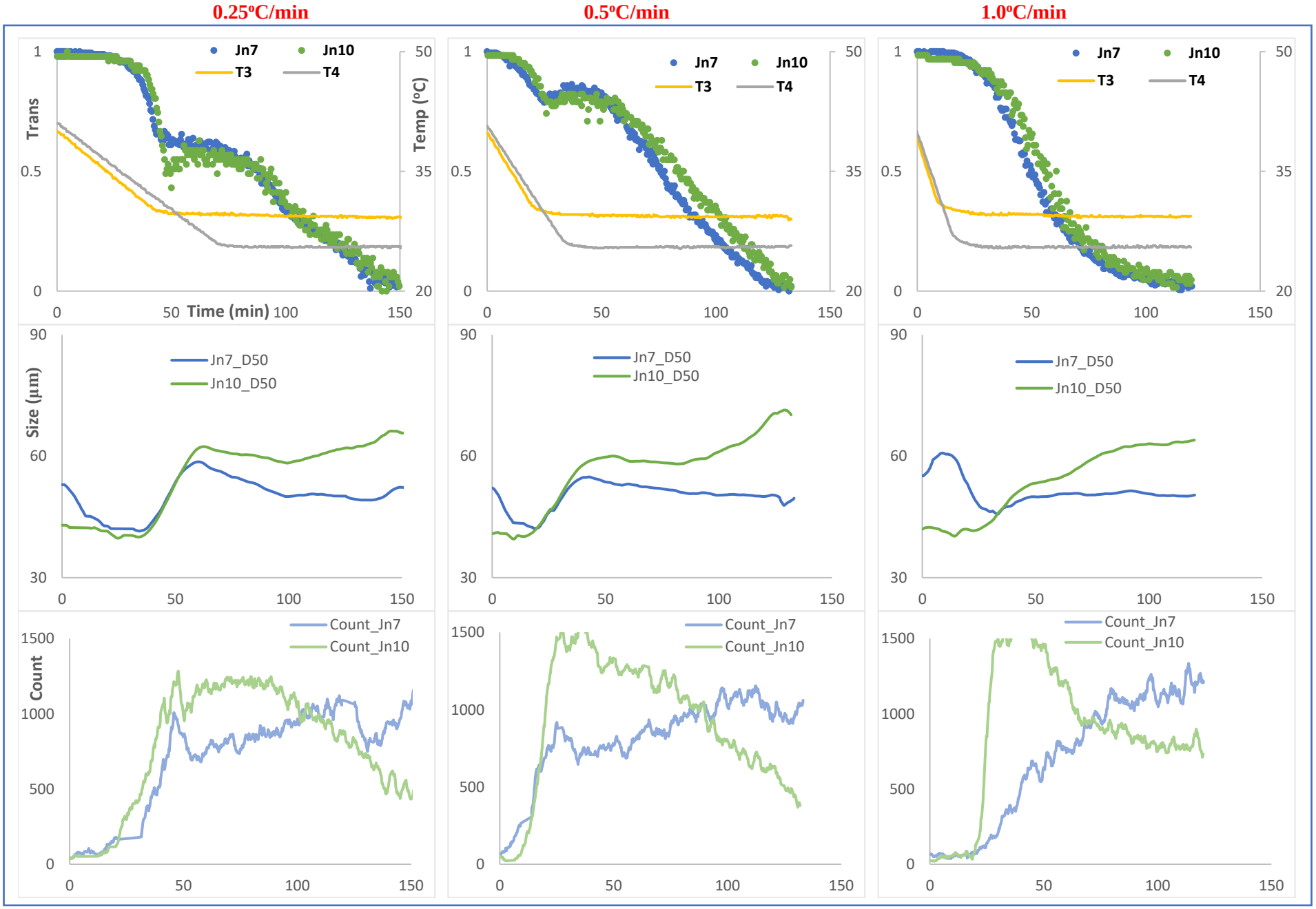

Fig 6.2: Turbidity and size profiles obtained for varied temperature ramping in the COBC during continuous crystallisation

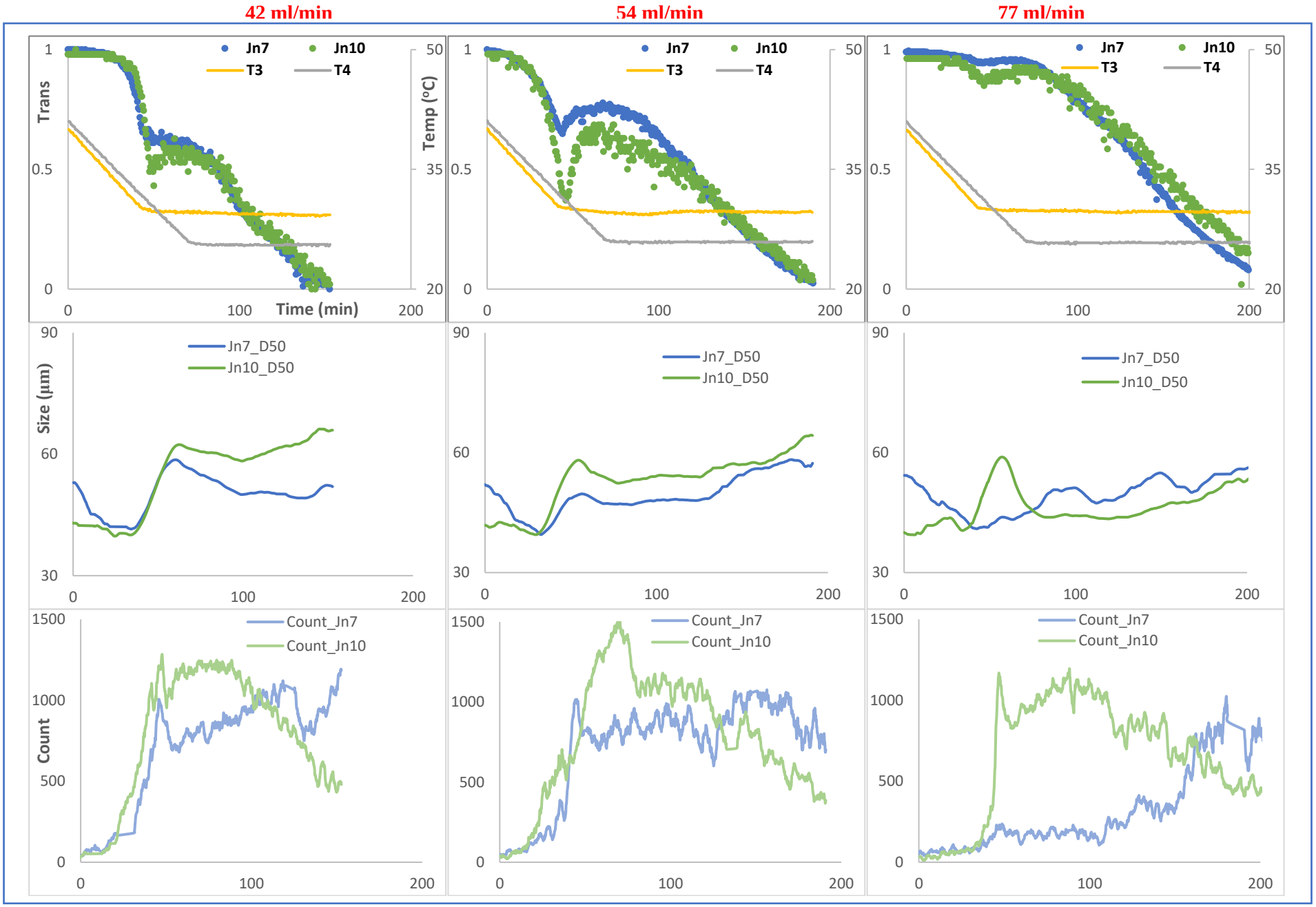

Fig 6.3: Turbidity and size profiles obtained for varied flowrates in the COBC during continuous crystallisation

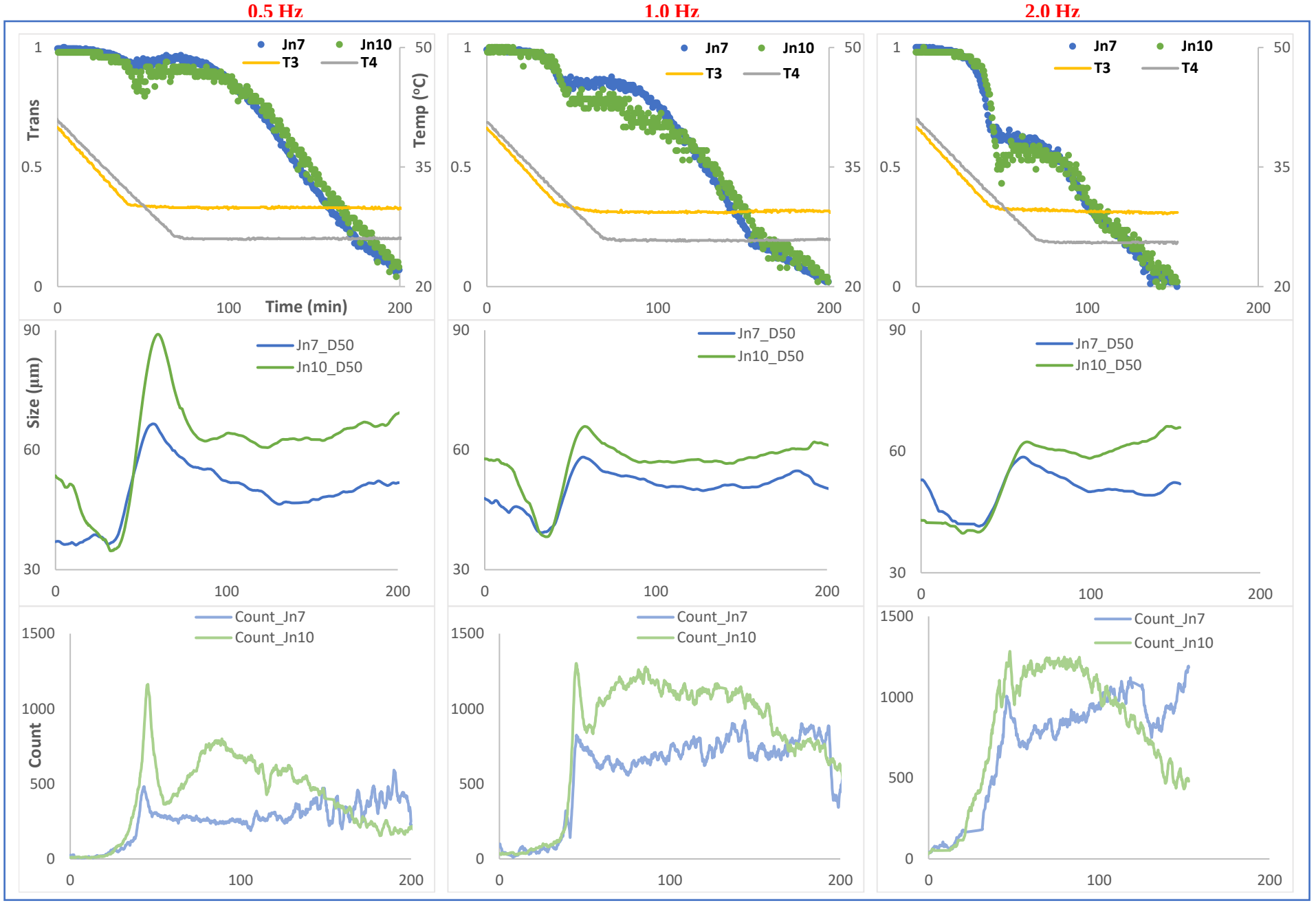

Fig 6.4: Turbidity and size profiles obtained for varied mixing intensity in the COBC during continuous crystallisation

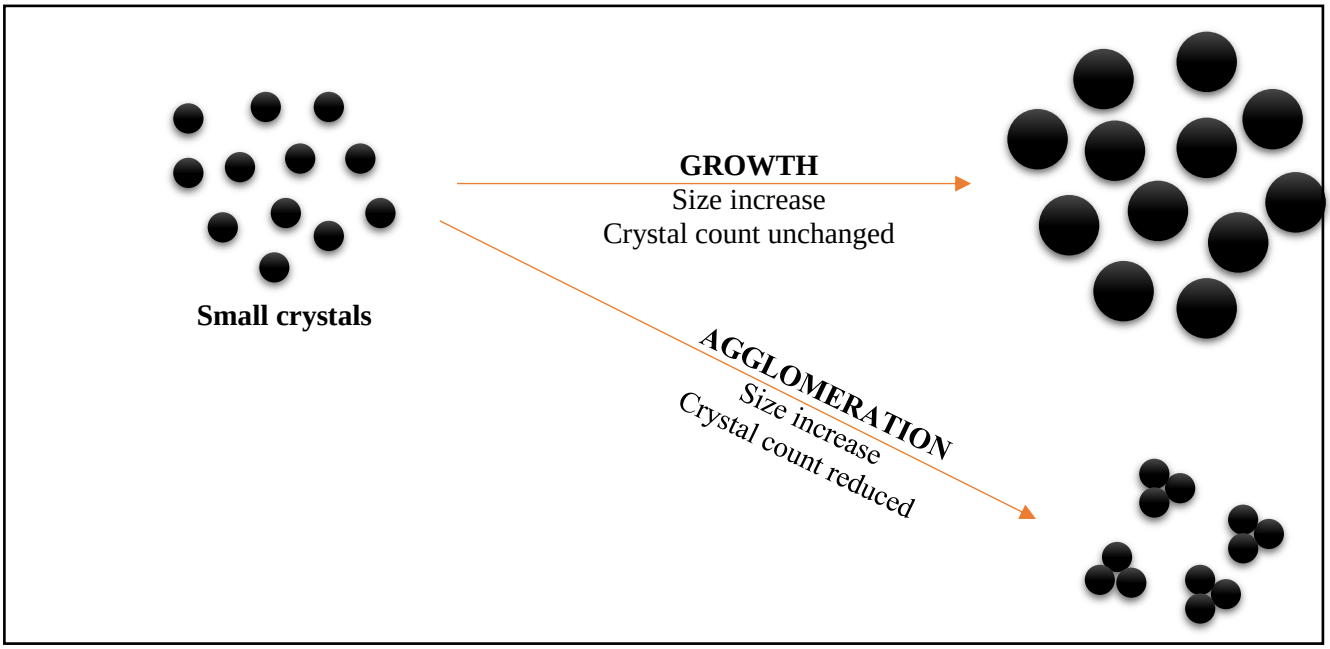

Fig 6.5: Rough schematic demonstrating the difference between crystal growth and agglomeration

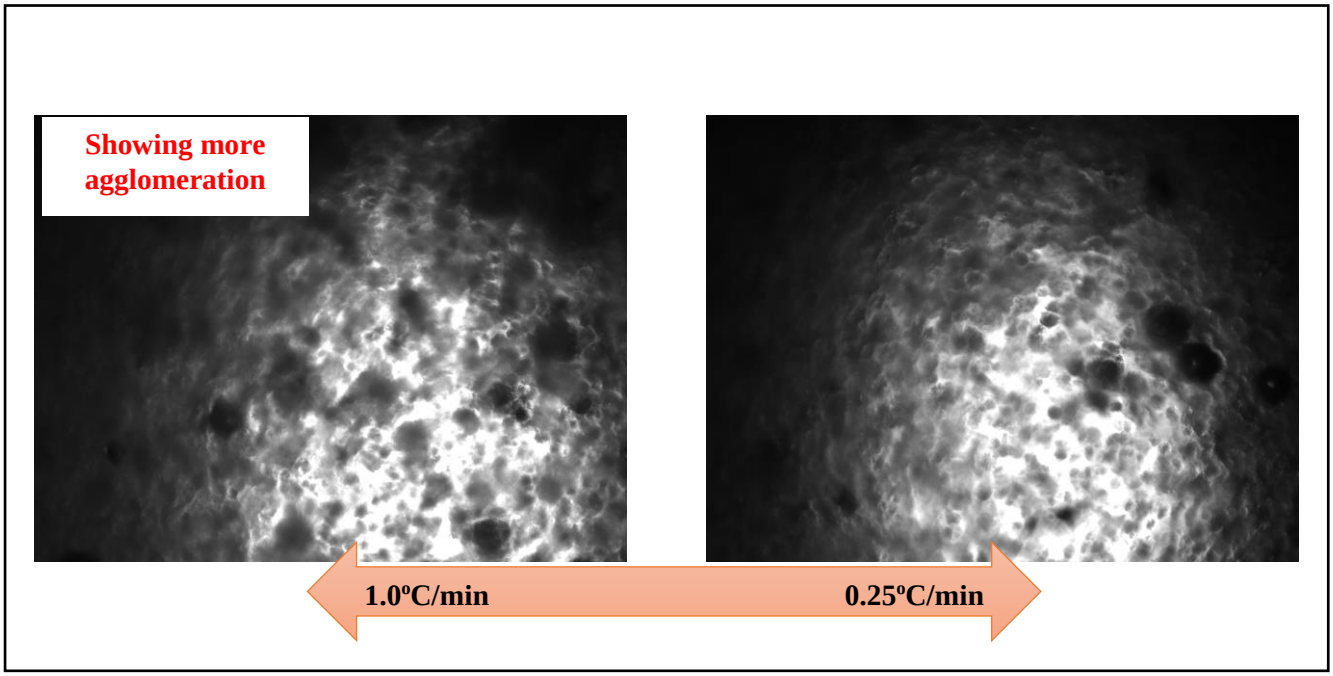

Fig 6.6: Sample online images of palm oil crystals within the COBC (from Perdix camera) showing the effect of temperature ramping

6.3 Conclusion

Continuous crystallisation of palm oil (a typical melt system) was carried in a continuous oscillatory baffled crystalliser (COBC) where the effects of temperature ramping, flowrate (residence time), and mixing intensity (oscillatory Reynolds number) on the steady state properties were examined. It was observed that:

- For all the temperature ramping considered, a temporal steady state size was observed at 50.64 ± 0.19 μm and 62.10 ± 0.94 μm at Jn7 and Jn10 respectively, with an overall size change of 6 – 10% over a 30-min period. The corresponding % transmittance (relating to solute consumption) was continuously decreasing with time, but the overall change in % transmittance with time was within similar order of magnitude for all ramps considered. An overall size change of ~3% corresponded to ~56% change in % transmittance over a 30-min period (a > 10-fold proportion).

- There was evidence of crystal size increase along the tube length as seen from the consistent higher mean size of crystals at Jn10 by an average of 11 μm for the rampings considered. However, this was attributed to agglomeration as opposed to crystal growth due to the minimal change in the % transmittance (≤10%) along the tube length. The rate of this agglomeration event was on the increase with time but it was averaged at 0.027 μm/s.

- Temporal steady state size was achieved for the flowrates examined with a 3 – 5% size change over last 15-min period considered. Lower mean size was observed at fast flowrate and this was attributed to the short residence time limiting the degree of crystallisation. The % transmittance also reflected this inference, such that its evolution with time also reduced by similar ratio by which the flowrate was increased.

- While spatial size increase was observed from Jn7 to Jn10 at low flowrate as expected, the reverse was the case at high flowrate, and this was again associated with the short residence time. The spatial difference in % transmittance ranged from 1 – 6% hence was considered fairly insignificant.

- At the mixing intensities considered, temporal steady state of mean size was achieved with ≤10% change for a 30-min period. A ~6% mean size reduction was observed when the oscillation frequency was increased by a factor of 4 – an attrition effect. Meanwhile, the corresponding transmittance data showed a ~59% decrease (i.e. increased solute consumption) – a nucleation effect. It was therefore concluded that mixing had more effect on the nucleation rate than the attrition rate.

- Size increase between Jn7 and Jn10, with minimal % transmittance change was observed at all mixing conditions examined; also, the rate of size increase was within similar order of magnitude. Mixing effect was more prominent with respect to solute consumption (see above paragraph).

- Note that this is the first time that temporal and spatial data of crystal sizes and solute consumption are obtained and analysed for different operating parameters. Carrying out these steady state analyses is an unchartered territory with respect to palm oil (a typical fat material) crystallisation and some interesting but useful correlations and discoveries were made.

CHAPTER 7- RECOMMENDED FUTURE WORK

This research has covered extensively some of the fundamentals of melt crystallisation using palm oil as its model system through experimental studies and some mathematical manipulations; the application of a novel mixing technology – oscillatory baffled crystalliser – was successfully explored. However, during the course of the studies carried out, some questions arose that birthed the possibility of taking this research even further, and the collation of these form the below recommendations for future work.

7.1 Extended studies on continuous crystallisation

Over the course of this research, particular in the studies relating to continuous crystallisation, a number of fascinating discoveries were made, but time constraints limited the extent to which these discoveries were explored further, such that inconclusive inferences were drawn. One of these include the concept of fouling which was inferred as a possibility at the high flowrate considered. Another is the possibility of solute concentration feeding the agglomeration event. These are just a few of the wide range of studies that could be carried out on fat crystallisation in the continuous oscillatory baffled crystalliser, using this research as a *building block*

7.2 Process Analytical Technology

One of the major challenges faced during this research is the availability of an appropriate PAT tool for online quantitative measurement of solute concentration due to the peculiarity of the oil system being examined. This challenge became prominent during the continuous crystallisation study such that qualitative measurements were resorted to instead. The limitation of this approach is quite apparent, hence it could be given more consideration such that more appropriate PAT technique can be sourced and adopted to get more real-time measurements, making it easier to explain some of the mysterious observations and therefore draw more accurate conclusions. Some extensive work had been carried out previously in this regard, but mostly for other organic compounds[106, 240, 241]. Adoption of these studies to continuous fat crystallisation would be of great insight.

7.3 Extended filtration studies

The filtration studies could be investigated further by exploring other parameters that influence the filtration (and product) properties, e.g. vacuum pressure, cake width/depth, media resistance, etc. Also, a filtration step can be incorporated into the continuous study by installing a suitable filtration mechanism to the exit of the COBC such that both the crystallisation and filtration process can run continuously. An example of a suitable mechanism is the membrane filter press (see **Fig 7.1** below), as this can easily be connected to the COBC such that the crystallised suspension exiting the crystalliser can be pumped directly into the filter press to undergo the filtration process without any downtime.

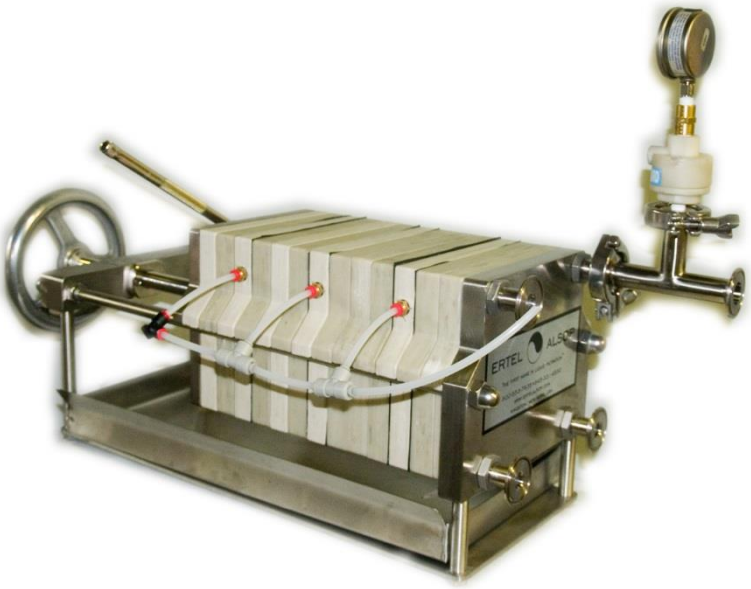

Fig 7.1: A picture of a typical membrane filter press (S*ource: ErtelAlsop*)

Whilst this would help validate some of the inferences drawn, it would also provide a more holistic understanding of the inter-dependence of crystallisation and filtration with respect to fat crystallisation. Furthermore, the latter would move the research closer to its ultimate goal of automating the entire solids particles manufacturing from synthesis to formulated products.

7.4 Modelling

In addition to experimental property measurements, steady states based on the evolution of parameters can be predicted through modelling and then compared with experimental results for validation; a common approach is the use of population balance model – it involves mass balance analyses based on the occurrences that make up the crystallisation process. A sample

model equation developed for steady state operation in a plug flow crystalliser is shown below[242]:

$$u_x \frac{\delta n}{\delta x} + G \frac{\delta n}{\delta L} = 0 \qquad (7.1)$$

Where x = distance along the length of the crystalliser; ux = average net velocity of fluid flow; n = number density; G = crystal growth rate; L = crystal size.

Results obtained and validation can also be compared with those of solution crystallisation to establish similarities and differences.

7.5 Other fat systems

This research was centred on a fat system (palm oil) with a particular feed triglyceride composition. Since studies on palm oil crystallisation was successfully carried out in the COBC, other fat systems (both palm oil from another source or a different type entirely, e.g. milk fat) should be explored such that the effect of triglyceride compositions on the crystallisation properties and resulting product quality can be established. For instance, the effect of chain length of the fatty acids that make up the triglycerides on the growth rate has been reported to be significant[80]; hence it would be useful to consider this with respect to the oscillatory mixing technology. This would also help to reaffirm the versatility of the oscillatory baffled technology with regards to melt crystallisation.

7.6 Polymorphism

It has been established through series of studies and techniques that palm oil fat crystals possess more than one polymorph; this was elaborated upon in section **2.3.5**. Hence investigating how the parameters explored in this research influence the polymorphic behaviour of the palm stearin product would be a useful study in providing more information on the crystallisation process and the resulting product quality. Essentially, the dynamics of the COBC in relation to its effect on fat polymorphism can be explored.

APPENDICES

APPENDIX A – Iodine Value

Titration Methods

There were two methods used for this experiment; one was for the standardisation of the titrant, sodium thiosulphate (**Fig A1. 1**) and another, for the actual titration experiment for iodine value determination **(Fig A1. 2**).

Method 6 –

B 4 Thiosulfate

- $c(Na_2S_2O_3)$ = 0.1 mol/L

  If possible this titrant should be bought ready for use. Otherwise weigh out 25 g $Na_2S_2O_3$ x 5 H_2O into a 1000 mL volumetric flask, dissolve in CO_2-free dist. H_2O, use this to make it up to the mark and mix.

Recommended accessories

- 6.0431.100 Pt Titrode with 6.2104.020 electrode cable
- 6.3026.220 Exchange Unit

Titer determination

Potassium iodate is dried overnight in a drying oven at 180 °C and allowed to cool down in a desiccator for at least 2 h.

Approx. 50 mg KIO_3 is weighed out into the titration beaker with an accuracy of 0.1 mg and dissolved in approx. 80 mL dist. H_2O. Add approx. 1 g potassium iodide and 10 mL $w(H_2SO_4)$ = 25% and titrate immediately with $c(Na_2S_2O_3)$ = 0.1 mol/L to after the first endpoint.

1 mL $c(Na_2S_2O_3)$ = 0.1 mol/L corresponds to 3.567 mg KIO_3 (C01)

Titer = C00 / C01 / EP1

EP1 = mL thiosulfate solution up to endpoint
C00 = weight of KIO_3 in mg
C01 = 3.567

Fig A1. 1 A screenshot of the titration method used for thiosulfate standardisation

Method 27 –

E 3 Iodine number

Recommended ccessories

- 6.0431.100 Pt Titrode with 6.2104.020 electrode cable
- 6.3026.220 Exchange Unit(s)

Reagents

- Titrant: $c(Na_2S_2O_3)$ = 0.1 mol/L. See Method 6, Section B.
- Reaction solution: c(ICl) = 0.1 mol/L in glacial acetic acid
  16.2 g iodine monochloride is dissolved in glacial acetic acid, made up to 1 liter with it and mixed.
- Glacial acetic: w(acetic acid) = 96...98%
- Catalyst solution: w(Mg acetate) = 3% in glacial acetic acid
  45 g $Mg(OOCCH_3)_2$ x 4 H_2O is dissolved in glacial acetic acid, made up to 1 liter with it and mixed.
- Potassium iodide solution: w(KI) = 10%
  50 g KI is dissolved in dist. H_2O, made up to 500 mL and mixed. It is stored in a dark bottle and protected against light.

Blank value of reaction solution

20 mL glacial acetic acid, 25.0 mL reaction solution and 10 mL catalyst solution are placed in an Erlenmeyer flask with an SGJ stopper. The flask is sealed and placed in the dark for exactly 5 min. 15 mL KI is then added, the mixture is then transferred quantitatively to the titration beaker with dist. H_2O and immediately titrated with $c(Na_2S_2O_3)$ = 0.1 mol/L to after the first endpoint.

The titrant consumption (EP1) is stored in the Titrino as a Common Variable (e.g. C31).

BV = EP1 (mL) = C31

Analysis

Depending on the expected iodine number, 0.1...1 g sample is weighed out into an Erlenmeyer flask with an SGJ stopper and dissolved in 20 mL glacial acetic acid. After the addition of 25.0 mL reaction solution and 10 mL catalyst solution the flask is sealed and placed in the dark for exactly 5 min. 15 mL KI is then added, the mixture is then transferred quantitatively to the titration beaker with dist. H_2O and immediately titrated with $c(Na_2S_2O_3)$ = 0.1 mol/L to after the first endpoint.

Calculations

Iodine number (IN) = g iodine per 100 g sample

IN = (C31 – EP1) x C01 x C30 / C00

EP1 = mL thiosulfate solution for sample
C00 = sample weight in g
C01 = 1.269 (equivalent weight of iodine)
C30 = titer of thiosulfate solution (Method 6)
C31 = BV (mL thiosulfate solution)

Remarks

- For vegetable fats and oils the iodine number lies between 75 and 150 g iodine per 100 g. Exceptions are coconut fat with 6...11 and palm oil with approx. 50 g I_2 / 100 g.
- Care must be taken that at least 25 mL thiosulfate are consumed by the sample. If the consumption is lower than there is the risk that too low iodine numbers will be obtained.
- For olive and sunflower oil we have found that the sample weights should be less than 0.4 g.

Fig A1. 2 A screenshot of the method used for Iodine Value Determination of palm oil in this research

Titration Result Data

The table below contains the data of results obtained from the titration experiment for the iodine value determination:

Key: *Conc (ol)* = olein concentration; *S_Size* = sample size; *BV* = blank value; *EP1* = titration end point; *IV* = iodine value; *IV (calc.)* = calculated iodine value

Table A1. 1 Results data for IV determination of palm olein/stearin blends

System	Conc (ol)	S_Size (g)	BV (ml)	EP1 (mL)	IV	IV (calc.)
Olein	**1.00**	**1.00**	47.20	3.73	54.70	54.70
Blend	0.85	1.06	47.42	5.84	52.32	51.89
Blend	0.70	1.00	47.24	7.78	49.65	49.08
Blend	0.55	1.00	47.61	10.28	46.96	46.27
Blend	0.40	1.02	47.33	12.37	43.98	43.46
Blend	0.25	1.00	47.20	14.93	40.6	40.65
Blend	0.10	1.00	47.36	16.42	38.92	37.83
Stearin	**0.00**	**1.00**	47.35	18.07	35.96	35.96

APPENDIX B – Solubility

Calorimetry

The table below shows the solubility data of stearin in olein using the Hildebrand equation.

Key: x_s = stearin fraction; x_o = olein fraction; x_t = total sample

Table B1. 1 Solubility data obtained from Hildebrand equation

T(°C)	T (K)	1/T	ln(x)	x_s (mol)	x_s (g)	x_o (mol)	x_o (g)	x_t (g)	x_s (g/g)
10	283.15	0.00353	-3.076	0.046	38.305	0.954	806.957	845.26	0.045
15	288.15	0.00347	-2.600	0.074	61.663	0.926	783.149	844.81	0.073
20	293.15	0.00341	-2.140	0.118	97.664	0.882	746.453	844.12	0.116
25	298.15	0.00335	-1.695	0.184	152.317	0.816	690.747	843.06	0.181
30	303.15	0.00330	-1.266	0.282	234.097	0.718	607.391	841.49	0.278
35	308.15	0.00325	-0.850	0.427	354.802	0.573	484.359	839.16	0.423
40	313.15	0.00319	-0.447	0.639	530.651	0.361	305.120	835.77	0.635
45	318.15	0.00314	-0.057	0.944	783.677	0.056	47.216	830.89	0.943

Molar mass of olein was taken as 846 g/mol (*assuming C18:1 forms the bulk of the FA content*)

REFERENCE

1. Lawton, S., et al., *Continuous Crystallization of Pharmaceuticals Using a Continuous Oscillatory Baffled Crystallizer*. Organic Process Research & Development, 2009. **13**(6): p. 1357-1363.
2. Mullin, J.W., *9 - Crystallizer design and operation*, in *Crystallization (Fourth Edition)*, J.W. Mullin, Editor. 2001, Butterworth-Heinemann: Oxford. p. 403-477.
3. Mersmann, A., *Design of Crystallizers*, in *Crystallization Technology Handbook*. 2001, CRC Press.
4. Ulrich, J. and H.C. Bülau, *7 - Melt crystallization*, in *Handbook of Industrial Crystallization (Second Edition)*, A.S. Myerson, Editor. 2002, Butterworth-Heinemann: Woburn. p. 161-179.
5. Mersmann, A., *Physical and Chemical Properties of Crystalline Systems*, in *Crystallization Technology Handbook*. 2001, CRC Press.
6. Mullin, J.W., *8 - Industrial techniques and equipment*, in *Crystallization (Fourth Edition)*. 2001, Butterworth-Heinemann: Oxford. p. 315-402.
7. Zhang, X., et al., *Comparative Analysis of Thermal Behavior, Isothermal Crystallization Kinetics and Polymorphism of Palm Oil Fractions.* Molecules, 2013. **18**(1): p. 1036-1052.
8. Kellens, M., et al., *Palm oil fractionation.* European Journal of Lipid Science and Technology, 2007. **109**(4): p. 336-349.
9. Mullin, J.W., *3 - Solutions and solubility*, in *Crystallization (Fourth Edition)*, J.W. Mullin, Editor. 2001, Butterworth-Heinemann: Oxford. p. 86-134.
10. Miers, H. and F. Isaac, *The Spontaneous Crystallisation of Binary Mixtures.* Proceedings of the Royal Society of London, 1907. **79**(531): p. 322-351.
11. Mitchell, N.A. and P.J. Frawley, *Nucleation kinetics of paracetamol–ethanol solutions from metastable zone widths.* Journal of Crystal Growth, 2010. **312**(19): p. 2740-2746.
12. Khamskii, E.V. and A. Tybulewicz, *Crystallization from solutions*. 1969, New York; London: Consultants Bureau.
13. Balibar, S., B. Castaing, and C. Laroche, *Nucleation and orientation of 4He crystals.* J. Physique Lett., 1980. **41**(12): p. 283-285.
14. Hunt, J.D. and K.A. Jackson, *Nucleation of the Solid Phase by Cavitation in an Undercooled Liquid which expands on Freezing*. Nature, 1966. **211**(5053): p. 1080-1081.
15. Nore, P. and A. Mersmann, *Batch precipitation of barium carbonate.* Chemical Engineering Science, 1993. **48**(17): p. 3083-3088.
16. Mersmann, A., C. Heyer, and A. Eble, *Activated Nucleation*, in *Crystallization Technology Handbook*. 2001, CRC Press.
17. Volmer, M. and A. Weber, *Nucleus formation in supersaturated systems.* IInternational Journal of Research in Physical Chemistry & Chemical Physics, 1926. **119**: p. 277-301.
18. Mullin, J.W., *5 - Nucleation*, in *Crystallization (Fourth Edition)*. 2001, Butterworth-Heinemann: Oxford. p. 181-215.
19. He, G., et al., *Determination of Critical Supersaturation from Microdroplet Evaporation Experiments.* Crystal Growth & Design, 2006. **6**(5): p. 1175-1180.
20. Christoffersen, J., E. Rostrup, and M.R. Christoffersen, *Relation between interfacial surface tension of electrolyte crystals in aqueous suspension and their solubility; a simple derivation based on surface nucleation.* Journal of Crystal Growth, 1991. **113**(3–4): p. 599-605.
21. Myerson, A.S. and R. Ginde, *2 - Crystals, crystal growth, and nucleation*, in *Handbook of Industrial Crystallization (Second Edition)*, S.M. Allan, Editor. 2002, Butterworth-Heinemann: Woburn. p. 33-65.
22. Pruppacher, H.R. and J.D. Klett, *Microphysics of Clouds and Precipitation*. 1978: Reidel. 714.
23. Fletcher, N.H., *The physics of rainclouds*. 1962: University Press. 386.
24. Valeton, J.J.P., *Growth and dissolution of crystals.* Journal for Crystallography, 1924. **59**: p. 135-169.
25. Volmer, M. and O.H. Foreign Technology Div Wright-Pattersonafb. *Kinetics of Phase Formation(Kinetik der Phasenbildung)*. 1939; Available from: http://handle.dtic.mil/100.2/ADA800534.
26. Mullin, J.W., *6 - Crystal growth*, in *Crystallization (Fourth Edition)*. 2001, Butterworth-Heinemann: Oxford. p. 216-288.
27. Garside, J. and S.J. Jančić, *Growth and dissolution of potash alum crystals in the subsieve size range.* AIChE Journal, 1976. **22**(5): p. 887-894.
28. Kougoulos, E., A.G. Jones, and M.W. Wood-Kaczmar, *Estimation of crystallization kinetics for an organic fine chemical using a modified continuous cooling mixed suspension mixed product removal (MSMPR) crystallizer.* Journal of Crystal Growth, 2005. **273**(3–4): p. 520-528.
29. Garside, J. and R.J. Davey, *INVITED REVIEW SECONDARY CONTACT NUCLEATION: KINETICS, GROWTH AND SCALE-UP*. Chemical Engineering Communications, 1980. **4**(4-5): p. 393-424.

30. White, E.T. and P.G. Wright, *Magnitude of size dispersion effects in crystallization.* Chemical Engineering Progress, Symposium Series 1971. **67**(110): p. 81-87.
31. Mullin, J.W., M. Chakraborty, and K. Mehta, *Nucleation and growth of ammonium sulphate crystals from aqueous solution.* Journal of Applied Chemistry, 1970. **20**(12): p. 367-371.
32. Ulrich, J. and C. Strege, *Some aspects of the importance of metastable zone width and nucleation in industrial crystallizers.* Journal of Crystal Growth, 2002. **237**: p. 2130-2135.
33. Nývlt, J., *Kinetics of nucleation in solutions.* Journal of Crystal Growth, 1968. **3–4**(0): p. 377-383.
34. Nývlt, J., *Induction period of nucleation and metastable zone width.* Collection of Czechoslovak chemical communications, 1983. **48**(7): p. 1977-1983.
35. Chrisman, R.W., R.S. Harner, and R.D. McLachlan, *Method for determining the onset of crystallization*. 1987, Google Patents: US.
36. Harner, R.S., et al., *Use of a Fiber-Optic Turbidity Probe to Monitor and Control Commercial-Scale Unseeded Batch Crystallizations.* Organic Process Research & Development, 2008. **13**(1): p. 114-124.
37. Wright, A., S. Narine, and A. Marangoni, *Comparison of experimental techniques used in lipid crystallization studies.* Journal of the American Oil Chemists' Society, 2000. **77**(12): p. 1239-1242.
38. Dunuwila, D.D., L.B. Carroll II, and K.A. Berglund, *An investigation of the applicability of attenuated total reflection infrared spectroscopy for measurement of solubility and supersaturation of aqueous citric acid solutions.* Journal of Crystal Growth, 1994. **137**(3): p. 561-568.
39. Chew, J.W., P.S. Chow, and R.B. Tan, *Automated in-line technique using FBRM to achieve consistent product quality in cooling crystallization.* Crystal Growth & Design, 2007. **7**(8): p. 1416-1422.
40. Geoff, T., K.W. Smith, and F.W. Cain, *Solvent Fraction of Palm Oil*, in *International News on Fats, Oils and Related Materials : INFORM*. 2006, AOCS Press. p. 324-326.
41. Cheon, Y.-H., K.-J. Kim, and S.-H. Kim, *A study on crystallization kinetics of pentaerythritol in a batch cooling crystallizer.* Chemical Engineering Science, 2005. **60**(17): p. 4791-4802.
42. Omar, W. and J. Ulrich, *Application of Ultrasonics in the On-line Determination of Supersaturation.* Crystal Research and Technology, 1999. **34**(3): p. 379-389.
43. Ni, X. and A. Liao, *Effects of mixing, seeding, material of baffles and final temperature on solution crystallization of l-glutamic acid in an oscillatory baffled crystallizer.* Chemical Engineering Journal, 2010. **156**(1): p. 226-233.
44. Söhnel, O. and J. Garside, *Precipitation: basic principles and industrial applications*. 1992: Butterworth-Heinemann.
45. Ulrich, J. *Some aspects in the purification by directed crystallization*. Chemical Engineering Symposium, 1988. **18**, 172-175.
46. Peters-Erjawetz, S., et al., *Milk fat fractionation by solid-layer melt crystallization.* Journal of the American Oil Chemists' Society, 1999. **76**(5): p. 579-584.
47. Matsuoka, M. and H. Fukushima, *Determination of solid-liquid equilibrium.* Bunri Gijutsu (Separation Process Engineering), 1986. **16**: p. 4-10.
48. Ransley, D.L., *Xylenes and Ethylbenzene*, in *Encyclopedia of Chemical Technology*, Kirk-Othmer, Editor. 1984, John Wiley & Sons: New York. p. 709.
49. Ulrich, J. and J. Bierwirth, *Melt Layer Crystallization*, in *Science and Technology of Crystal Growth*, J.P. Eerden and O.S.L. Bruinsma, Editors. 1995, Springer Netherlands. p. 245-258.
50. Jancic, S.J., *Fractional Crystallisation*, in *Industrial Crystallisation*, J. Nyvlt and S. Zacek, Editors. 1987, Elsevier Science Publishers: Amstersdam. p. 57-70.
51. Taylor, H.S., *States of Aggregation (Tammann, G.).* Journal of Chemical Education, 1926. **3**(1): p. 119.
52. Turnbull, D. and J.C. Fisher, *Rate of Nucleation in Condensed Systems.* The Journal of Chemical Physics, 1949. **17**(1): p. 71-73.
53. Mullin, J.W. and C.L. Leci, *Some nucleation characteristics of aqueous citric acid solutions.* Journal of Crystal Growth, 1969. **5**(1): p. 75-76.
54. Wintermantel, K. and W. Kast, *Wärme- und Stoffaustausch bei der Kristallisation an gekühlten Flächen. Teil II: Ergebnisse bei bewegten wäßrigen Lösungen und Xylol-Gemischen.* Chemie Ingenieur Technik, 1973. **45**(9-10): p. 728-731.
55. Wintermantel, K., *Die effektive Trennwirkung beim Ausfrieren von Kristallschichten aus Schmelzen und Lösungen – eine einheitliche Darstellung.* Chemie Ingenieur Technik, 1986. **58**(6): p. 498-499.
56. Burton, J.A., R.C. Prim, and W.P. Slichter, *The Distribution of Solute in Crystals Grown from the Melt. Part I. Theoretical.* The Journal of Chemical Physics, 1953. **21**(11): p. 1987-1991.
57. Rutter, J.W. and B. Chalmers, *A PRISMATIC SUBSTRUCTURE FORMED DURING SOLIDIFICATION OF METALS.* Canadian Journal of Physics, 1953. **31**(1): p. 15-39.
58. Scholz, K., *Die Schichtkristallisation als thermisches Trennverfaren*. 1993, VDI: Germany.
59. Mullins, W.W. and R.F. Sekerka, *Stability of a Planar Interface During Solidification of a Dilute Binary Alloy.* Journal of Applied Physics, 1964. **35**(2): p. 444-451.

60. Biles, J.A., *Fractional solidification. Vol. I. Edited by M. Zief and W. R. Wilcox. Marcel Dekker, Inc., 95 Madison Ave., New York, NY 10019 1967. xvi + 714 pp. 16 × 23.5 cm. Price $28.75*. Journal of Pharmaceutical Sciences, 1968. **57**(8): p. 1452-1452.
61. Henning, S. and J. Ulrich, *Description of the Migration of Liquid Inclusions in Growing Crystalline Layers.* Chemical Engineering Research and Design, 1997. **75**(2): p. 233-236.
62. Foubert, I., K. Dewettinck, and P.A. Vanrolleghem, *Modelling of the crystallization kinetics of fats.* Trends in food science & technology, 2003. **14**(3): p. 79-92.
63. Avrami, M., *Kinetics of phase change. I General theory.* The Journal of Chemical Physics, 1939. **7**(12): p. 1103-1112.
64. Avrami, M., *Kinetics of phase change. II transformation-time relations for random distribution of nuclei.* The Journal of Chemical Physics, 1940. **8**(2): p. 212-224.
65. Evans, U.R., *The laws of expanding circles and spheres in relation to the lateral growth of surface films and the grain-size of metals.* Transactions of the Faraday Society, 1945. **41**(0): p. 365-374.
66. Meares, P., *Polymers: structure and bulk properties*. 1965: Van Nostrand Reinhold.
67. Hay, J., *Application of the modified avrami equations to polymer crystallisation kinetics.* British Polymer Journal, 1971. **3**(2): p. 74-82.
68. Sperling, L., *Introduction to physical polymer science, 1992*. John Wiley & Sons, New York.
69. Cazé, C., et al., *A new method to determine the Avrami exponent by d.s.c. studies of non-isothermal crystallization from the molten state.* Polymer, 1997. **38**(3): p. 497-502.
70. Lu, M.G., M.J. Shim, and S.W. Kim, *Dynamic DSC Characterization of Epoxy Resin by Means of the Avrami Equation.* Journal of Thermal Analysis and Calorimetry. **58**(3): p. 701-709.
71. Bhattacharyya, A.R., et al., *Crystallization and orientation studies in polypropylene/single wall carbon nanotube composite.* Polymer, 2003. **44**(8): p. 2373-2377.
72. Wang, X. and J.J. Vlassak, *Crystallization kinetics of amorphous NiTi shape memory alloy thin films.* Scripta Materialia, 2006. **54**(5): p. 925-930.
73. Campos, R., S. Narine, and A. Marangoni, *Effect of cooling rate on the structure and mechanical properties of milk fat and lard.* Food Research International, 2002. **35**(10): p. 971-981.
74. Galwey, A.K. and M.E. Brown, *Thermal decomposition of ionic solids: chemical properties and reactivities of ionic crystalline phases*. Vol. 86. 1999: Elsevier.
75. Sharples, A., *Introduction to polymer crystallization.* 1966.
76. Pal, S. and A.K. Nandi, *Cocrystallization mechanism of poly(3-alkyl thiophenes) with different alkyl chain length.* Polymer, 2005. **46**(19): p. 8321-8330.
77. Marangoni, A.G., *Fat crystal networks*. Vol. 140. 2004: CRC Press.
78. Mazzanti, G., A.G. Marangoni, and S.H. Idziak, *Modeling phase transitions during the crystallization of a multicomponent fat under shear.* Physical Review E, 2005. **71**(4): p. 041607.
79. Khanna, Y.P. and T.J. Taylor, *Comments and recommendations on the use of the Avrami equation for physico-chemical kinetics.* Polymer Engineering & Science, 1988. **28**(16): p. 1042-1045.
80. Himawan, C., V. Starov, and A. Stapley, *Thermodynamic and kinetic aspects of fat crystallization.* Advances in colloid and interface science, 2006. **122**(1): p. 3-33.
81. Becker, R., *Die Keimbildung bei der Ausscheidung in metallischen Mischkristallen.* Annalen der Physik, 1938. **424**(1-2): p. 128-140.
82. Vyazovkin, S., *Isoconversional Kinetics of Thermally Stimulated Processes*. 2015: Springer International Publishing.
83. Michèle, P., F. Loïc, and S. Michel, *From the drawbacks of the Arrhenius-f (α) rate equation towards a more general formalism and new models for the kinetic analysis of solid–gas reactions.* Thermochimica Acta, 2011. **525**(1): p. 93-102.
84. Takeuchi, M., S. Ueno, and K. Sato, *Crystallization kinetics of polymorphic forms of a molecular compound constructed by SOS (1, 3-distearoyl-2-oleoyl-sn-glycerol) and SSO (1, 2-distearoyl-3-oleoyl-rac-glycerol).* Food Research International, 2002. **35**(10): p. 919-926.
85. Söhnel, O. and J.W. Mullin, *Interpretation of crystallization induction periods.* Journal of Colloid And Interface Science, 1988. **123**(1): p. 43-50.
86. Ng, W., *A study of the kinetics of nucleation in a palm oil melt.* Journal of the American Oil Chemists' Society, 1990. **67**(11): p. 879-882.
87. Sangwal, K., *A novel self-consistent Nývlt-like equation for metastable zone width determined by the polythermal method.* Crystal Research and Technology, 2009. **44**(3): p. 231-247.
88. World, O. *The Independent Forecasting Service for Oilseeds, Oils & Meals*. 2001-2003; Available from: http://www.oilworld.biz/app.php?ista=4218b48123fbd8e6cafc4f97a12c899c.
89. Blamire, P.J., *Triglycerides*, in *Science at a Distance*, P.S.L.G. 2, Editor. 2000.
90. Bresson, S., M.E. Marssi, and B. Khelifa, *Raman spectroscopy investigation of various saturated monoacid triglycerides.* Chemistry and Physics of Lipids, 2005. **134**(2): p. 119-129.

91. Timms, R.E., *Fractionation of palm oil: Current status, future possibilities*, in *International News on Fats, Oils and Related Materials : INFORM*. 2007, AOCS Press. p. 59-62.
92. Calliauw, G., *Edible Oil Processing: DRY FRACTIONATION*. 2011: Belgium. p. 10.
93. Illingworth, D., *Fractionation of fats*, in *Physical Properties of Lipids*, A.G. Marangoni and S.S. Narine, Editors. 2002, Marcel Dekker: New York. p. 411-477.
94. Gijs, H.C., G. Véronique, and F.J.D.G. Wim, *Principles of palm olein fractionation: a bit of science behind the technology.* Lipid Technol, 2007. **19**(7): p. 152-155.
95. Harris, J. *Solvent Fractionation*. Edible OIl Processing, 2011.
96. Don, W.G. and H.P. Robert, *CRYSTALLIZATION FROM SOLUTION*, in *Perry's Chemical Engineers' Handbook, Eighth Edition*. 2008, McGraw Hill Professional, Access Engineering.
97. Don, W.G. and H.P. Robert, *FILTRATION*, in *Perry's Chemical Engineers' Handbook, Eighth Edition*. 2008, McGraw Hill Professional, Access Engineering.
98. Kellens, M., *New developments in the fractionation of palm oil*. 1993.
99. Schick, M.J., *Handbook of lipid research 4–the physical chemistry of lipids, by Donald M. Small, Plenum, New York, 1986, 672 pp. Price: $89.50.* Journal of Polymer Science Part C: Polymer Letters, 1987. **25**(2): p. 86-87.
100. Taylor, A.M., *The Crystallisation and dry fractionation of Malaysian Palm oil.* Oleagineux, 1976. **31**: p. 73-79.
101. Timms, R.E., *Fractional crystallisation – the fat modification process for the 21st century.* European Journal of Lipid Science and Technology, 2005. **107**(1): p. 48-57.
102. Gibbs, J.W., *On the Equilibrium of Heterogeneous Substances.* The Connecticut Academy of Arts and Sciences 1874. **3**(10): p. 343-524.
103. Mullin, J.W., *1 - The crystalline state*, in *Crystallization (Fourth Edition)*. 2001, Butterworth-Heinemann: Oxford. p. 1-31.
104. Chen, C., et al., *Isothermal crystallization kinetics of refined palm oil.* Journal of the American Oil Chemists' Society, 2002. **79**(4): p. 403-410.
105. Braipson-Danthine, S. and V. Gibon, *Comparative analysis of triacylglycerol composition, melting properties and polymorphic behavior of palm oil and fractions.* European Journal of Lipid Science and Technology, 2007. **109**(4): p. 359-372.
106. Hammond, R.B., et al., *Application of In-Process X-ray Powder Diffraction for the Identification of Polymorphic Forms during Batch Crystallization Reactions.* Crystal Growth & Design, 2004. **4**(5): p. 943-948.
107. Che Man, Y.B., et al., *Composition and thermal profile of crude palm oil and its products.* Journal of the American Oil Chemists' Society, 1999. **76**(2): p. 237-242.
108. Garti, N. and K. Sato, *Crystallization and polymorphism of fats and fatty acids*. 1988: M. Dekker.
109. Smith, K.W., F.W. Cain, and G. Talbot, *Crystallisation of 1, 3-dipalmitoyl-2-oleoylglycerol and tripalmitoylglycerol and their mixtures from acetone.* European Journal of Lipid Science and Technology, 2005. **107**(9): p. 583-593.
110. Litwinenko, J., et al., *Relationship between crystallization behavior, microstructure, and mechanical properties in a palm oil-based shortening.* Journal of the American Oil Chemists' Society, 2002. **79**(7): p. 647-654.
111. Normah, I., C. Cheow, and C. Chong, *Crystal habit during crystallization of palm Oil: Effect of time and temperature.* International Food Research Journal, 2013. **20**(1).
112. Kellens, M. *Developments in fat fractionation technology*. in *Fats and oils and fats group symposium*. 1994. London: Society of Chemical Industry.
113. Krishnamurthy, R. and M. Kellens, *Fractionation and winterization*, in *Edible Oil and Fat Products: Processing Technology, Bailey's Industrial Oil and Fat Products*, Y.H. Hui, Editor. 1996, John Wiley: Champaign, USA. p. 301-337.
114. Deffense, E., *Dry fractionation technology in 2000.* European Journal of Lipid Science and Technology, 2000. **102**(3): p. 234-236.
115. Frank Roche, T.P., Jonathan Seville, *Non-stop Pharma*, in *TCE: The chemical engineer*. 2013. p. 28-31.
116. Paul, E.L., H.-H. Tung, and M. Midler, *Organic crystallization processes.* Powder Technology, 2005. **150**(2): p. 133-143.
117. Trout, P.B. *Next-Wave Model*. World Pharmaceutical Frontiers, 2009. 74-76.
118. Alexis Pellek, P.V.A. *Continuous Processing: Moving with or against the Manufacturing Flow*. Pharmaceutical Technology, 2008. **9**, 52-58.
119. Staff, A. *CONTINUOUS MANUFACTURE AND CRYSTALLISATION OF APIS – JUST A PIPEDREAM?* 2012; Available from: http://www.amrismartsourcing.com/manufacturing/continuous-manufacture-and-crystallisation-of-apis-just-a-pipedream/#.WcaJOrKGPcu.

120. Kresta, S.M. and R.S. Brodkey, *Turbulence in mixing applications*, in *Handbook of industrial mixing: science and practice*, E.L. Paul, V.A. Atiemo-Obeng, and S.M. Kresta, Editors. 2004, John Wiley & Sons, Inc: US. p. 19-87.
121. Technology, U.o., *Mixing*. Faculty of Chemical, Environmental and Biological Science and Technology: China. p. 1-66.
122. Zhou, G. and S.M. Kresta, *Impact of tank geometry on the maximum turbulence energy dissipation rate for impellers.* AIChE Journal, 1996. **42**(9): p. 2476-2490.
123. Rielly, C.D. and A.J. Marquis, *A particle's eye view of crystallizer fluid mechanics.* Chemical Engineering Science, 2001. **56**(7): p. 2475-2493.
124. *Agitation and Mixing*. Available from: https://www.slideshare.net/knowledge1995/agitaion-and-mixing.
125. Stonestreet, P. and A.P. Harvey, *A Mixing-Based Design Methodology for Continuous Oscillatory Flow Reactors.* Chemical Engineering Research and Design, 2002. **80**(1): p. 31-44.
126. Stephanoff, K., I.J. Sobey, and B. Bellhouse, *On flow through furrowed channels. Part 2. Observed flow patterns.* J. Fluid Mech, 1980. **96**(1): p. 27-32.
127. Chan, K. and M. Baird, *Wall friction in oscillating liquid columns.* Chemical Engineering Science, 1974. **29**(10): p. 2093-2099.
128. Baird, M. and J. Garstang, *Power consumption and gas hold-up in a pulsed column.* Chemical Engineering Science, 1967. **22**(12): p. 1663-1673.
129. Fitch, A.W., H. Jian, and X. Ni, *An investigation of the effect of viscosity on mixing in an oscillatory baffled column using digital particle image velocimetry and computational fluid dynamics simulation.* Chemical Engineering Journal, 2005. **112**(1–3): p. 197-210.
130. Dickens, A., M. Mackley, and H. Williams, *Experimental residence time distribution measurements for unsteady flow in baffled tubes.* Chemical engineering science, 1989. **44**(7): p. 1471-1479.
131. Mackley, M. and X. Ni, *Mixing and dispersion in a baffled tube for steady laminar and pulsatile flow.* Chemical Engineering Science, 1991. **46**(12): p. 3139-3151.
132. Sobey, I.J., *The occurrence of separation in oscillatory flow.* Journal of Fluid Mechanics, 1983. **134**: p. 247-257.
133. Stonestreet, P. and P.M.J. Van Der Veeken, *The Effects of Oscillatory Flow and Bulk Flow Components on Residence Time Distribution in Baffled Tube Reactors.* Chemical Engineering Research and Design, 1999. **77**(8): p. 671-684.
134. Levenspiel, O. and W. Smith, *Notes on the diffusion-type model for the longitudinal mixing of fluids in flow.* Chemical Engineering Science, 1957. **6**(4): p. 227-235.
135. Baird, M. and P. Stonestreet, *Energy dissipation in oscillatory flow within a baffled tube.* Chemical engineering research & design, 1995. **73**(5): p. 503-511.
136. Nagy, Z.K., et al., *Recent advances in the monitoring, modelling and control of crystallization systems.* Chemical Engineering Research and Design, 2013. **91**(10): p. 1903-1922.
137. Haryati, T., P. K., and BuanaL., *Determination of Oil Content by Gas Chromatography.* Malysian Oil Science Technology, 1995. **4**: p. 190-192.
138. Geeraert, E. and P. Sandra, *Capillary GC of triglycerides in fats and oils using a high temperature phenylmethylsilicone stationary phase. Part II. The analysis of chocolate fats.* Journal of the American Oil Chemists' Society, 1987. **64**(1): p. 100-105.
139. Swe, P., Y. Man, and H. Ghazali, *Improved NARP-HPLC method for separating triglycerides of palm olein and its solid fractions obtained at low temperature storage.* Food Chemistry, 1996. **56**(2): p. 181-186.
140. Hamdy, A.H.E.-. and E.G. Perkins, *High Performance reversed phase chromatography of Natural triglyceride mixtures: Critical pair separation.* Journal of the American Oil Chemists' Society, 1981. **58**(9): p. 867-872.
141. Dong, M.W. and J.L. Dicesare, *Improved separation of natural oil triglycerides by liquid chromatography using columns packed with 3-μm particles.* Journal of the American Oil Chemists' Society, 1983. **60**(4): p. 788-791.
142. Deffense, E., *Application de la chromatographie liquide haute performance à l'analyse des triglycérides des graisses végétales et animales et de leurs fractions obtenues par cristallisation fractionnée = High performance liquid chromatography analysis of triglycerides and their fractions obtained by fractional crystallization in vegetable and animal fats.* Revue française des corps gras, 1984. **31**(3): p. 123 - 129.
143. Malaysia, I.P.M.K.S., *Determination of fatty acid methyl esters by gas-liquid chromatography*, in *PORIM Test Methods*. 1995, Palm Oil Research Institute of Malaysia: Malaysia. p. 92-101.
144. AOCS, *Official Methods and Recommended Practices of the American Oil Chemist's Society.* . 4th ed. Aditions and Revisions: Method C 1-25. 1992: AOCS Press, Champaign.
145. Zaliha, O., et al., *Crystallization properties of palm oil by dry fractionation.* Food Chemistry, 2004. **86**(2): p. 245-250.

146. Siew, W.-L. and W.-L. Ng, *Characterisation of Crystals in Palm Olein.* Journal of the Science of Food and Agriculture, 1996. **70**(2): p. 212-216.
147. Okiy, D.A., *Interaction of triglycerides and diglycerides of palm oil.* Oleagineux, 1978. **33**(12): p. 625-628.
148. Lo, S.-K., et al., *Diacylglycerol Oil—Properties, Processes and Products: A Review.* Food and Bioprocess Technology, 2008. **1**(3): p. 223-233.
149. Ab Latip, R., et al., *Palm-based diacylglycerol fat dry fractionation: effect of crystallisation temperature, cooling rate and agitation speed on physical and chemical properties of fractions.* PeerJ, 2013. **1**: p. e72.
150. Inc, A.E. *Oil and Fat Processing*. 2007 10/4/2014]; Available from: https://www.amano-enzyme.co.jp/eng/productuse/oil.html.
151. Blamire, P.J., *Diglyceride*, in *Science at a Distance*, P.S.L.G. 2, Editor. 2000.
152. Lutton, E.S., *Lipid structures.* Journal of the American Oil Chemists' Society, 1972. **49**(1): p. 1-9.
153. Instrument Specialists, I. *DSC – DIFFERENTIAL SCANNING CALORIMETRY*. 2016 [cited 2017 2nd October 2017]; Available from: http://instrument-specialists.com/thermal-analysis-applications/differential-scanning-calorimetry-dsc/.
154. Tan, C.P. and Y.B. Che Man, *Differential scanning calorimetric analysis of palm oil, palm oil based products and coconut oil: effects of scanning rate variation.* Food Chemistry, 2002. **76**(1): p. 89-102.
155. Saadi, S., et al., *Application of differential scanning calorimetry (DSC), HPLC and pNMR for interpretation primary crystallisation caused by combined low and high melting TAGs.* Food Chemistry, 2012. **132**(1): p. 603-612.
156. Busfield, W.K. and P. Proschogo, *Thermal analysis of palm stearine by DSC.* Journal of the American Oil Chemists' Society, 1990. **67**(3): p. 171-175.
157. Fredrick, E., et al., *Influence of Monoglycerides on the Crystallization Behavior of Palm Oil.* Crystal Growth & Design, 2008. **8**(6): p. 1833-1839.
158. De Graef, V., et al., *Crystallization Behavior and Texture of Trans-Containing and Trans-Free Palm Oil Based Confectionery Fats.* Journal of Agricultural and Food Chemistry, 2007. **55**(25): p. 10258-10265.
159. YCW, *Quality and Identity Characteristics – Part 2 – Chemical Characteristics*, in *Oil Palm Knowledge Base*. 2014.
160. Paquot, C., *2.205 - Determination of the Iodine Value (I.V.)*, in *Standard Methods for the Analysis of Oils, Fats and Derivatives (Sixth Edition)*, C. Paquot, Editor. 1979, Pergamon. p. 66-70.
161. Pétursson, S., *Clarification and expansion of formulas in AOCS recommended practice Cd 1c-85 for the calculation of Iodine value from FA composition.* Journal of the American Oil Chemists' Society, 2002. **79**(7): p. 737-738.
162. Bergman, J., et al., *Registration of 'Finch'safflower.* Crop Science, 1989. **29**(3): p. 829-829.
163. Misra, N., S. Batra, and A. Rathore, *Effect of storage moulds on the nutritional components of Foeniculum vulgare Mill.* International Journal of Tropical Plant Diseases, 1988. **6**(1): p. 67-72.
164. Schynowski, F. and W. Schwack, *Photochemistry of parathion on plant surfaces: relationship between photodecomposition and iodine number of the plant cuticle.* Chemosphere, 1996. **33**(11): p. 2255-2262.
165. Mittelbach, M., *Diesel fuel derived from vegetable oils, VI: Specifications and quality control of biodiesel.* Bioresource Technology, 1996. **56**(1): p. 7-11.
166. Cocks, L.V. and C. van Rede, *Laboratory handbook for oil and fat analysts*. 1966: Academic P.
167. Rossell, J.B., *Classical Analysis of Oils and fats*, in *Analysis of Oils and Fats*. 1987, Elsevier applied science publishers: London. p. 10-12.
168. Kyriakidis, N. and T. Katsiloulis, *Calculation of iodine value from measurements of fatty acid methyl esters of some oils: Comparison with the relevant American Oil Chemists Society method.* Journal of the American Oil Chemists' Society, 2000. **77**(12): p. 1235-1238.
169. Man, Y.C., G. Setiowaty, and F. Van de Voort, *Determination of iodine value of palm oil by Fourier transform infrared spectroscopy.* Journal of the American Oil Chemists' Society, 1999. **76**(6): p. 693-699.
170. Haryati, T., et al., *Determination of iodine value of palm oil by differential scanning calorimetry.* Journal of the American Oil Chemists' Society, 1997. **74**(8): p. 939-942.
171. Gee, P., *Iodine Value Determination by FTIR Spectroscopy.* Mal. Oil Sci. Tech, 1995. **4**: p. 182-185.
172. Siebert, F. and P. Hildebrandt, *Theory of Infrared Absorption and Raman Spectroscopy*, in *Vibrational Spectroscopy in Life Science*. 2008, WILEY-VCH Verlag GmbH & Co: Weinheim. p. 11-61.
173. Arnold, R. and T. Hartung, *Infrared spectroscopic determination of degree of unsaturation of fats and oils.* Journal of food science, 1971. **36**(1): p. 166-168.
174. Van de Voort, F., et al., *Rapid and direct Iodine value and saponification number determination of fats and oils by attenuated total reflectance/fourier transform infrared spectroscopy.* Journal of the American Oil Chemists' Society, 1992. **69**(11): p. 1118-1123.

175. Zhou, Y. and R. Hartel, *Phase behavior of model lipid systems: Solubility of high-melting fats in low-melting fats.* Journal of the American Oil Chemists' Society, 2006. **83**(6): p. 505-511.
176. Hannewijk, J., A. Haighton, and P. Hendrikse, *Dilatometry of fats.* Analysis and Characterization of Oils, Fats and Fat Products, 1964. **1**: p. 121-182.
177. Timms, R., *The solubility of milk fat, fully hardened milk fat, and milk fat hard fraction in liquid oils [vegetable oils used to soften butter]*. Australian Journal of Dairy Technology (Australia), 1978.
178. Hartel, R.W., *Crystallization in Foods*. 2001: Springer.
179. Hannewijk, J., *Crystallisation of Fats: General Considerations.* Chemical Weekly, 1964. **60**: p. 309-320.
180. Gokcen, N., *Temperature dependence of solubility of nonelectrolytes.* Journal of the Chemical Society, Faraday Transactions 1: Physical Chemistry in Condensed Phases, 1973. **69**: p. 438-443.
181. Guggenheim, E., *Thermodynamics, 1967*. NothMHolland, AmsterM dam, 1967.
182. Perrot, P., *A to Z of Thermodynamics*. 1998: Oxford University Press.
183. Stahly, G.P., *Diversity in Single- and Multiple-Component Crystals. The Search for and Prevalence of Polymorphs and Cocrystals.* Crystal Growth & Design, 2007. **7**(6): p. 1007-1026.
184. Calliauw, G., et al., *Recent developments in the production of soft-PMF and superolein*, in *EuroFedLipid Congress*. 2006: Madrid, Spain.
185. Miskandar, M.S. *Palm oil for solid fat application*. in *26th Palm Oil Familiarisation Programme*. 2006. Kuala Lumpur.
186. Tan, Y., *Quality monitoring (chemical and instrumental technique). 26th Palm Oil Familiarisation Programme*. Kuala Lumpur, July, 2006: p. 9-19.
187. Paquot, C., et al., *Standard methods for the analysis of oils, fats, and derivatives*. 1987: Blackwell Scientific Publications.
188. Malaysia, I.P.M.K.S., *Determination of solid fat content by nuclear magnetic resonance*, in *PORIM Test Methods*. 1995, Palm Oil Research Institute of Malaysia: Malaysia. p. 127-131.
189. AINIE, K., et al., *MPOB test methods : a compendium of test on palm oil products, palm kernel products, fatty acids, food related products and others*, ed. K. Ainie. 2004, Selangor, Malysia: Malaysian Palm Oil Board.
190. Timms, R., *Computer program to construct isosolid diagrams for fat blends.* Chemistry and Industry, 1979.
191. HAYATI, I., et al., *Melting characteristic and solid fat content of milk fat and palm stearin blends before and after enzymatic interesterification.* Journal of Food Lipids, 2000. **7**(3): p. 175-193.
192. Lida, H. and A.R. Ali, *Physico-chemical characteristics of palm-based oil blends for the production of reduced fat spreads.* Journal of the American Oil Chemists' Society, 1998. **75**(11): p. 1625-1631.
193. Kaisersberger, E., *DSC investigations of the thermal characterization of edible fats and oils.* Thermochimica Acta, 1989. **151**: p. 83-90.
194. Dijkstra, A., *Modification processes and food uses.* The Lipid Handbook; Gunstone, FD; Harwood, JL; Dijkstra, AJ, Eds, 2012: p. 263-353.
195. Hishamuddin, E., A.G. Stapley, and Z.K. Nagy, *Application of laser backscattering for monitoring of palm oil crystallisation from melt.* Journal of Crystal Growth, 2011. **335**(1): p. 172-180.
196. Van Putte, K. and B. Bakker, *Crystallization kinetics of palm oil.* Journal of the American Oil Chemists' Society, 1987. **64**(8): p. 1138-1143.
197. Chawla, P., *Measurement of the size distribution of fat crystals using a laser particle counter.* Journal of the American Oil Chemists' Society, 1990. **67**(5): p. 329-332.
198. Fitzgerald, A.M., et al., *Measurement of particle size distribution of tripalmitin crystals in a model solution using a laser diffraction method.* Journal of the American Oil Chemists' Society, 2001. **78**(10): p. 1013-1020.
199. Miskandar, M., et al., *Palm oil crystallization: Effects of cooling time and oil content.* Journal of Food Lipids, 2004. **11**(3): p. 190-207.
200. De Graef, V., et al., *Influence of shear flow on polymorphic behavior and microstructural development during palm oil crystallization.* European Journal of Lipid Science and Technology, 2009. **111**(3): p. 290-302.
201. Vuillequez, A., et al. *Thermal and Structural Behavior of Palm Oil. Influence of Cooling Rate on Fat Crystallization*. in *Macromolecular symposia*. 2010. Wiley Online Library.
202. Yu, Z., R. Tan, and P. Chow, *Effects of operating conditions on agglomeration and habit of paracetamol crystals in anti-solvent crystallization.* Journal of Crystal Growth, 2005. **279**(3): p. 477-488.
203. Heath, A.R., et al., *Estimating average particle size by focused beam reflectance measurement (FBRM).* Particle & Particle Systems Characterization, 2002. **19**(2): p. 84-95.
204. Ruf, A., J. Worlitschek, and M. Mazzotti, *Modeling and experimental analysis of PSD measurements through FBRM.* Particle & Particle Systems Characterization, 2000. **17**(4): p. 167-179.

205. Herrera, M. and R. Hartel, *Effect of processing conditions on crystallization kinetics of a milk fat model system.* Journal of the American Oil Chemists' Society, 2000. **77**(11): p. 1177-1188.
206. Shi, Y., B. Liang, and R.W. Hartel, *Crystal morphology, microstructure, and textural properties of model lipid systems.* Journal of the American Oil Chemists' Society, 2005. **82**(6): p. 399-408.
207. Swe, P.Z., Y.B.C. Man, and H.M. Ghazali, *Improved NARP-HPLC method for separating triglycerides of palm olein and its solid fractions obtained at low temperature storage.* Food Chemistry, 1996. **56**(2): p. 181-186.
208. Haryati, T., et al., *Determination of iodine value of palm oil based on triglyceride composition.* Journal of the American Oil Chemists' Society, 1998. **75**(7): p. 789-792.
209. Gotoh, N., et al., *Quantification method for triglyceride molecular species in fish oil with high performance liquid chromatography-ultraviolet detector-evaporative light scattering detector.* Journal of Oleo Science, 2006. **55**(9): p. 457-463.
210. Bullock, S. *High Resolution Analysis of Triglycerides in Vegetable Oils by HPLC with ELSD*. 2.
211. Henderson, D.W., *Thermal analysis of non-isothermal crystallization kinetics in glass forming liquids.* Journal of Non-Crystalline Solids, 1979. **30**(3): p. 301-315.
212. Toro-Vazquez, J., et al., *Crystallization kinetics of palm stearin in blends with sesame seed oil.* Journal of the American Oil Chemists' Society, 2000. **77**(3): p. 297-310.
213. Tieko Nassu, R. and L. Guaraldo Gonçalves, *Solid fat content determination: Comparison between pNMR and DSC techniques.* Grasas y aceites, 1995. **46**(6): p. 337-343.
214. Ng, W.L. *Nucleation from palm oil melt*. in *Proceedings-PORIM international palm oil development conference-chemistry, technology and marketing, 5-9 Sep. 1989, Kuala Lumpur, Malaysia*. 1990. PORIM.
215. Ng, W.L., *A study of the kinetics of nucleation in a palm oil melt.* Journal of the American Oil Chemists' Society, 1990. **67**(11): p. 879-882.
216. Fredrick, E., et al., *Influence of monoglycerides on the crystallization behavior of palm oil.* Crystal growth and design, 2008. **8**(6): p. 1833-1839.
217. Man, Y.C. and P. Swe, *Thermal analysis of failed-batch palm oil by differential scanning calorimetry.* Journal of the American Oil Chemists' Society, 1995. **72**(12): p. 1529-1532.
218. Chemistry, K. *Bond Enthalpy (Bond Energy)*. Kinetics and Equilibrium; Available from: http://www.kentchemistry.com/links/Kinetics/BondEnergy.htm.
219. HEL-Group. *Technology: Turbidity*. Automated solubility monitoring unit 2014 [cited 2014 7th May]; Available from: http://www.helgroup.com/reactor-systems/crystallisation-particle-studies/crystal-eyes/technology/.
220. Ni, X. and A. Liao, *Effects of Cooling Rate and Solution Concentration on Solution Crystallization of l-Glutamic Acid in an Oscillatory Baffled Crystallizer.* Crystal Growth & Design, 2008. **8**(8): p. 2875-2881.
221. Liang, J., *Process Scale Dependence of Batch Crystallisation l-glutamic Acid from Aqueous Solution in Relation to Reactor Internals Reactant Mixing and Process Conditions.* Heriot-Watt University, Edinburgh, 2002.
222. Kim, K.-J. and A. Mersmann, *Estimation of metastable zone width in different nucleation processes.* Chemical Engineering Science, 2001. **56**(7): p. 2315-2324.
223. Timms, R., *Choice of solvent for fractional crystallization of palm oil*, in *Palm Oil Product Technology in the Eighties*, E. Pushparajah and M. Rajasurai, Editors. 1983, CSIRO Division of Food Research Highett, Vic. p. 277-290.
224. Chiang, C.-Y., V. Starov, and D. Lloyd, *Crystallization kinetics of a polymer-solvent system. I: Derivation of model equations.* Colloid journal of the Russian Academy of Sciences, 1995. **57**(5): p. 715-724.
225. Kawamura, K., *The DSC thermal analysis of crystallization behavior in palm oil.* Journal of the American Oil Chemists' Society, 1979. **56**(8): p. 753-758.
226. Wright, A.J., et al., *The effect of minor components on milk fat crystallization.* Journal of the American Oil Chemists' Society, 2000. **77**(5): p. 463-475.
227. Pereira, R.P. and A.M. Rocco, *Nanostructure and crystallisation kinetics of poly (ethylene oxide)/poly (4-vinylphenol-co-2-hydroxyethyl methacrylate) blends.* Polymer, 2005. **46**(26): p. 12493-12502.
228. Kloek, W., P. Walstra, and T. van Vliet, *Crystallization kinetics of fully hydrogenated palm oil in sunflower oil mixtures.* Journal of the American Oil Chemists' Society, 2000. **77**(4): p. 389-398.
229. Garti, N. and K. Sato, *Crystallization Processes in Fats and Lipid Systems*. 2001: Taylor & Francis.
230. Sato, K. and T. Kuroda, *Kinetics of melt crystallization and transformation of tripalmitin polymorphs.* Journal of the American Oil Chemists' Society, 1987. **64**(1): p. 124-127.
231. Brown, C.J., et al., *Evaluation of crystallization kinetics of adipic acid in an oscillatory baffled crystallizer.* CrystEngComm, 2014. **16**(34): p. 8008-8014.

232. Ghotra, B.S., S.D. Dyal, and S.S. Narine, *Lipid shortenings: a review.* Food Research International, 2002. **35**(10): p. 1015-1048.
233. Vanhoutte, B., et al., *Monitoring milk fat fractionation: Filtration properties and crystallization kinetics.* Journal of the American Oil Chemists' Society, 2003. **80**(3): p. 213-218.
234. DeMan, J., *Effect of cooling procedures on consistency, crystal structure and solid fat content of milk fat.* Dairy Industries, 1964. **29**: p. 244-246.
235. Herrera, M.L. and R.W. Hartel, *Effect of processing conditions on physical properties of a milk fat model system: Rheology.* Journal of the American Oil Chemists' Society, 2000. **77**(11): p. 1189-1196.
236. Reis, N., et al., *Residence times and mixing of a novel continuous oscillatory flow screening reactor.* Chemical Engineering Science, 2004. **59**(22): p. 4967-4974.
237. Brown, C.J., J.A. Adelakun, and X.-w. Ni, *Characterization and modelling of antisolvent crystallization of salicylic acid in a continuous oscillatory baffled crystallizer.* Chemical Engineering and Processing: Process Intensification, 2015. **97**: p. 180-186.
238. Kitaigorodsky, A.I.W., Nicholas, *Order and Disorder in the World of Atoms*. 1st ed. 1980, Moscow: Mir Publishers.
239. Neves-Saraiva, R., *The characterisation of mixing for oscillatory flow within baffled tubes.* University of Cambridge Cambridge UK, 1998.
240. Abebe, S.B., et al., *The information content in NIR spectral data for slurries of organic crystals.* Powder Technology, 2008. **179**(3): p. 176-183.
241. Grön, H., et al., *Dynamic In-Process Examination of Particle Size and Crystallographic Form under Defined Conditions of Reactant Supersaturation as Associated with the Batch Crystallization of Monosodium Glutamate from Aqueous Solution.* Industrial & Engineering Chemistry Research, 2003. **42**(20): p. 4888-4898.
242. Ridder, B.J., A. Majumder, and Z.K. Nagy, *Population balance model-based multiobjective optimization of a multisegment multiaddition (MSMA) continuous plug-flow antisolvent crystallizer.* Industrial & Engineering Chemistry Research, 2014. **53**(11): p. 4387-4397.